

72-4608

PERKINS, Richard Alex, 1945-  
THE DIFFUSION OF CHROMIUM IN NICKEL  
OXIDE.

The Ohio State University, Ph.D., 1971  
Engineering, metallurgy

University Microfilms, A XEROX Company, Ann Arbor, Michigan

THE DIFFUSION OF CHROMIUM IN

NICKEL OXIDE

DISSERTATION

Presented in Partial Fulfillment of the Requirements for  
the Degree Doctor of Philosophy in the Graduate  
School of the Ohio State University


By

Richard Alex Perkins, B.S.

\* \* \* \* \*

The Ohio State University  
1971

Approved by

  
\_\_\_\_\_  
Adviser  
Department of Metallurgical  
Engineering

PLEASE NOTE:

Some Pages have indistinct  
print. Filmed as received.

UNIVERSITY MICROFILMS

## ACKNOWLEDGMENTS

The author wishes to thank Dr. Robert A. Rapp, thesis adviser, for his assistance in setting up the experimental program and interpreting the data.

Also, the author wishes to acknowledge the helpful discussions and assistance of Dr. K. Wylie, Dr. W. Crow and Albert Caffo in performing the experimental work.

International Nickel Company is gratefully thanked for providing the fellowship to the department of Metallurgical Engineering which provided the financial support for this work. The Ohio State University Computer Center is also acknowledged for contributing the computer time used in this work.

VITA

August 27, 1945      Born - Decatur, Illinois

1967.....      B. S. University of Missouri at Rolla, Rolla, Missouri

1967-1968.....      Research Associate, The Ohio State University,  
Columbus, Ohio

1968-1971.....      International Nickel Fellow, The Ohio State University,  
Columbus, Ohio

## CONTENTS

	Page
ACKNOWLEDGMENTS . . . . .	ii
VITA . . . . .	iii
TABLES . . . . .	vi
FIGURES . . . . .	vii
I. INTRODUCTION AND LITERATURE SURVEY . . . . .	1
A. NiO and Its Defect Structure	
B. Cr-doped NiO and Its Defect Structure	
C. Diffusion Theory	
D. Diffusion Studies in NiO	
II. STATEMENT OF PURPOSE . . . . .	20
III. THEORY . . . . .	21
A. Equilibrium and Complexing of $F^{3+}$ in Divalent MX	
B. Diffusion of Aliovalent Impurities	
C. Application to Chromium Diffusion in NiO	
IV. EXPERIMENTAL MATERIALS AND PROCEDURE . . . . .	46
A. Sample Preparation	
B. Pressure Calibration	
C. Sectioning Apparatus	
D. Counting Apparatus	
E. Procedure	
V. RESULTS AND DISCUSSION . . . . .	67
VI. SUMMARY AND CONCLUSIONS . . . . .	99
APPENDIXES	
A. . . . .	101
B. . . . .	105

CONTENTS (Continued)

	Page
APPENDIXES (Continued)	
C. . . . .	109
REFERENCES. . . . .	119

TABLES

Table	Page
1. Concentration of Thermally Created Native Nickel in NiO as a Function of Temperature and Oxygen Pressure . . . . .	7
2. Concentration of Two- and Three-member Complexes as a Function of Temperature and Impurity Concentration. . . . .	38
3. Results of the Spectrographic Analysis of the NiO Single Crystals. . . . .	48
4. Results of the Analyses of the Diffusion Profiles for Chromium in NiO. . . . .	85
5. Diffusion Data for Chromium in NiO . . . . .	110



## FIGURES

Figure	Page
1. Defect Equilibria in Cr-doped NiO for $[V_{Ni}'] \ll [V_{Ni}'']$ . After Meier <sup>12</sup> . . . . .	4
2. Schematic Phase Diagram for the Ni-Cr-O System . . . . .	8
3. Degree of Association as a Function of $RT/\Delta G_3^0$ for $[F_{TOT}] = 10^{-4}$ Cation Fraction. . . . .	30
4. Degree of Association as a Function of $RT/\Delta G_3^0$ for $[F_{TOT}] = 10^{-3}$ Cation Fraction. . . . .	31
5. Degree of Association as a Function of $RT/\Delta G_3^0$ for $[F_{TOT}] = 10^{-2}$ Cation Fraction. . . . .	32
6. Degree of Association as a Function of $RT/\Delta G_3^0$ for $[F_{TOT}] = 10^{-1}$ Cation Fraction. . . . .	33
7. Schematic Diagram of the Jump Order for Diffusion of a Three-member Complex . . . . .	36
8. Concentration Dependence of the Impurity Diffusion Coefficient from the Impurity-Vacancy Complexes for $RT/\Delta G_3^0 = 0.05$ . . . . .	40
9. Concentration Dependence of the Impurity Diffusion Coefficient from the Impurity-Vacancy Complexes for $RT/\Delta G_3^0 = 0.1$ . . . . .	41
10. Concentration Dependence of the Impurity Diffusion Coefficient from the Impurity-Vacancy Complexes for $RT/\Delta G_3^0 = 0.2$ . . . . .	42
11. Concentration Dependence of the Impurity Diffusion Coefficient from the Impurity-Vacancy Complexes at $RT/\Delta G_3^0 = 0.3$ . . . . .	43
12. Schematic Illustration of the Apparatus Used to Perform the Diffusion Anneals at $P_{O_2} = 1.0$ . . . . .	49
13. Cell Unit Assembly for the Diffusion Anneals at $P_{O_2} = 1.0$ . . . . .	52

## FIGURES (Continued)

Figure	Page
14. Schematic Illustration of the Apparatus Used to Perform the Diffusion Anneals at $P_{O_2} = 10^{-2}$ and $10^{-5}$ . . . . .	54
15. Cell Unit Assembly for the Diffusion Anneals at $P_{O_2} = 10^{-2}$ and $10^{-5}$ . . . . .	57
16. Apparatus Used to Section the NiO Crystals . . . . .	61
17. Apparatus Used to Measure the Thickness of the Sections Removed from the NiO Crystals. . . . .	63
18. Solubility Limit of Chromium in NiO as a Function of Temperature . . . . .	71
19. Diffusion Profile for Chromium in NiO at $1100^{\circ}C$ and $P_{O_2} = 1.0$ . . . . .	73
20. Normalized Diffusion Coefficient of Chromium as a Function of the Chromium Concentration at $1100^{\circ}C$ and $P_{O_2} = 1.0$ . . . . .	76
21. Concentration Profile of Chromium and Nickel Vacancies Diffusing into NiO. . . . .	77
22. Effect of Positive Holes Upon the Diffusion of Vacancies Ahead of the Chromium . . . . .	81
23. Reduced Diffusion Profile for Chromium in NiO at $1100^{\circ}C$ and $P_{O_2} = 1.0$ . . . . .	83
24. Saturation Diffusion Coefficient of Chromium as a Function of Temperature. . . . .	88
25. Concentration of Chromium-Vacancy Complexes as a Function of Temperature and Chromium Concentration . . . . .	89
26. Log D as a Function of $1/T$ for $10^{-3}$ Cation Fraction of Chromium-Vacancy Complexes. . . . .	92
27. Log D as a Function of $1/T$ for $1.2 \times 10^{-2}$ Cation Fraction of Chromium . . . . .	95
28. Diffusion Coefficient of Chromium as a Function of Chromium Concentration and Temperature . . . . .	96
29. Normalized Diffusion Coefficient of Chromium as a Function of the Chromium Concentration at $1100^{\circ}C$ and $1300^{\circ}C$ . . . . .	97

## I. INTRODUCTION AND LITERATURE SURVEY

Nickel-based alloys containing chromium are important for service at high temperatures in oxidizing atmospheres, so the oxidation of pure and chromium-doped nickel has been studied extensively.

Pure nickel, after a period of initial oxide formation, oxidizes in accordance with the parabolic rate law at temperatures above about 700°C, indicating diffusion controlled oxidation.<sup>1-4</sup> Diffusion studies in single crystal NiO at around 1200°C have indicated that the diffusion coefficient of nickel is approximately three orders of magnitude greater than the diffusion coefficient of oxygen.<sup>5,6</sup> Therefore the oxidation of pure nickel is seemingly controlled by the motion of nickel ions through the NiO scale which is compact.

The parabolic oxidation rate constant of nickel increases rapidly with small additions of chromium.<sup>1,2,7-11</sup> The prevailing theory<sup>13</sup> states that the presence of chromium in the NiO scale increases the cation vacancy concentration and increases the diffusion rate of nickel through the scale. This doping effect would be dependent upon the diffusion of chromium into NiO from NiCr<sub>2</sub>O<sub>4</sub> particles.

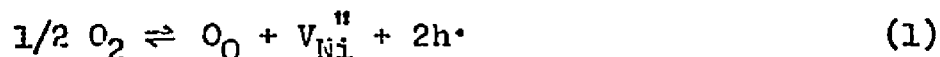
While the results of the present investigation should be pertinent to dilute Ni-Cr alloy oxidation, the study is best characterized as an investigation of the diffusion of an aliovalent dopant (Cr<sup>3+</sup>) in the lattice of an inorganic compound (NiO). Initially, the defect structure of pure and Cr-doped NiO is discussed. Then the theory of diffusion of

divalent dopants in alkali halides is presented along with experimental results which support the theory. Finally, the results of investigations involving the diffusion of trivalent impurities in NiO are discussed.

#### A. NiO and Its Defect Structure

Nickelous oxide, NiO, has the NaCl-type lattice structure--interpenetrating face-centered-cubic lattices of nickel and oxygen ions--with a lattice parameter of 4.1768Å.<sup>14</sup> Thermoelectric power<sup>15,16</sup> and electrical conductivity, Seebeck effect and optical transmission measurements<sup>17</sup> have shown that NiO is a metal-deficit, p-type semiconductor; therefore, vacancies exist in the nickel sublattice along with positive holes or Ni<sup>3+</sup> ions. Morin<sup>18</sup> has proposed that the holes in NiO exist in the 2p and 3d energy levels of the nickel atoms.

The degree of ionization of the cation vacancies in the nickel substructure has been a subject of debate in the literature. If the cation vacancies are doubly ionized, the excess oxygen is incorporated into the lattice by the reaction:



According to the notation of Kröger and Vink,  $O_O$  is a normal oxygen ion on an oxygen site,  $V_{Ni}''$  is a vacant nickel site with a charge of "minus two" relative to the normally occupied site, and  $h^{\bullet}$  is a positive hole or Ni<sup>3+</sup> ion. From the law of mass action, assuming the activity of  $O_O$  is unity relative to a "perfect NiO lattice standard state," the equilibrium constant for Eq. (1) is given as:

$$K = \frac{[V_{Ni}^{''}] p^2}{P_{O_2}^{1/2}} \quad (2)$$

The number of defects is small compared to the number of lattice sites so the activities of the defects can be replaced by their concentrations (Henry's Law). If positive holes and doubly charged cation vacancies are essentially the only charged species in the lattice, the simplified electrical neutrality condition becomes:

$$p = [V_{Ni}^{''}] \quad (3)$$

Substituting Eq. (3) into Eq. (2) and rearranging gives:

$$p = K^{1/3} P_{O_2}^{1/6} \quad (4)$$

Therefore the electrical conductivity, which is directly proportional to the hole concentration, should be directly proportional to  $P_{O_2}^{1/6}$  if the cation vacancies are doubly ionized. In a similar manner the conductivity can be shown to be proportional to  $P_{O_2}^{1/4}$  if the vacancies are singly ionized. A singly ionized cation vacancy is a vacant nickel site with a trapped positive hole or  $Ni^{3+}$  adjacent to the vacancy. For doubly ionized vacancies the positive holes are completely dissociated from the vacancies. However if trivalent impurity cations are present in concentrations greater than the native vacancy concentration, the dependence of the conductivity on  $P_{O_2}$  will be  $1/4$  for doubly ionized cation vacancies and  $1/2$  for singly ionized cation vacancies. In Fig. 1 the Kröger and Vink diagram for chromium-doped NiO for the case

$[V_{Ni}^{''}] \gg [V_{Ni}^{\cdot}]$  is shown. In Zone II where the chromium-induced va-

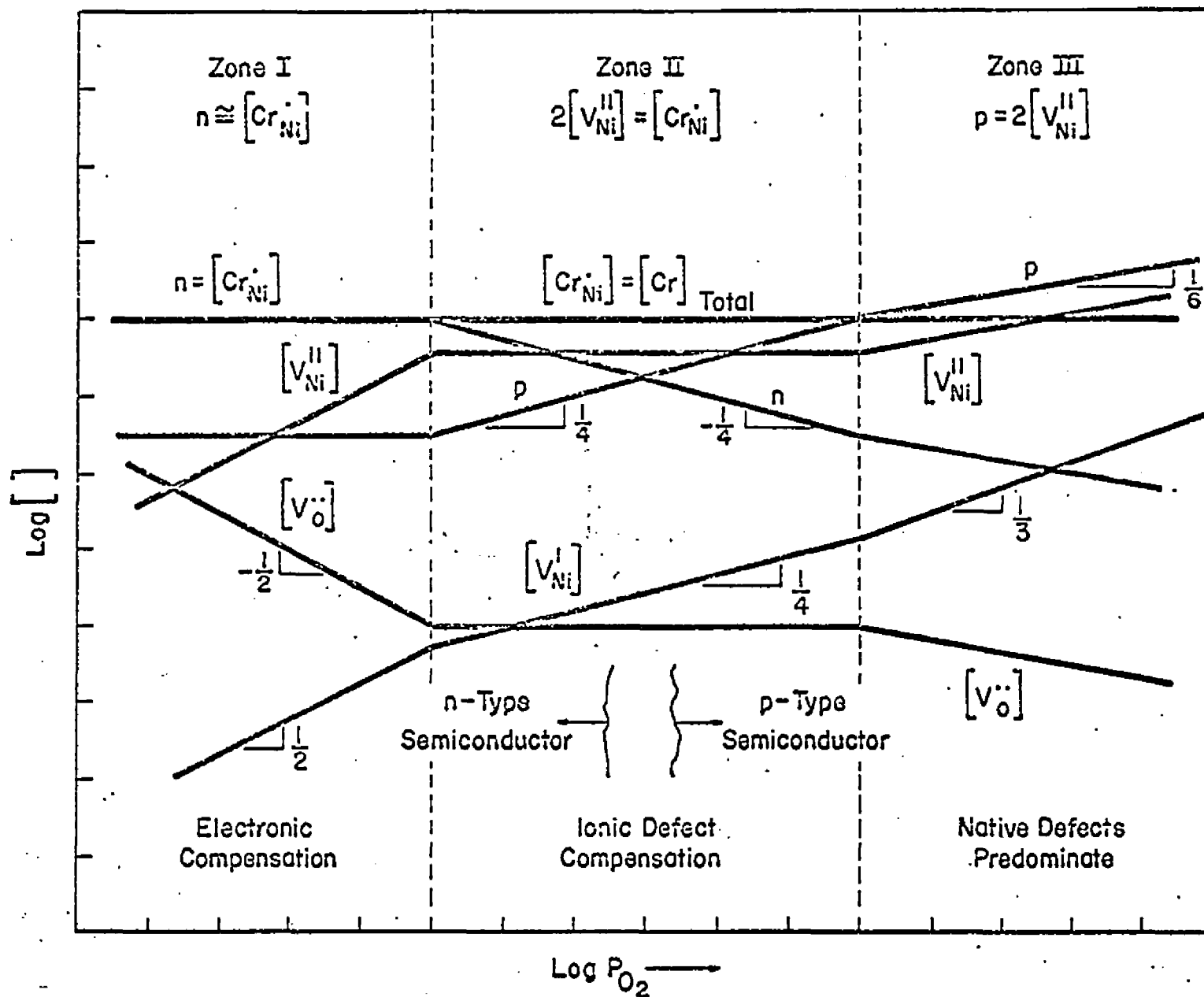


Fig. 1. -- Defect Equilibria in Cr-doped NiO for  $[V_{Ni}^I] \ll [V_{Ni}^{II}]$ .  
 After Meier.<sup>12</sup>

cancies predominate,  $p$  is proportional to  $P_{O_2}^{1/4}$ , and Zone III where the native vacancies predominate,  $p$  is proportional to  $P_{O_2}^{1/6}$ .

The first extensive study of the electrical behavior of NiO was performed by Baumbach and Wagner.<sup>19</sup> They found the conductivity of NiO to be proportional to  $P_{O_2}^{1/4}$ , but the nickel used to form the oxide samples contained small amounts of iron and manganese which might have doped the lattice. Eror<sup>20</sup> and Bransky and Tallan<sup>21</sup> also found a  $P_{O_2}^{1/4}$  dependence for the conductivity of NiO. The results of these investigations were interpreted as indicating that singly ionized cation vacancies are the predominant defects in NiO. Mitoff<sup>22</sup> has reported a  $P_{O_2}^{1/6}$  dependence of the conductivity of NiO. Meier and Rapp<sup>23</sup> have observed the conductivity to be proportional to  $P_{O_2}^{1/n}$  where  $n$  approached 6 at temperatures above 850°C for high purity specimens and  $n$  approached 4 for lower temperatures and less pure specimens. These results were interpreted to indicate that doubly ionized cation vacancies are the predominate defects in NiO--at least at temperatures above 850°C according to Meier and Rapp. Tripp and Tallan<sup>24</sup> have recently reported a  $P_{O_2}^{1/5}$  dependence for the conductivity. They interpreted this result as indicating that the cation vacancies are doubly ionized but that the impurity concentration of their specimens was too large to observe the  $P_{O_2}^{1/6}$  dependence which would be expected.

In the present work the cation vacancies are assumed to be doubly ionized, so that in pure NiO the defect equilibrium is assumedly described by Eq. (1). The concentration of native defects can be calculated as a function of the temperature and oxygen pressure using the expression obtained by Tret'yakov and Rapp<sup>25</sup> from coulometric titration:

$$[V_{Ni}^{''}] = 0.51 (P_{O_2})^{1/6} \exp (-19000 \pm 8700/RT) \quad (5)$$

the expression obtained by Mitoff<sup>22</sup> from gravimetric and conductivity data:

$$[V_{Ni}^{''}] = 0.11 (P_{O_2})^{1/6} \exp (-17800/RT) \quad (6)$$

or the expression obtained by Tripp and Tallan<sup>24</sup> also from gravimetric and conductivity data:

$$[V_{Ni}^{''}]_{eff} = 0.168 (P_{O_2})^{1/5} \exp (-19800 \pm 3500/RT) \quad (7)$$

In Eq. (7)  $[V_{Ni}^{''}]_{eff}$  is the effective native vacancy concentration defined as the difference between the actual vacancy concentration and the vacancies created by the aliovalent impurities. The concentration of thermally produced native vacancies calculated from these expressions are tabulated in Table 1 for the temperatures and oxygen pressures used in this work. From an analysis of the impurities in the NiO crystal, the concentration of native vacancies created by the presence of aliovalent cation impurities, i.e. cations whose valence states differ from that of the host cations, can be estimated. The concentration of native thermal vacancies is rather low so that the aliovalent impurities of even nominally pure NiO can be important in determining the actual vacancy concentration.

#### B. Cr-doped NiO and Its Defect Structure

The schematic phase diagram for the Ni-Cr-O system is drawn in Fig. 2. Some of the composition limits for the various phases are not known, but the coexistence of the phases was obtained from the stability



TABLE 1.--Concentration of the Thermally Created Native Nickel Vacancies in NiO as a Function of Temperature and Oxygen Pressure

T (°C)	P <sub>O<sub>2</sub></sub> (atm)	[V <sub>Ni</sub> <sup>''</sup> ] <sup>a</sup> (cat frac)	[V <sub>Ni</sub> <sup>''</sup> ] <sup>b</sup> (cat frac)	[V <sub>Ni</sub> <sup>''</sup> ] <sub>eff</sub> <sup>c</sup> (cat frac)
1000	1.0	2.9 x 10 <sup>-4</sup>	1.0 x 10 <sup>-4</sup>	6.9 x 10 <sup>-5</sup>
1100	1.0	5.1 x 10 <sup>-4</sup>	1.7 x 10 <sup>-4</sup>	1.2 x 10 <sup>-4</sup>
	10 <sup>-2</sup>	2.4 x 10 <sup>-4</sup>	7.8 x 10 <sup>-5</sup>	4.8 x 10 <sup>-5</sup>
	10 <sup>-5</sup>	7.3 x 10 <sup>-5</sup>	2.5 x 10 <sup>-5</sup>	1.2 x 10 <sup>-5</sup>
1200	1.0	8.3 x 10 <sup>-4</sup>	2.6 x 10 <sup>-4</sup>	2.0 x 10 <sup>-4</sup>
	10 <sup>-2</sup>	3.9 x 10 <sup>-4</sup>	1.2 x 10 <sup>-4</sup>	8.0 x 10 <sup>-5</sup>
	10 <sup>-5</sup>	1.2 x 10 <sup>-4</sup>	3.8 x 10 <sup>-5</sup>	2.0 x 10 <sup>-5</sup>
1300	1.0	1.2 x 10 <sup>-3</sup>	3.9 x 10 <sup>-4</sup>	3.0 x 10 <sup>-4</sup>
	10 <sup>-2</sup>	5.8 x 10 <sup>-4</sup>	1.8 x 10 <sup>-4</sup>	1.2 x 10 <sup>-4</sup>
	10 <sup>-5</sup>	1.8 x 10 <sup>-4</sup>	5.7 x 10 <sup>-5</sup>	3.0 x 10 <sup>-5</sup>

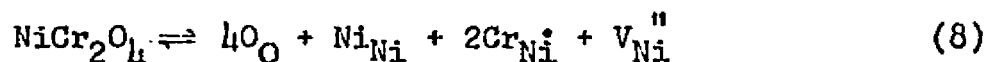
<sup>a</sup>Calculated from expression of Tret'yakov and Rapp

<sup>b</sup>Calculated from expression of Mitoff

<sup>c</sup>Calculated from expression of Tripp and Tallan

diagrams constructed by Giggins and Pettit<sup>11</sup> and Ray et al.<sup>26</sup> From the phase diagram, NiCr<sub>2</sub>O<sub>4</sub> is shown to coexist with either NiO or Cr<sub>2</sub>O<sub>3</sub>.

When NiO is in equilibrium with NiCr<sub>2</sub>O<sub>4</sub> the defect equilibrium is described by:



where Cr<sub>Ni</sub><sup>•</sup> is a chromium ion on a nickel site with an excess charge of

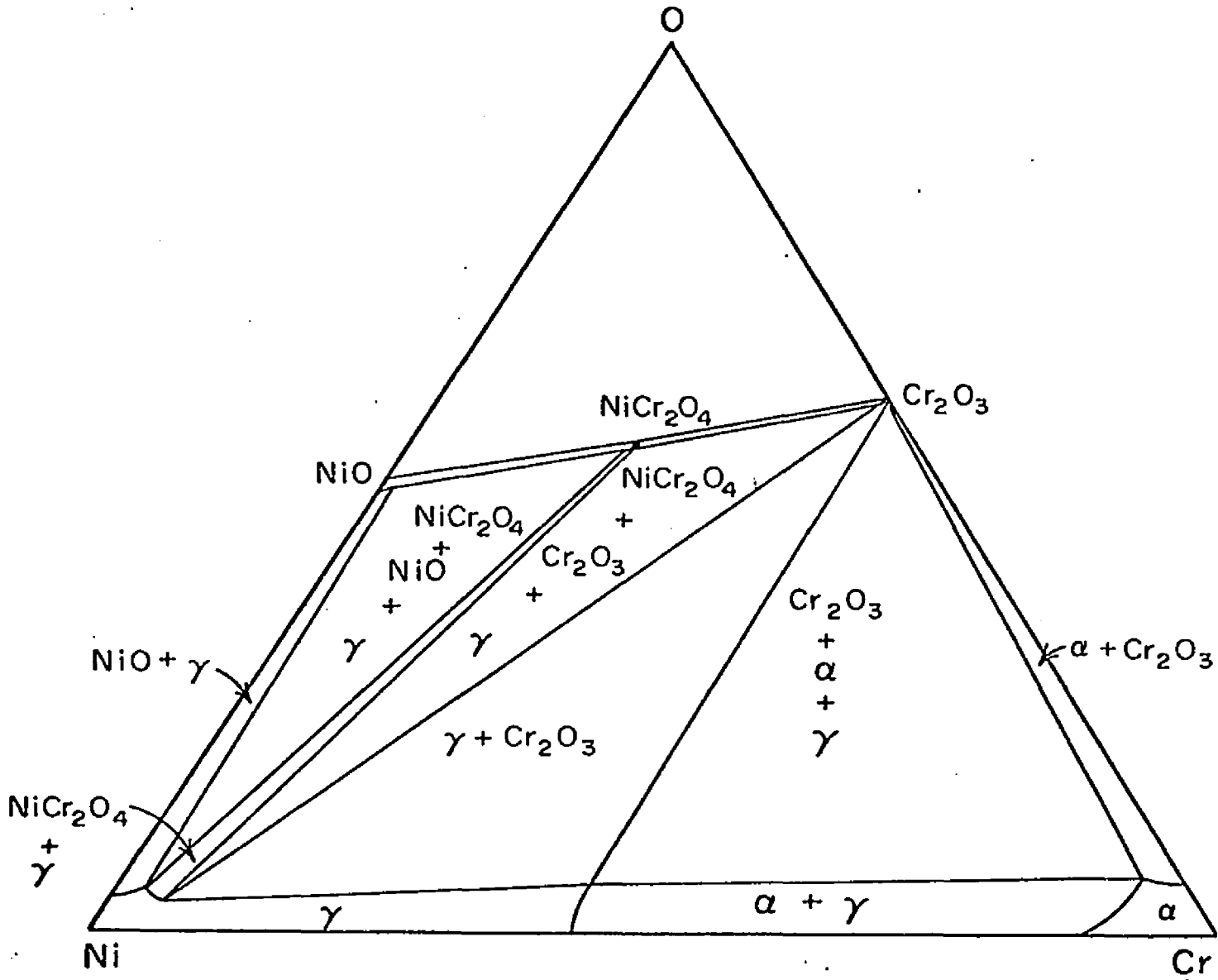


Fig. 2.--Schematic Phase Diagram for the Ni-Cr-O System.

"plus one." If the concentration of native vacancies is greatly exceeded by the chromium ion concentration, the simplified electrical neutrality condition becomes:

$$[\text{Cr}_{\text{Ni}}^{\bullet}] = 2 [\text{V}_{\text{Ni}}^{\prime\prime}] \quad (9)$$

Substitution of Eq. (9) into Eq. (2) gives:

$$p = (2K_1)^{1/2} \frac{P_{\text{O}_2}^{1/4}}{[\text{Cr}_{\text{Ni}}^{\bullet}]^{1/2}} \quad (10)$$

so that the conductivity of Cr-doped NiO should be proportional to  $P_{\text{O}_2}^{1/4}$  and  $[\text{Cr}_{\text{Ni}}^{\bullet}]^{-1/2}$  for doubly ionized vacancies. Application of the law of mass action to Eq. (8) gives:

$$K_2 = \frac{[\text{Cr}_{\text{Ni}}^{\bullet}]^2 [\text{V}_{\text{Ni}}^{\prime\prime}]}{a_{\text{NiCr}_2\text{O}_4}} \quad (11)$$

Because  $\text{NiCr}_2\text{O}_4$  is a relatively tight compound, its activity is essentially independent of the activities of its component species. Therefore the activity of  $\text{NiCr}_2\text{O}_4$  coexisting with Cr-saturated NiO is approximately unity for all  $P_{\text{O}_2}$ . Substitution of Eq. (9) into Eq. (11) gives:

$$[\text{Cr}_{\text{Ni}}^{\bullet}]_{\text{Saturation}} = (2K_3)^{1/3} \neq f(P_{\text{O}_2}) \quad (12)$$

so that the solubility of Cr in NiO should be independent of  $P_{\text{O}_2}$  if the chromium ions are compensated by doubly ionized cation vacancies. From the  $P_{\text{O}_2}^{1/4}$ -dependence and the  $[\text{Cr}_{\text{Ni}}^{\bullet}]^{-1/2}$ -dependence of the conductivity of the chromium solubility which they observed, Meier and Rapp<sup>23</sup> con-

cluded that the experimental range of Cr-doped NiO existence is the right-hand portion of Zone II in the Kroger and Vink diagram shown in Fig. 1.

Attractive coulombic force will exist between the negatively charged cation vacancies and positively charged chromium ions which may cause the two species to be associated as a complex. The long-range coulombic interaction between unassociated chromium ions and cation vacancies can be calculated from the Debye-Huckel theory for concentrated electrolytes.<sup>27</sup> The fact that the ions in a crystalline system can only occupy discrete lattice sites as opposed to ions moving continuously in a solution is not likely to be significant at small dopant concentrations. At small concentrations the average separation between charges is much larger than the lattice spacing so the discreteness of the lattice site is not very important. From the Debye-Huckel theory, the electrical energy,  $V_e$ , of the electrolyte solution is given by:

$$V_e = -\frac{\sum N_i z_i^2}{2} \frac{e^2 K}{D(1 + K a_i)} \quad (13)$$

where  $N_i$  is the number of ions of each species present in the electrolyte,  $z_i$  is the valence of each species,  $e$  is the charge of the electron,  $D$  is the dielectric constant of the electrolyte,  $a_i$  is the characteristic diameter of each species, and  $K$  is the Debye-Huckel screening constant which is defined as:

$$\frac{1}{K} = \left( \frac{DkT}{8\pi e^2 \sum_i n_i z_i^2} \right)^{1/2} \quad (14)$$

Therefore in Cr-doped NiO, in addition to the chromium ions and cation vacancies, there will be an equilibrium number of complexes formed between the chromium and vacancies in the lattice.

### C. Diffusion Theory

When a particular cationic species diffuses in an MX crystal lattice, the rate of diffusion is dependent upon the number of cations of that species which are capable of moving. If the species diffuses by a vacancy mechanism, then only those cations which have a vacancy on one of their nearest neighbor cation sites are capable of a diffusion jump. For the case of completely random or uncorrelated self-diffusion, the diffusion coefficient for the random walk analysis is given by:<sup>28</sup>

$$D = (1/6) T^1 r^2 \quad (15)$$

where  $T^1$  is the average number of jumps made by every ion in unit time and  $r$  is the jump distance. The average number of jumps is given by  $Zx\omega_1$ , where  $x$  is the concentration of native cation vacancies,  $Z$  is the coordination number of the cation sublattice and  $\omega_1$  is the jump frequency for the exchange between a cation and a cation vacancy. For self-diffusion, the number of cations which are capable of migration is given by  $Zx$  which is the number of cation sites adjacent to cation vacancies at nearest neighbor sites.

For the diffusion of impurity cations of the same valence as the host cations, the diffusion coefficient is given by:

$$D = (1/6) T^1 r^2 f \quad (16)$$

where  $f$  is the correlation factor which accounts for any interdependence

between successive jumps of the impurity ions. In this case the average number of jumps is given by  $Zxc\omega_2$  where  $c$  is the concentration of the impurity and  $\omega_2$  is the jump frequency for the impurity-vacancy exchange. For a vacancy-impurity pair, the correlation factor is approximately:<sup>29</sup>

$$f = \frac{\omega_1}{\omega_1 + \omega_2} \quad (17)$$

Substitution for  $T$  and  $f$  in Eq. (2) yields:

$$D = (1/6)Zxc \left( \frac{\omega_1 \omega_2}{\omega_1 + \omega_2} \right) r^2 \quad (18)$$

In this case the number of impurity ions which are able to move is given by  $Zxc$  where  $Zx$  is the number of cation sites which are nearest neighbor sites of the native cation vacancies and  $c$  is the fraction of these sites which will be occupied by impurity ions.

For the diffusion of aliovalent cations, the situation is more complicated because gross electrical neutrality must be maintained in the crystal and there will be a coulombic force between the impurities and vacancies. The concentration of aliovalent impurities which are able to move is dependent upon the concentration of cation vacancies and the coulombic force between the impurities and vacancies. Therefore the diffusion coefficient of aliovalent impurities would be expected to be dependent upon its own concentration.

For divalent impurities in alkali halides, e.g.  $\text{Cd}^{2+}$  in  $\text{NaCl}$ , each  $\text{Cd}^{2+}$  present in the lattice is compensated electrically by a cation

vacancy which is singly charged. Therefore the vacancy concentration is increased and the electrical neutrality condition becomes:

$$[\text{Cd}_{\text{Na}}^{\bullet}] = [V_{\text{Na}}'] \quad (19)$$

where in the Kroger and Vink notation  $\text{Cd}_{\text{Na}}^{\bullet}$  is a cadmium ion on a sodium site with a " plus one " charge relative to a normally occupied sodium site and  $V_{\text{Na}}'$  is a vacant sodium site with a " minus one " charge relative to a normal site. Also because the vacancies and cadmium are of opposite charges they will be attracted to each other. In this case the number of impurity ions capable of migration will be affected by the increase in the vacancy concentration with the cadmium concentration and the attractive force between cation vacancies and cadmium ions.

Up the basis of the association model of Stasiw and Teltow,<sup>30</sup> Lidiard<sup>28</sup> theoretically treated the diffusion of  $\text{Cd}^{2+}$  in NaCl assuming that: 1) complexes are formed between the cation vacancies and cadmium ions because of the attractive force between them, 2) a complex is created when a vacancy and a cadmium ion are on nearest neighbor cation sites, 3) cadmium moves only when it is in a complex and therefore the complex is considered to diffuse as an entity, and 4) the complexes are tightly bound. With these assumptions, the one-dimensional flux of cadmium is given by:

$$J = -D_0 \frac{d}{dx} (Npc) \quad (20)$$

where  $D_0$  is the diffusion coefficient of the complex,  $c$  is the cadmium concentration,  $p$  is the degree of association between the cadmium and

vacancies, and  $N$  is the number of solvent cations. The degree of association is obtained from the association reaction:



where  $(\text{Cd}_{\text{Na}} \text{V}_{\text{Na}})$  is a cadmium-vacancy complex. Application of the law of mass action to Eq. (21) yields:

$$K_{\text{eq}} = \frac{[(\text{Cd}_{\text{Na}} \text{V}_{\text{Na}})]}{[\text{Cd}_{\text{Na}}] [\text{V}_{\text{Na}}']} \quad (22)$$

with the assumption that Henry's Law is obeyed so that concentrations of the species can be substituted for their activities. The equilibrium constant can be expressed as a function of temperature and Eq. (22) becomes:

$$\frac{pc}{(c - pc)(c - pc)} = Z \exp(\Delta G^0/RT) \quad (23)$$

where  $Z$  is the number of distinguishable configurations of the complex and  $\Delta G^0$  is the energy of association of the complex. Lidiard has assumed that the native vacancies can be ignored, and  $p$  is called the "degree of association" and is defined as the number of cadmium ions existing in complexes divided by the total number of cadmium ions present.

Because cadmium only moves when in a complex, Eq. (20) can be written as:

$$J = -D_0 \frac{d}{dx} (pc) \frac{d}{dx} (Nc) \quad (24)$$

where  $\frac{d}{dx} (Nc)$  is the cadmium concentration gradient and  $\frac{d}{dx} (pc)$  is the change in the concentration of complexes as a function of the cadmium



concentration. The diffusion coefficient for cadmium is then given by:

$$D_{\text{Cd}} = D_0 \frac{d}{dc} (pc) \quad (25)$$

and the concentration dependence is contained in  $\frac{d}{dc} (pc)$ . When the complexes are tightly bound, the dissociation-association equilibrium need not be considered explicitly so that the factor  $\frac{d}{dc} (pc)$  contains the whole of the concentration dependence of  $D_{\text{Cd}}$ . By evaluating  $\frac{d}{dc} (pc)$ , Lidiard obtained the concentration dependence of  $D_{\text{Cd}}$  to be:

$$D_{\text{Cd}} = D_0 \left\{ 1 - [1 + 48 c \exp (\Delta G^0/RT)]^{-1/2} \right\} \quad (26)$$

At the low-concentration, high-temperature limit, i.e. for a high degree of dissociation,  $D_{\text{Cd}}$  is directly proportional to  $c$ , and at the high-concentration, low-temperature limit, i.e. for a high degree of association,  $D_{\text{Cd}}$  approaches  $D_0$ .

Lidiard's model has been fit to the experimental results for several systems involving divalent impurities in alkali halides. For the diffusion of  $\text{Cd}^{2+}$  in  $\text{AgBr}$ <sup>31</sup>,  $\text{Pb}^{2+}$  in  $\text{KCl}$ <sup>32</sup>,  $\text{Cd}^{2+}$  in  $\text{KCl}$ <sup>33</sup>, and  $\text{Pb}^{2+}$  in  $\text{NaCl}$ <sup>34</sup>, Eq. (26) has been fit to the experimental results to describe the concentration dependence of the impurity diffusion coefficient. To make this evaluation of Lidiard's theory, the local diffusion coefficient along the concentration profile was obtained from the appropriate solution of the diffusion equation. The diffusion coefficient at various concentrations was placed in Eq. (26) and  $\Delta G^0$  and  $D_0$  were calculated using a method of successive approximations. From the average values of  $D_0$  and  $\Delta G^0$  for data from a diffusion profile, the theoretical depen-

dence of the diffusion coefficient upon the impurity concentration can be obtained. The theoretical model fit the experimental results very well in the systems mentioned, and in each case the conclusion was offered that the impurity diffused by impurity-vacancy complexes.

Therefore, in compounds with very ionic bonding, the rate of diffusion of an aliovalent impurity which diffuses via a vacancy mechanism is dependent upon the concentration of impurity-vacancy complexes present at a given temperature and impurity concentration. The basic assumptions of the diffusion mechanism of complexes are that the impurity diffuses via vacancies and the attractive force between the impurities and vacancies causes an equilibrium concentration of stable complexes to be present in the lattice.

#### D. Diffusion Studies in NiO

The self-diffusion of nickel in NiO has been studied by several investigators. Choi and Moore<sup>35</sup> have reported the activation energy of nickel self-diffusion in NiO as 45.6 kcal. However they reported that the concentration of trivalent impurities in their crystals was comparable to the total cation vacancy concentration. At temperatures greater than 1100°C, Shim and Moore<sup>5</sup> reported an activation energy of 44.2 kcal but they did not mention the impurity content of their crystals. Over the temperature range 740°-1400°C, Lindner and Akerstrom<sup>36</sup> obtained an activation energy of 56.0 kcal. Crow<sup>37</sup> reported an activation energy of 54.7 kcal from 1100°-1400°C in crystals with a very low aliovalent impurity content. Crow also observed a  $P_{O_2}$ -dependence of the self-diffusion coefficient which indicated that the cation vacancy concentration

was determined by the oxygen pressure. The lower activation energy probably applies to the case where the cation vacancy concentration is constant and determined by the aliovalent impurities, i.e. extrinsic behavior. The higher activation energy probably applies to the case where the cation vacancy is in equilibrium with the temperature and  $P_{O_2}$ , i.e. intrinsic behavior.

More recently the diffusion of impurities, i.e. cobalt, iron, and chromium, in NiO has received attention.<sup>37-40</sup> Seltzer<sup>40</sup> has studied the diffusion of  $^{51}\text{Cr}$  into NiO by evaporating a small amount of  $^{51}\text{Cr}$  onto the NiO surface and then annealing the crystal. From analysis of the diffusion profile the diffusion coefficient was concentration-dependent at high chromium concentrations which Seltzer attributed to the self-doping effect of the chromium. At low chromium concentrations, the diffusion coefficient was found to be constant presumably because the number of vacancies created by the chromium ions in the lattice decreased with the chromium concentration until the native defects predominated and the doping effect was negated. Considering only the concentration-independent portion of his diffusion profiles, Seltzer obtained the following Arrhenius-type equation for the diffusion coefficient of chromium in NiO as a function of temperature:

$$D = 9.36 \times 10^{-5} \exp \left[ \frac{-47.0 \pm 3.0 \text{ kcal}}{RT} \right] \frac{\text{cm}^2}{\text{sec}} \quad (27)$$

Since this value was obtained from the low concentration region where significant self-doping should not occur,  $D$  can be considered to be the self-diffusion coefficient of chromium in NiO.

Greskovich<sup>38</sup> has also studied the diffusion of chromium into NiO by contacting a NiO single crystal and a Cr<sub>2</sub>O<sub>3</sub> pellet and allowing the NiCr<sub>2</sub>O<sub>4</sub> spinel to form at the interface. The interdiffusion of chromium from the NiO-NiCr<sub>2</sub>O<sub>4</sub> interface into the NiO crystal and of nickel in the NiO to the NiO-NiCr<sub>2</sub>O<sub>4</sub> interface was measured while the spinel layer was growing. The interdiffusion coefficient is defined as:

$$D = (N_{Ni}D_{Cr} + N_{Cr}D_{Ni}) \quad (28)$$

where  $N_{Ni}$  and  $N_{Cr}$  are the cation fractions of nickel and chromium, respectively, and  $D_{Ni}$  and  $D_{Cr}$  are the diffusion coefficients of nickel and chromium, respectively. Greskovich found the interdiffusion coefficient to be directly proportional to the mole fraction of Cr<sub>2</sub>O<sub>3</sub> in the NiO and the diffusion of chromium to be the rate-determining step in the counter diffusion of nickel and chromium in NiO. These results lead to the conclusion that chromium diffusion in NiO is dependent upon its own concentration. By extrapolation of his linear plots of the interdiffusion coefficient versus chromium concentration to  $N_{Cr} = 0$ , Greskovich obtained the following Arrhenius-type equation for the self-diffusion of chromium in essentially pure NiO:

$$D = 1.4 \times 10^{-3} \exp \left[ \frac{-55.0 \text{ kcal}}{RT} \right] \frac{\text{cm}^2}{\text{sec}} \quad (29)$$

The diffusion of iron in NiO has also been studied<sup>37,39</sup> and indicated that iron also acted as a self-dopant. Crow<sup>37</sup> found that the diffusion coefficient of iron in NiO was nearly independent of the oxygen pressure. This result indicated that iron assumed the +3 valence state

and therefore created cation vacancies when dissolved in NiO in a concentration which exceeded the number of native defects. The iron retained a plus-three valence over the experimental  $P_{O_2}$  range and negated the oxygen pressure dependence which would otherwise determine the native vacancy concentration and effect the diffusion coefficient.

## II. STATEMENT OF PURPOSE

The principal purpose of this investigation was to examine theoretically and experimentally the diffusion of a trivalent impurity ion in a divalent oxide lattice. In contrast to the previous work in compounds with very ionic bonding, NiO exhibits predominate electronic (p-type) conduction, and the bonding is rather covalent. The mechanism involving complexing of the impurities with cation vacancies is tested and evaluated from the experimental determination of concentration profiles of  $^{51}\text{Cr}$  into NiO in the following manner:

- a) an empirical determination of the diffusion coefficient of chromium as a function of the chromium concentration is made from the experimental diffusion profiles,
- b) determination of the dependence of the concentration profiles upon the oxygen activity is made,
- c) the data are fit to a modification of the Lidiard theory to get the bonding energy and diffusion coefficient of the complexes, and the equilibrium concentration of complexes is calculated,
- d) a comparison of the experimental concentration dependence of the chromium diffusion coefficient to the theoretical functional form of the theory is made.

### III. THEORY

When a trivalent cation,  $F^{3+}$ , is dissolved in an MX lattice where M and X are divalent and MX has the NaCl type crystal structure, the  $F^{3+}$  ion occupying an M site possesses a charge of +1 relative to the normally occupied site. In order to maintain electrical neutrality in the crystal, either negatively charged ionic or electronic defects must be created. For the case treated here, the assumption that fully charged cation vacancies are created is made. If the concentration of native defects in the crystal is greatly exceeded by the impurity-created vacancies, the electrical neutrality condition is:

$$C = [F_{\text{tot}}] = [F_M^{\bullet}] = 2 [V_M^{\prime\prime}] \quad (30)$$

where  $V_M^{\prime\prime}$  denotes a vacancy on an M site which has a charge of "minus two" relative to the normally occupied site and  $F_M^{\bullet}$  denotes an F ion on an M site which has a "plus one" charge relative to the normally occupied site.

#### A. Equilibrium and Complexing of $F^{3+}$ in Divalent MX

Because of their opposing electrostatic charges, an attractive coulombic force exists between the cation vacancies and the F ions. An association or complex is said to exist when a cation vacancy and F ion are on nearest neighboring cation sites. Because the charge on a vacancy is "minus two" and the charge on an F ion is "plus one," two simple types

of complexes can exist--one type consists of a vacancy with one F ion on a nearest neighbor cation site which could result in a complex with a "minus one" charge, and the other type consists of a vacancy with two F ions on nearest neighbor sites resulting in an electrostatically neutral complex. These two types of complexes, along with several others which are disregarded because they involve the occupancy of second-nearest-neighbor sites, have been observed by electron spin resonance studied in specimens of chromium-doped NiO at room temperature.<sup>41</sup>

The two types of complexes should exist independently and simultaneously in the lattice; in fact, according to the temperature, an equilibrium concentration for each complex and for free dopants and vacancies exists. The first type of complex--which will hereafter be referred to as the two-member complex--is formed by the reaction:



A vacancy and an impurity ion which are initially unassociated, i.e. at next-nearest-neighbor sites or farther, react to form a two-member complex. Application of the law of mass action, an approach conceived by Stasiw and Teltow<sup>30</sup> and applied by Lidiard<sup>28</sup> to complexes in alkali halides as previously mentioned, yields:

$$K_2(T) = \frac{[(V_M F_M)^\cdot]}{[V_M''] [F_M^\bullet]} \quad (32)$$

where the brackets represent concentrations (moles/cm<sup>3</sup>), and  $K_2(T)$  is a function of temperature only. If at any given temperature in a unit volume there are  $n_2$  impurity ions existing in two-member complexes and  $N_F$  total impurity of dopant ions, Eq. (32) becomes:



$$K_2 (T) = N_c n_2 / (N_F - n_2) (1/2 N_F - n_2) \quad (33)$$

where  $N_c$  is the number of solvent cations, and the revised electrical neutrality condition is:

$$2 [v_M''] + [(v_{N^+M})'] = [F_M'] \neq [F_{tot}] \quad (34)$$

Lidiard has considered the Helmholtz energy ( $F$ ) of an alkali halide crystal which is perfect except for one type of aliovalent cation impurity. By assuming that the vibrational term of  $F$  is independent of the arrangement of the impurities in the lattice, and by considering an impurity content low enough to neglect the mutual interactions of the unassociated charges, Lidiard derived the equilibrium constant given by:

$$K_2 (T) = Z_2 \exp (\Delta G_2^0 / RT) \quad (35)$$

where  $Z_2$  is the number of distinguishable orientations of the complex and  $\Delta G_2^0$  is the Gibbs free energy of association of the complex.  $\Delta G_2^0$  is defined as the work gained at constant temperature and pressure in bringing a vacancy from a distant position to a nearest neighbor site of an impurity ion.

For the NaCl crystal structure of NiO,  $Z_2$  is the number of nearest neighbor cation sites in the nickel sublattice which is 12. The combination of Eqs. (33) and (35) with the result expressed in terms of cation fraction and  $p$ , the degree of association, yields:

$$\frac{p_2}{[F_{tot}] (1 - p_2) (1/2 - p_2)} = 12 \exp (\Delta G_2^0 / RT) \quad (36)$$

where the cation fraction of the chromium impurity is

$$F_{\text{tot}} = N_F/N_c \quad (37)$$

and the degree of association for the two-member complex is defined as

$$p_2 = n_2/N_F \quad (38)$$

The second type of complex – referred to hereafter as the three-member complex – is formed by the reaction:



and again application of the law of mass action states that:

$$K_3 (T) = [(F_M V_M F_M)] / [V_M''] [F_M^{\bullet}]^2 \quad (40)$$

rewriting Eq. (40) in terms of  $N_F$ ,  $N_c$ , and  $n_3$  which is the number of impurity ions existing in three-member complexes gives:

$$K_3 (T) = N_c^2 n_3 / (N_F - n_3)^3 \quad (41)$$

and the electrical neutrality condition is again given by Eq. (30).

Again  $K_3 (T)$  can be shown to be:

$$K_3 (T) = Z_3 \exp (\Delta G_3^{\circ}/RT) \quad (42)$$

where  $\Delta G_3^{\circ}$  is the Gibbs free energy of association for the three-member complex.

There are 66 possible configurations of the three-member complex; however, only 6 of these configurations are linear arrangements which result in a stable electrostatic force distribution. Therefore the assumption is made that the probability of the complex existing in one

of these six stable configurations is much greater than the probability of being in one of the other 60 unstable configurations, and  $Z_3$  is assumed to be approximately six. The combination of Eqs. (41) and (42) with the result expressed in terms of cation fraction and degree of association yields:

$$\frac{p_3}{[F_{\text{tot}}]^2 (1 - p_3)^3} = 6 \exp(\Delta G_3^0/RT) \quad (43)$$

where  $p_3$  is the degree of association of the three-member complexes

$$p_3 = \frac{n_3}{N_F} = \frac{2 [(F_M V_M F_M)]}{[F_{\text{tot}}]^3} \quad (44)$$

The two types of complexes have been considered to be independent, but in a real lattice the formation of the two types will be inter-related at most temperatures. From consideration of only the coulombic forces between the vacancies and impurities, the enthalpy of formation of the three-member complex is slightly less than twice the enthalpy of formation of the two-member complex. Because polarization and short-range, closed-shell interactions are not considered but may increase the enthalpy of formation of the three-member complex relative to the two-member,  $\Delta G_2^0$  is assumed to be approximately  $1/2 \Delta G_3^0$ . Then at very low temperatures the three-member complexes should predominate. At higher temperatures the two-member complexes should predominate because the entropy contribution tends to dissociate (randomize) complexes. On this basis, the following four zones would be expected in a plot of  $p_2$  and  $p_3$

as a function of increasing temperature at a given impurity concentration: (1) Zone I – all the vacancies are in three-member complexes; (2) Zone II – all vacancies are either in three- or two-member complexes; (3) Zone III – vacancies exist in two and three-member complexes but also unassociated; (4) Zone IV – vacancies exist in two-member complexes and unassociated.

In Zone I, the degree of association of three-member complexes, which is obtained directly by solving the cubic equation for  $p_3$  which results from Eq. (43), is given by:

$$p_3 = 1 + \left\{ -\frac{1}{2X} + \left( \frac{1}{4X^2} + \frac{1}{27X^3} \right)^{1/2} \right\}^{1/3} + \left\{ -\frac{1}{2X} - \left( \frac{1}{4X^2} + \frac{1}{27X^3} \right)^{1/2} \right\}^{1/3} \quad (45)$$

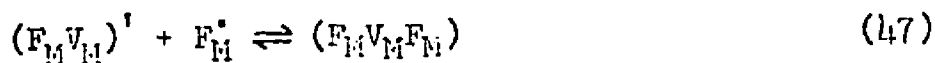
where

$$X = Z_3 [F_{\text{tot}}]^2 \exp(\Delta G_3^0/RT) \quad (46)$$

Zone I will occur only at very low temperatures where  $X$  will be very large. The degree of association of the three-member complexes will therefore be essentially equal to one throughout Zone I, and no two-member complexes will be present.

As the temperature is increased the three-member complexes will be broken up by thermal vibrations, and both two- and three-member complexes will coexist along with unassociated impurity ions. The coexist-

ence reaction is:



The law of mass action yields:

$$K_{II}(T) = \frac{1/2 p_3}{(1 - p_3 - p_2) (p_2) [F_{tot}]} \quad (48)$$

and the temperature dependence of  $K_{II}(T)$  is:

$$K_{II}(T) = \frac{K_3(T)}{K_2(T)} = \frac{Z_3}{Z_2} \exp(\Delta G_3^0/2RT) \quad (49)$$

The degree of association of the two- and three-member complexes is obtained by solving two simultaneous equations. The first equation which is obtained by combining Eqs. (48) and (49) is:

$$p_2 = -\frac{p_3}{2} + \frac{1}{2} \pm \left( \frac{p_3^2}{4} - \frac{p_3}{2} + \frac{1}{4} - \frac{p_3}{2Y} \right)^{1/2} \quad (50)$$

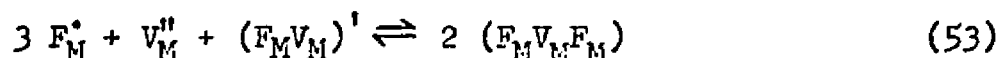
where

$$Y = \frac{Z_3}{Z_2} [F_{tot}] \exp(\Delta G_3^0/2RT) \quad (51)$$

The second equation which arises from the fact that all of the vacancies are assumed to be in complexes is:

$$p_3 + 2p_2 = 1 \quad (52)$$

Eqs. (50) and (51) define the degree of association in Zone II, but as the temperature is further increased the thermal vibrations will also break up the two-member complexes so that two-member complexes, three-member complexes, unassociated vacancies, and unassociated impurities will all be present in the lattice. The coexistence reaction for this system is:



The application of the law of mass action for this reaction yields:

$$K_{III}(T) = \frac{(1/2 p_3)^2}{[F_{tot}]^3 (1 - p_3 - p_2)^3 (1/2 - 1/2 p_3 - p_2) (p_2)} \quad (54)$$

and the temperature dependence of  $K_{III}(T)$  is given by:

$$K_{III}(T) = K_3(T) \cdot K_{II}(T) = \frac{Z_3^2}{Z_2} \exp(+3\Delta G_3^0/2RT) \quad (55)$$

In this zone,  $p_2$  will generally be from one to two orders of magnitude greater than  $p_3$ . Because the two-member complexes predominate,  $p_2$  is calculated from Eq. (56) given for Zone IV, and  $p_3$  is calculated by equating Eq. (54) to Eq. (55). This calculation then yields only approximate values of  $p_2$  and  $p_3$ , but the approximation is very good when  $p_2 \gg p_3$ .

As the temperature becomes very high the number of three-

member complexes becomes very small, and in Zone IV the assumption is made that only two-member complexes exist. The degree of association of the two-member complexes, which is obtained directly from Eq. (36), is given by:

$$p_2 = \frac{3}{4} + \frac{1}{2V} - \left( \frac{1}{16} + \frac{3}{4V} + \frac{1}{4V^2} \right)^{1/2} \quad (56)$$

where

$$V = Z_2 [F_{\text{tot}}] \exp ( \Delta G_3^0 / 2RT ) \quad (57)$$

From Eqs. (45), (50) and (56) the degree of association of two- and three-member complexes can be calculated and plotted as a function temperature at a given impurity concentration. In Figs. 3-6 the degree of association is plotted versus  $RT / \Delta G_3^0$  for increasing impurity concentration. The four zones are indicated by the vertical dashed lines. The dashed lines to the zone boundaries represent the actual solutions to the appropriate equations for each zone, but the discontinuities at the zone boundaries must be removed. The transition from one zone to another was obtained by visually smoothing the curves so the solid lines represents the degrees of association as a function of temperature as a smooth curve. The maximum for  $p_2$  moved to higher temperatures as the concentration increased, and at temperatures above the maximum, the two-member complexes predominate. At low temperatures the three-member complexes predominate but decrease rapidly as the temperature increases in Zone II.

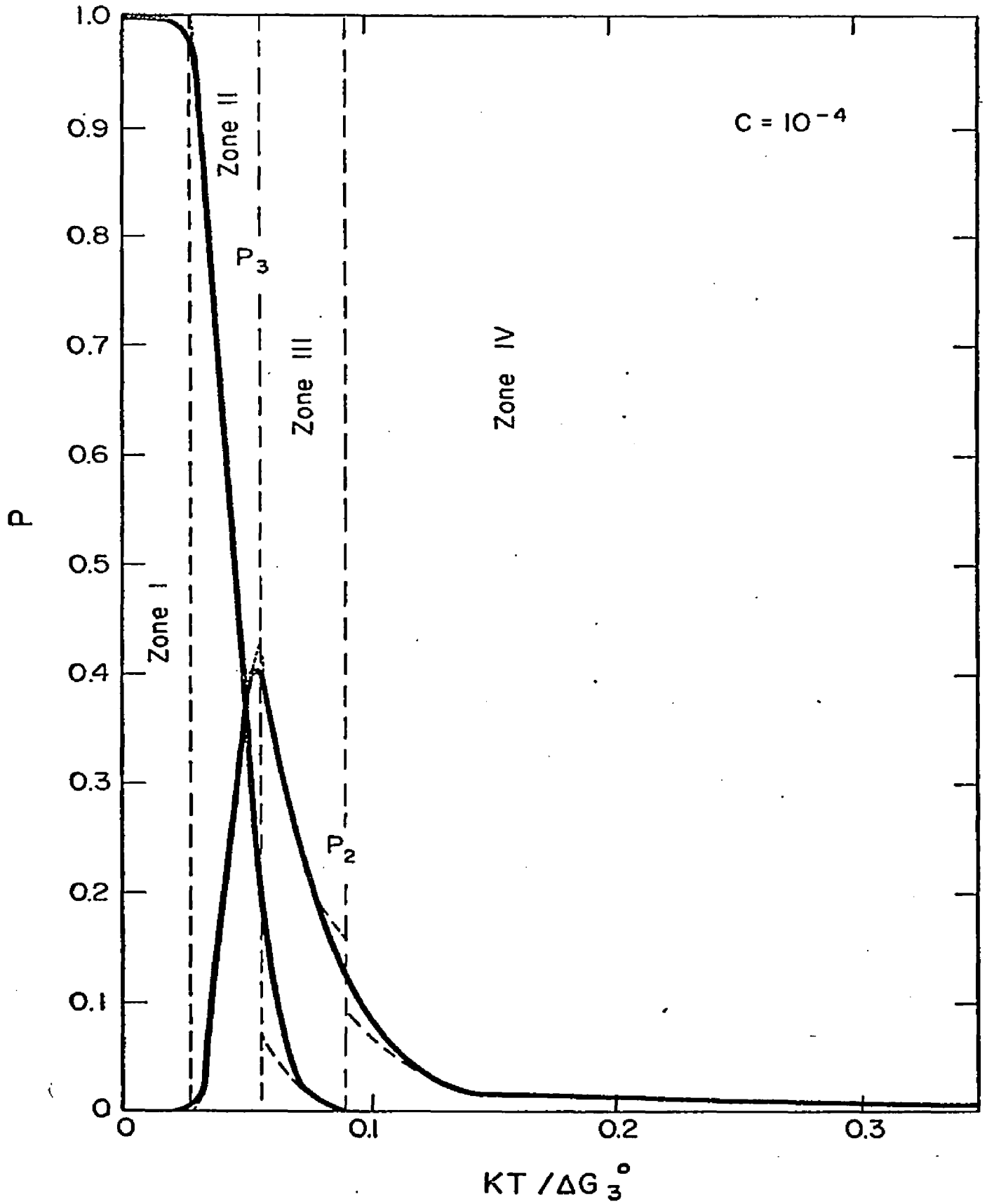


Fig. 3.--Degree of Association as a Function of  $RT/\Delta G_3^{\circ}$  for  $[F_{TOT}] = 10^{-4}$  Cation Fraction.



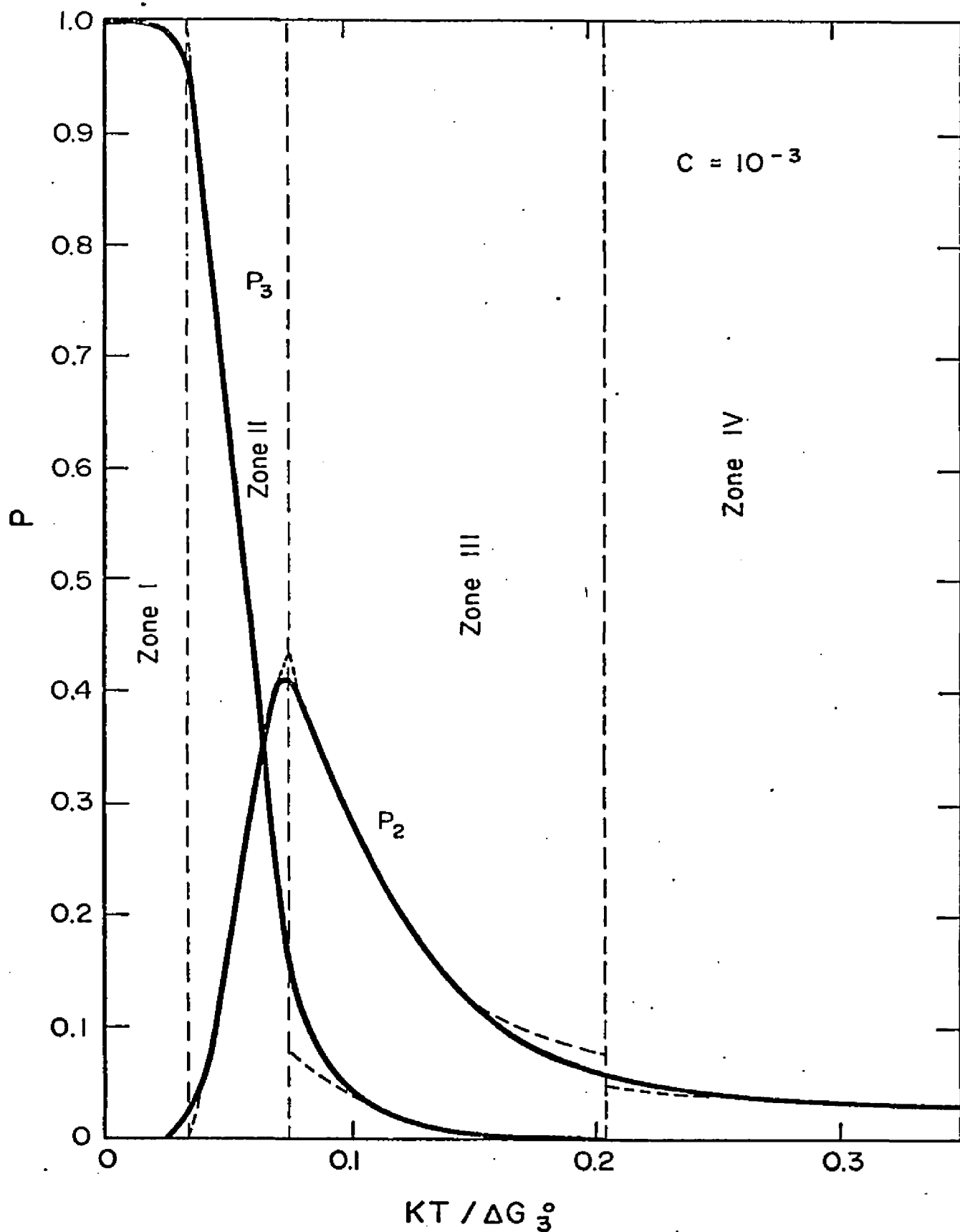


Fig. 4. --- Degree of Association as a Function of  $RT/\Delta G_3^0$  for  $[F_{TOT}] = 10^{-3}$  Cation Fraction.

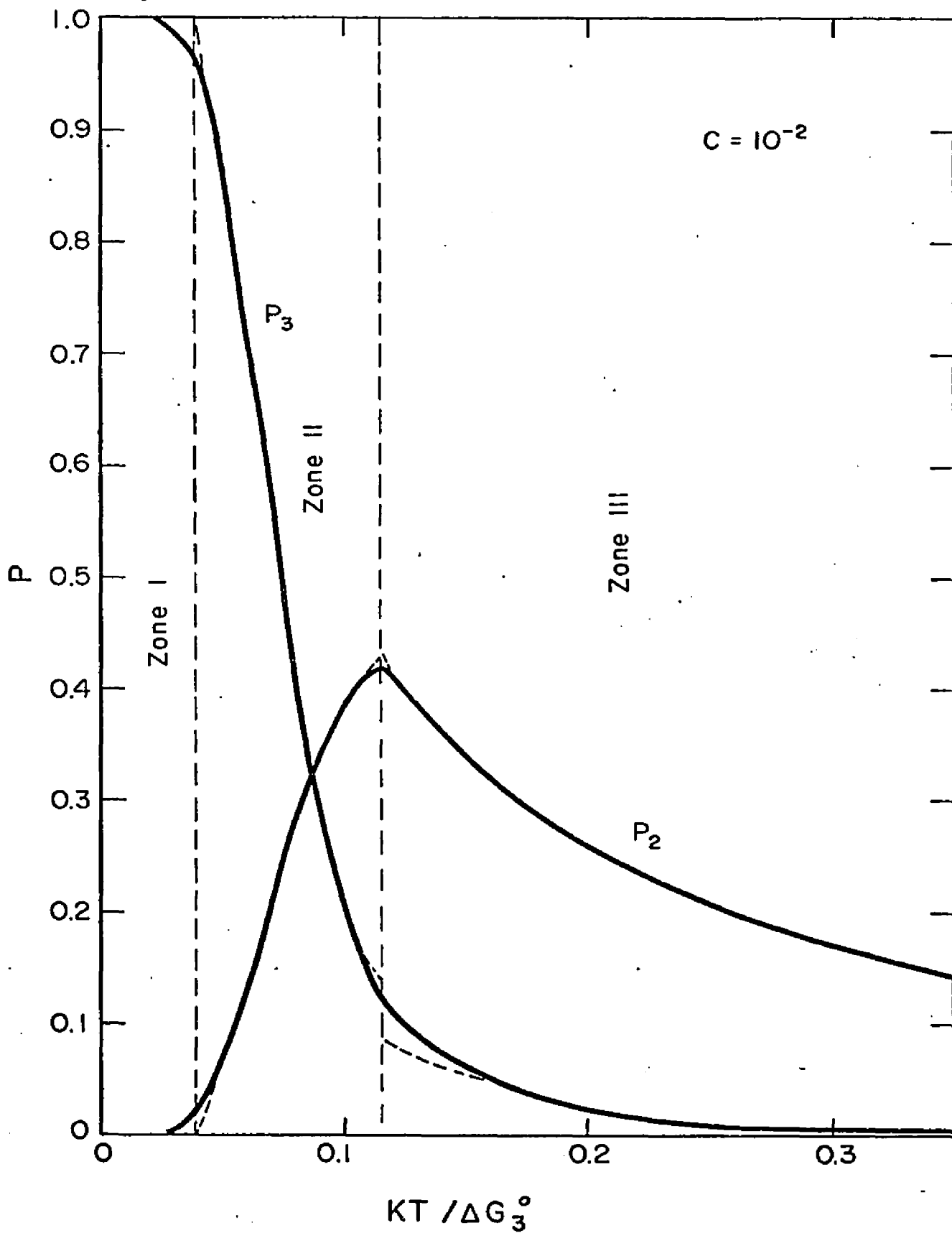


Fig. 5.--Degree of Association as a Function of  $KT/\Delta G_3^{\circ}$  for  $[F_{TOT}] = 10^{-2}$  Cation Fraction.

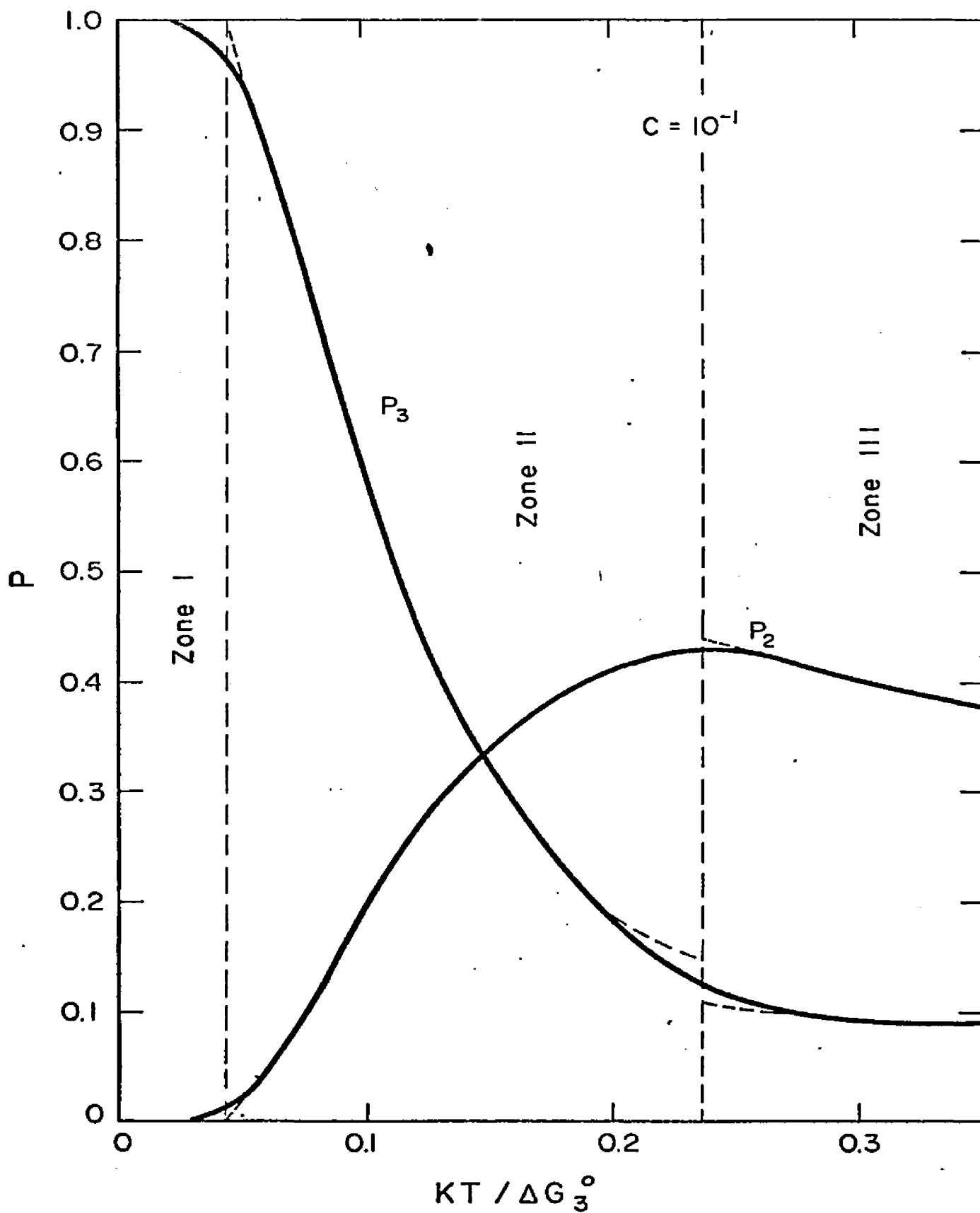


Fig. 6.--Degree of Association as a Function of  $RT/\Delta G_3^{\circ}$  for  $[F_{TOT}] = 10^{-1}$  Cation Fraction.

### B. Diffusion of Aliovalent Impurities

As previously discussed Lidiard has shown that the diffusion coefficient of a divalent impurity in an alkali halide is:

$$D_F = D_0 \frac{dp_c}{dc} \quad (58)$$

This result applies to only two-member complexes and therefore describes the diffusion in Zone IV for the trivalent impurity in a divalent MX lattice. In the other zones, both two- and three-member complexes are present, and the diffusion coefficient becomes:

$$D_F = D_0 (3) \frac{dp_3^c}{dc} + D_0 (2) \frac{dp_2^c}{dc} \quad (59)$$

In order to evaluate  $D_F$ , the diffusion coefficients of the complexes,  $D_0 (3)$  and  $D_0 (2)$ , must be obtained.

As given by Lidiard, the diffusion coefficient for the two-member complex is given by:

$$D_0 (2) = (1/6) T r^2 f \quad (60)$$

where  $T$  is the number vacancy-impurity exchanges per unit time,  $r$  is the jump distance and  $f$  is the correlation factor. Because  $r$  is  $\sqrt{2}a$  where  $a$  is the MX lattice parameter,  $T$  is  $\omega_2$  and the correlation factor is  $\omega_1/\omega_1 + \omega_2$ , Eq. (60) then becomes:

$$D_0 (2) = \frac{a^2}{3} \left( \frac{\omega_1 \omega_2}{\omega_1 + \omega_2} \right) \quad (61)$$

If the ionic radii of  $F^{3+}$  and  $M^{2+}$  are nearly similar, the trivalent charge of the F impurity would cause the potential energy barrier for an  $F-V_M$  jump to be greater than for an  $M-V_M$  jump; therefore,  $\omega_2 \ll \omega_1$ , and Eq. (61) reduces to:

$$D_0 (2) = \frac{a^2}{3} \omega_2 \quad (62)$$

The diffusion of a three-member complex is a more difficult process. For the complex to travel in the lattice, the vacancy would have to follow a cycle similar to that depicted in Fig. 7. The plane of the paper corresponds to a close-packed  $\{111\}$  plane of the M sublattice. For this diffusion sequence, the three-member complex is considered to exist when one of the F impurities is on a nearest neighbor site of the M vacancy and the other F impurity is at least on a fourth nearest neighbor site of the M vacancy. The cycle in Fig. 7 could be divided into two steps, from a) through d) and from e) through h). These two partial steps are similar to the diffusion of two-member complexes; however, the jump frequencies will vary greatly for the jumps in a), d) and e), so no comparison of the diffusion coefficients for the two complexes seems possible. The assumption that the correlation factor for the three-member complex is roughly the square of the correlation factor of the two-member complex can be made because the three-member complex movement can be divided into the successive movement of two member complexes. Eq. (59) then becomes:

$$D_F = \frac{\omega_1}{\omega_1 + \omega_2} \left( \frac{a^2}{3} \omega_2 \frac{dp_2^c}{dc} + D_0' (3) \frac{\omega_1}{\omega_1 + \omega_2} \frac{dp_3^c}{dc} \right) \quad (63)$$

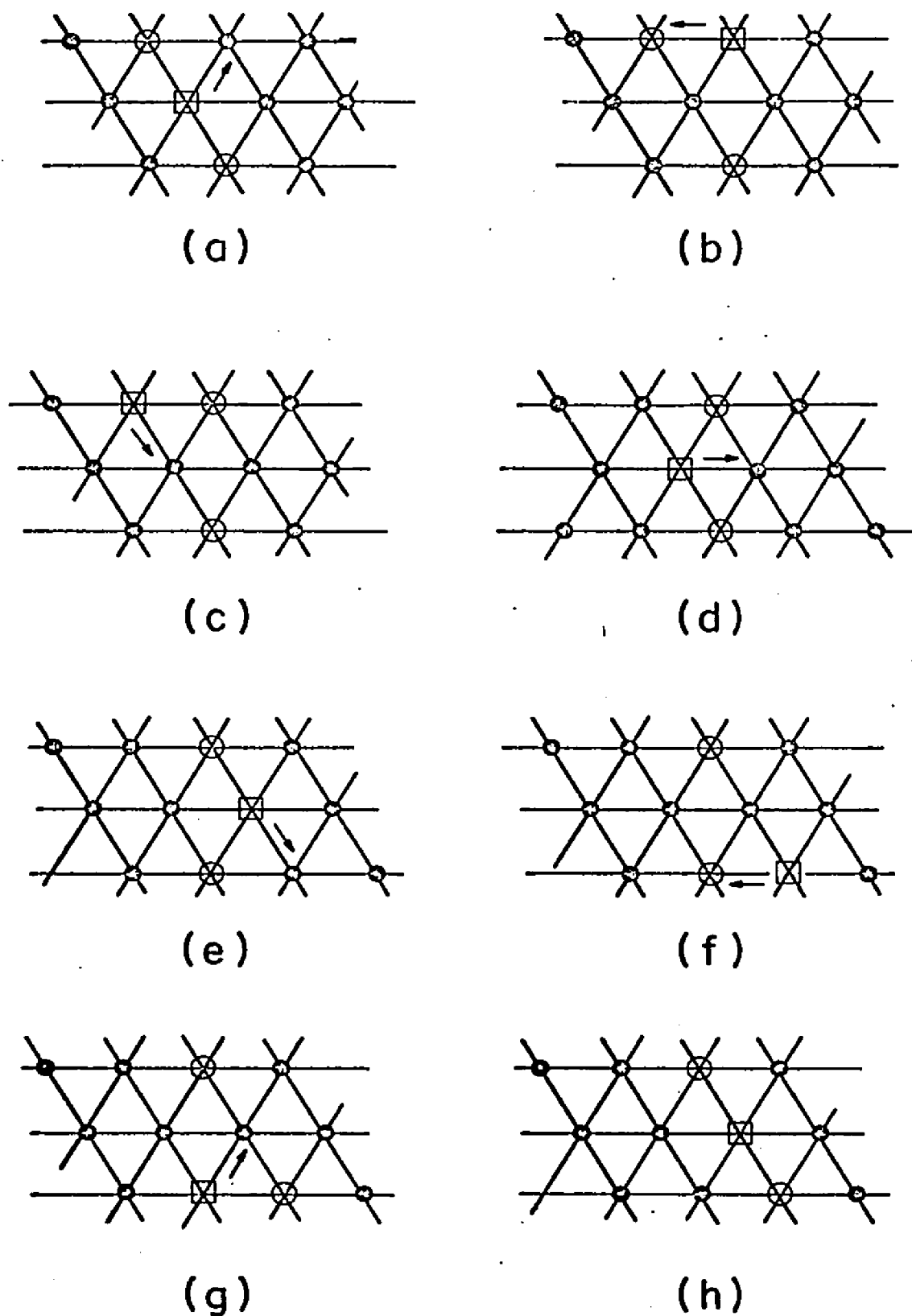


Fig. 7.--Schematic Diagram of the Jump Order for Diffusion of a Three-member Complex.

where  $D_0'$  (3) is the diffusion coefficient of the three-member complexes with the correlation factor removed. When  $\omega_2 \gg \omega_1$ , the contribution of the three-member complexes will be extremely small compared to that of the two member complexes. When  $\omega_2 \ll \omega_1$ , which is the expected case, both types of complexes may contribute to the impurity diffusion.

In Eq. (63) the concentration dependence of  $D_F$  is contained entirely in  $dp_2c/dc$  and  $dp_3c/dc$  because  $\omega_1$  and  $\omega_2$  should not vary with the impurity concentration. Therefore the evaluation of these gradients becomes necessary. In Table 2 the number of complexes are tabulated as a function of impurity concentration at constant temperature. The values of  $p_2$  and  $p_3$  used in the table were taken from the curves in Figs. 3-6. From the data in Table 2, a divided difference table for  $p_2c$  and  $p_3c$  as a function of  $c$  at constant temperature can be created, and the calculation of  $dp_2c/dc$  and  $dp_3c/dc$  is then possible using the derivative of the Newton formula for divided differences<sup>43</sup>. An analytical solution for  $dp_2c/dc$  or  $dp_3c/dc$  is possible only when one type of complex is present in the crystal. At low temperatures  $dp_3c/dc$  may be described analytically. The concentration dependence of  $D_F$  can now be determined from the concentration dependence of  $dp_2c/dc$  and  $dp_3c/dc$ .

In Figs. 8-11,  $dp_2c/dc$  and  $dp_3c/dc$  are plotted as a function of concentration from the results of the divided difference table at several temperatures. If the three-member complexes predominate, at low temperatures  $D_F$  would rapidly approach a constant value,  $D_0$  (3), as concentration increases. At higher temperatures,  $D_F$  would increase approximately linearly with the concentration. If the two-member complexes predominate, at low temperatures  $D_F$  would increase rapidly to a maximum

TABLE 2.--Concentration of Two- and Three-member Complexes as a Function of Temperature and Impurity Concentration

Conc (cat frac)	$RT/\Delta G_3^0 = 0.05$		$RT/\Delta G_3^0 = 0.1$	
	$p_2^c$ ( $10^{-4}$ cat frac)	$p_3^c$ ( $10^{-4}$ cat frac)	$p_2^c$ ( $10^{-4}$ cat frac)	$p_3^c$ ( $10^{-4}$ cat frac)
$10^{-4}$	0.37	0.283	0.071	0.001
$5 \times 10^{-4}$	1.12	2.75	1.035	0.055
$10^{-3}$	1.7	6.58	2.81	0.30
$5 \times 10^{-3}$	4.25	41.0	20.4	6.80
$10^{-2}$	7.0	85.0	38.8	22.3
$10^{-1}$	22.0	956	201	598
.15	23.2	1440	258	985

Conc (cat frac)	$RT/\Delta G_3^0 = 0.2$		$RT/\Delta G_3^0 = 0.3$	
	$p_2^c$ ( $10^{-4}$ cat frac)	$p_3^c$ ( $10^{-4}$ cat frac)	$p_2^c$ ( $10^{-4}$ cat frac)	$p_3^c$ ( $10^{-4}$ cat frac)
$10^{-4}$	$7.1 \times 10^{-3}$	$9.1 \times 10^{-6}$	$3.2 \times 10^{-3}$	$1.6 \times 10^{-6}$
$5 \times 10^{-4}$	0.165	0.001	0.076	$1.95 \times 10^{-4}$
$10^{-3}$	0.60	0.007	0.29	$1.5 \times 10^{-3}$
$5 \times 10^{-3}$	9.30	0.425	5.50	0.128
$10^{-2}$	25.9	1.90	14.8	0.69
$10^{-1}$	402	190	397	39.1
.15	560	381	637	153



and then decrease. At higher temperatures, the maximum would gradually disappear, and  $D_F$  would increase with concentration and approach  $1/2 D_0$  (2) asymptotically. The limit is  $1/2 D_0$  (2) because only half of the impurity ions in the crystal can be associated with the vacancies when all the vacancies exist in two-member complexes.

As shown in Fig. 7 the series of jumps necessary for the diffusion of a three-member complex is very restrictive. If  $\omega_2 \gg \omega_1$  the contribution of three-member complexes has been shown to be very small from consideration of its correlation factor. In the expected case,  $\omega_2 \ll \omega_1$  the vacancy will move rapidly around the impurities and the correlation factor is nearly one. Since the vacancy can move about the impurities, the probability of the impurities making the correct jumps is approximately  $1/6$  for each impurity jump in Fig. 7 while the probability of the impurities making a jump which would dissociate the complex is approximately  $1/2$  for each impurity jump. Therefore the probability that the complex would dissociate and diffuse as a two-member complex is greater than the probability that the three-member complex will diffuse as a stable unit. Therefore the contribution of the three-member complexes to the diffusion of the impurity is again very small, and the concentration dependence of  $D_F$  would be similar to that attributed to  $dp_2c/dc$ , neglecting the diffusion of three-member complexes.

There are two limiting cases for  $D_F$ . The first case is for very low temperatures where complete association occurs and only three-member complexes are assumed to be present. By differentiating Eq. (43) and applying the condition  $[F_{tot}]^2 \exp(-\Delta G_3^0/RT) \gg 1$ , the limiting condition  $dp_3c/dc = 1$  is obtained. Therefore, the diffusion coefficient

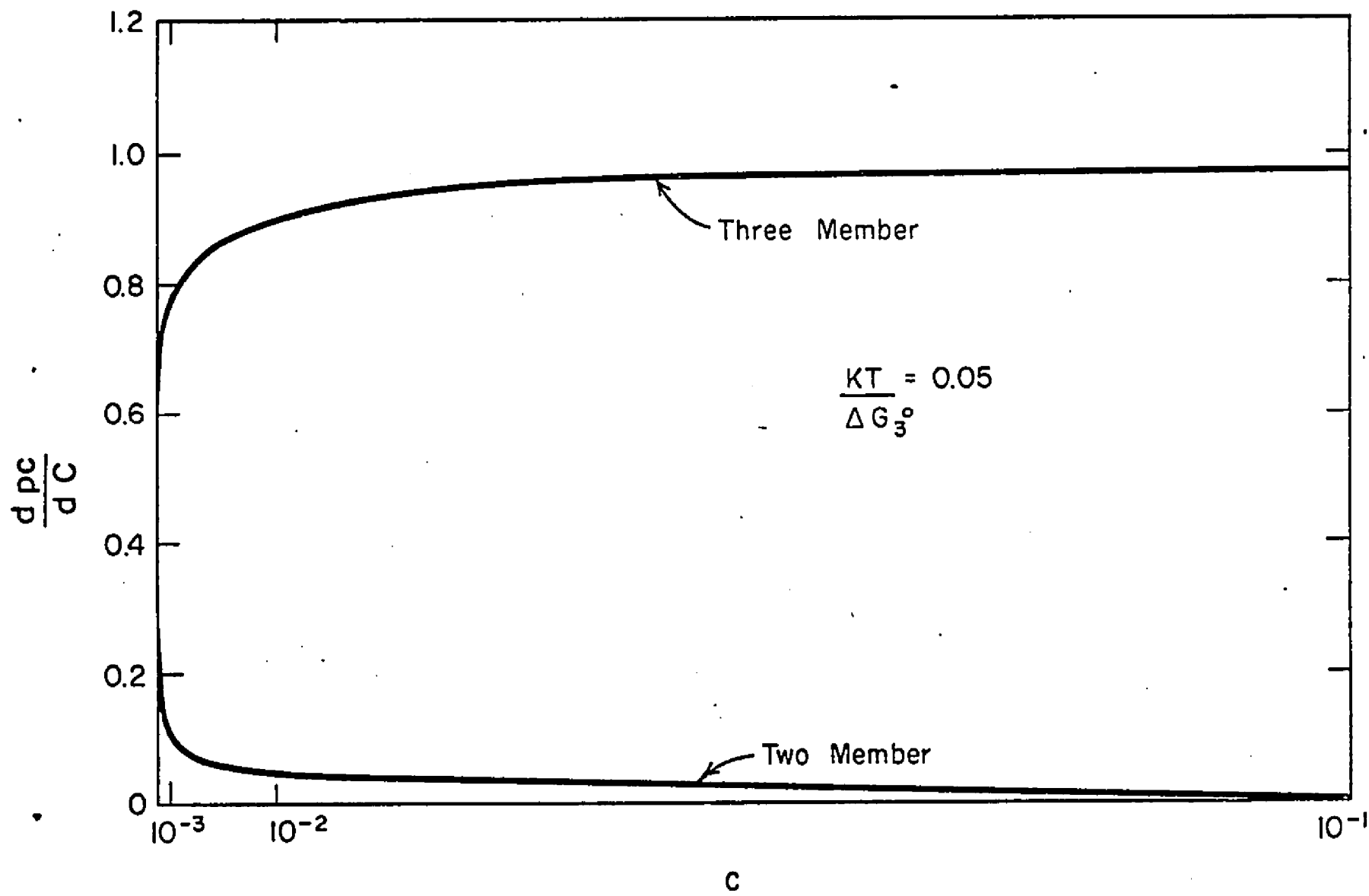


Fig. 8.--Concentration Dependence of the Impurity Diffusion Coefficient from the Impurity-Vacancy Complexes for  $RT/\Delta G_3^0 = 0.05$ .

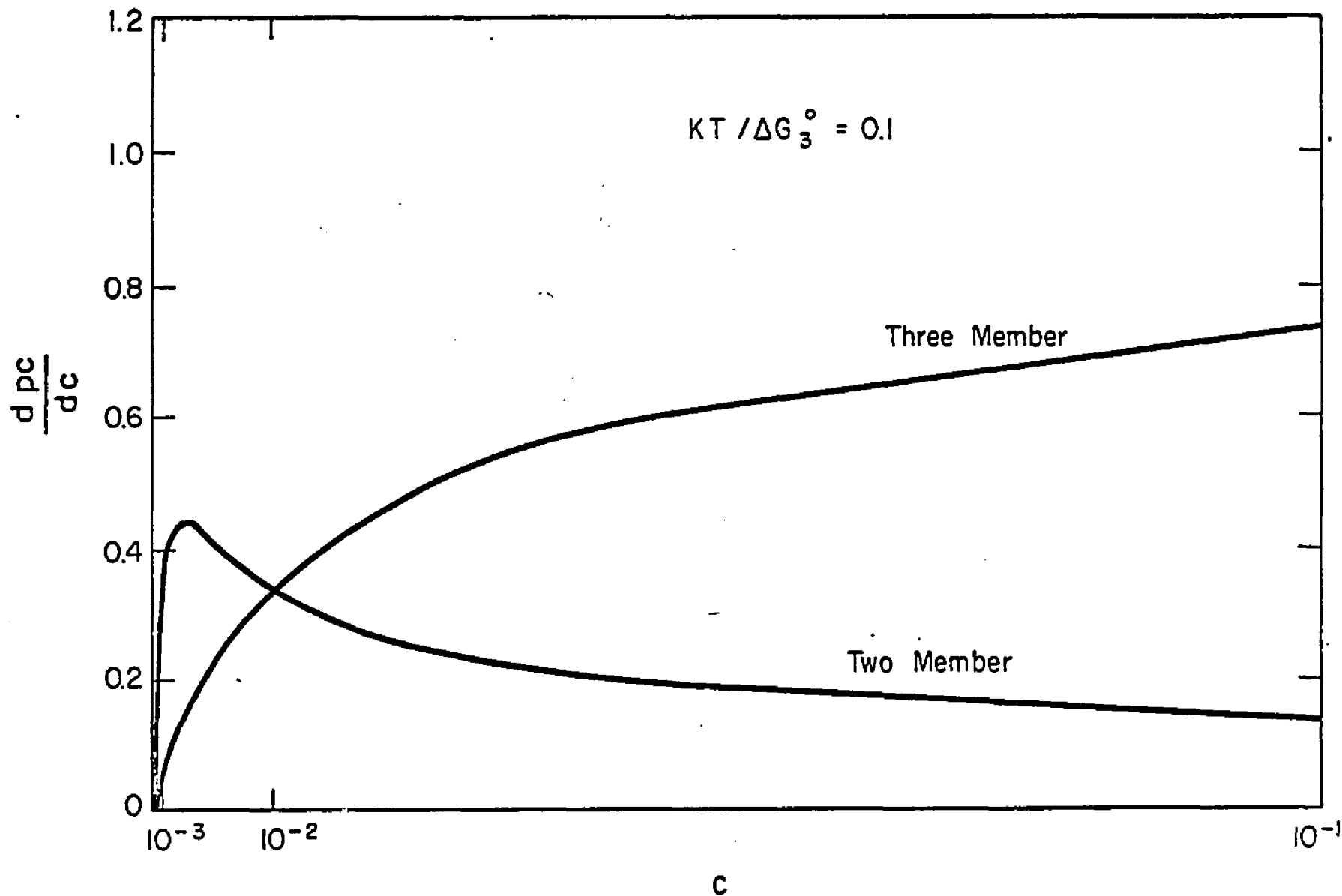


Fig. 9.--Concentration Dependence of the Impurity Diffusion Coefficient from the Impurity-Vacancy Complexes for  $RT/\Delta G_3^0 = 0.1$ .

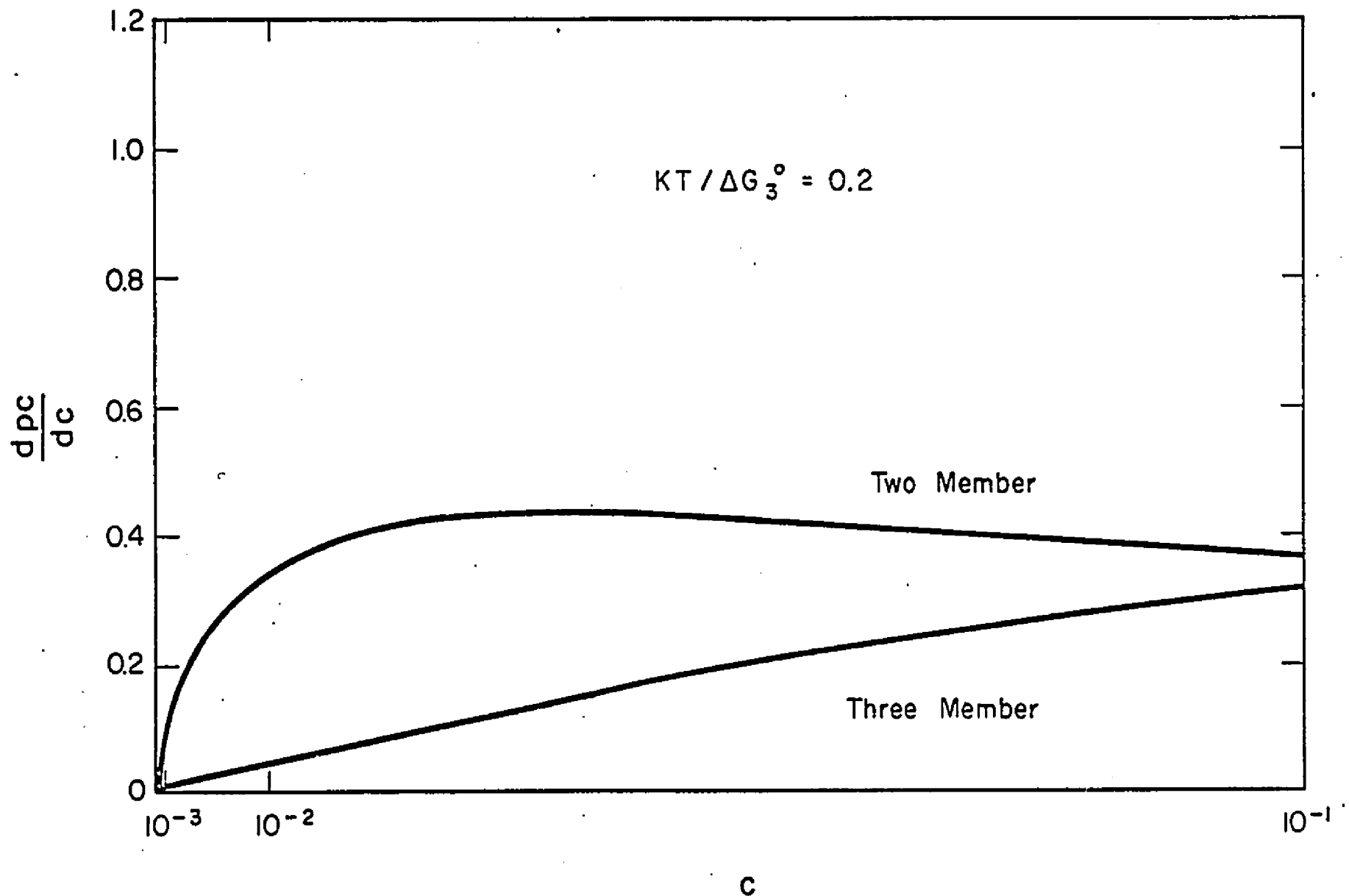


Fig. 10.--Concentration Dependence of the Impurity Diffusion Coefficient from the Impurity-Vacancy Complexes for  $RT/\Delta G_3^0 = 0.2$ .

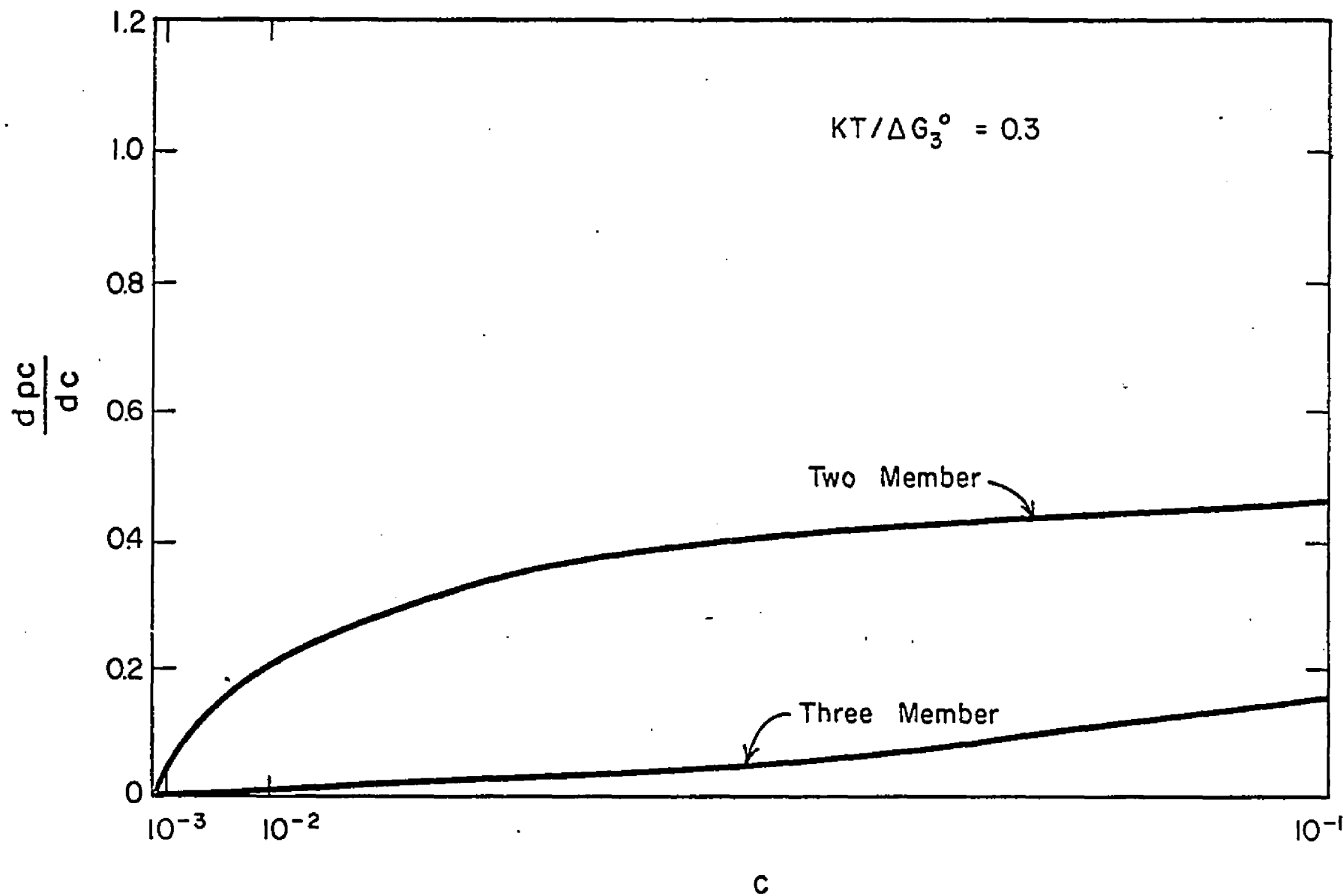


Fig. 11.--Concentration Dependence of the Impurity Diffusion Coefficient from the Impurity-Vacancy Complexes at  $RT/\Delta G_3^0 = 0.3$ .

at low temperatures should be constant and equal to the diffusion coefficient of the three-member complex, such that:

$$D_F = \left( \frac{\omega_1}{\omega_1 + \omega_2} \right)^2 D_0' \quad (64)$$

which is expected to be very small. The other limiting case holds for high temperatures where essentially all the three-member complexes are dissociated, and only two-member complexes along with unassociated impurities and vacancies exist. In this case the degree of complexing is very low. By differentiating Eq. (56) and applying the condition that  $[F_{\text{tot}}] \exp(\Delta G_3^0/2RT) \ll 1$ , the limiting condition is:

$$\frac{dp_2^c}{dc} = \left( \frac{3}{2} + (Z_2 [F_{\text{tot}}] \exp(\Delta G_3^0/2RT))^{-1} \right)^{-1} \quad (65)$$

Insertion of this limit into Eq. (63) yields:

$$D_F = \frac{a^2}{3} \left( \frac{\omega_1 \omega_2}{\omega_1 + \omega_2} \right) \left\{ \frac{3}{2} + (Z_2 [F_{\text{tot}}] \exp(\Delta G_3^0/2RT))^{-1} \right\}^{-1} \quad (66)$$

in which  $D_F$  is approximately proportional to the impurity concentration.

### C. Application to Chromium Diffusion in NiO

Chromium ions dissolved in the NiO lattice are trivalent and occupy nickel lattice sites.<sup>7,38,44</sup> Therefore, the chromium ions possess a charge of "plus one" relative to the normally occupied site. In order to maintain electrical neutrality in the crystal, either negatively

charged ionic or electronic defects must be created. Meier and Rapp<sup>23</sup> have shown that the compensating defects in Cr-doped NiO are cation vacancies which are doubly charged. The concentration of native cation vacancies, i.e., the equilibrium concentration in absolutely pure NiO, is relatively low as shown in Table 1, so that the concentration of cation vacancies created by the presence of trivalent chromium greatly exceeds the native vacancy concentration and essentially establishes the total vacancy concentration. The simplified electrical neutrality condition is then:

$$2 [V_{Ni}^{''}] = [Cr_{Ni}^{\cdot}] = [Cr_{tot}] \quad (67)$$

The defect structure of Cr-doped NiO conforms to the hypothetical model for dopant diffusion which was discussed. Therefore the diffusion coefficient for the diffusion of chromium in NiO should be described by Eq. (63) with the same limits and concentration dependence.

#### IV. EXPERIMENTAL MATERIALS AND PROCEDURE

##### A. Sample preparation

To study the concentration-dependent diffusion of chromium into NiO, for the diffusion anneals a pill of NiO saturated  $\text{NiCr}_2\text{O}_4$  spinel was placed on either side of a disc-shaped single crystal of NiO. The diffusion of chromium from the spinel into the NiO was measured by the use of a radioactive tracer-sectioning-counting technique.

The sintered, compacted powder, spinel pills were made from  $\text{Cr}_2\text{O}_3$  and NiO of 99.5% and 99.995% purity, respectively, obtained from Leico Industries, Incorporated. The  $\text{Cr}_2\text{O}_3$  was irradiated at the Battelle Memorial Research Reactor (West Jefferson, Ohio) to create radioactive  $^{51}\text{Cr}$  from  $^{50}\text{Cr}$  by neutron capture. The  $^{51}\text{Cr}$  decays by electron capture causing the emission of gamma rays and has a half-life of 27.8 days. The irradiated  $\text{Cr}_2\text{O}_3$  was then mixed with NiO in the correct proportions to form upon sintering one gram pellets of  $\text{NiCr}_2\text{O}_4$  with 5% excess NiO. The NiO +  $\text{Cr}_2\text{O}_3$  powder was ground by pestle and mortar and mixed in a 5 ml. polyethylene container rotating at 20 rpm for 18 hours. The powder was reground and then cold-pressed into discs 1/2 inch in diameter and about 1/8 inch thick under a load of 3000 pounds. The cold-pressed pills were placed in a bed of NiO +  $\text{Cr}_2\text{O}_3$  powder of the same composition in a stabilized-zirconia boat and sintered at 1200°C for two days in air. The surfaces of the pills were prepared for the diffusion anneal by hand polishing on successively finer emery paper using 0, 2/0,



3/0 and 4/0 grades of paper.

The single crystal discs were cleaved from two NiO boules purchased from Marubeni-Iida, Incorporated.\* The crystals were grown by a flame-fusion technique in an oxidizing atmosphere. The results of an optical emission spectrographic analysis of a disc from each crystal are given in Table 3. The analyses were performed at Battelle Memorial Institute, and the discs were annealed at  $1200^{\circ}\text{C}$  and  $P_{\text{O}_2} = 1.0$  atm for 24 hours before the analysis was made. The crystals are fairly pure with the major impurities being magnesium and calcium which are divalent and would not affect the native vacancy concentration. Nickelous oxide has the rock salt crystal structure and cleaves easily along the  $\{100\}$  planes. The boules were cleaved into discs along the  $\{100\}$  planes perpendicular to the cylindrical axis of the boules with a hardened tool steel cleaving tool 2 1/2 inches long and 1/4 inch square with one end ground to form a  $15^{\circ}$  wedge. The tool was placed on the boule at the desired position and lightly tapped. The discs were cleaved into smaller pieces as desired by a light tap on a razor blade held against the crystal. The crystals were polished with 1 through 4/0 emery paper and then with 0.3 micron alumina powder by a Syntron vibratory polishing machine to an optical finish. Each crystal was annealed for 24 hours at the temperature and oxygen pressure intended for its subsequent diffusion anneal and then repolished.

#### B. Pressure Calibration

Two types of apparatus were used to make the diffusion anneals.

---

\*Marubeni-Iida, Incorporated, Osaka, Japan

TABLE 3.--Results of the Spectrographic Analysis of the NiO Single Crystals

Impurity	Crystal #1 (ppmw)	Crystal #2 (ppmw)
Fe	20	10 <sup>T</sup>
Mg	70	300
Si	10 <sup>T</sup>	10 <sup>T</sup>
Cu	5	5 <sup>T</sup>
Co	10	10
Ca	7	3
Al	10 <sup>N</sup>	10 <sup>N</sup>
Cr	10 <sup>N</sup>	10 <sup>N</sup>
Mn	10 <sup>N</sup>	10 <sup>N</sup>

T = trace

N = not detected

The apparatus shown in Fig.12 was used for anneals at one atmosphere of oxygen. A non-inductively wound Marshall, Pt-40% Rh furnace was used in conjunction with a Wheelco on-off type temperature controller. A variable transformer provided power to the controller, and a shunt resistor was connected to the controller. An oscillator which superimposed a sine wave-type voltage with an amplitude of approximately 10 millivolts and a period of approximately 1/4 seconds upon the voltage measured by the thermocouple was connected in series with the thermocouple. This arrangement minimized the dead band of the controller so that the relay

Figure 12 Legend

- A Thermocouple leads
- B Mullite furnace tube
- C Liquid nitrogen cold trap
- D Bubblers

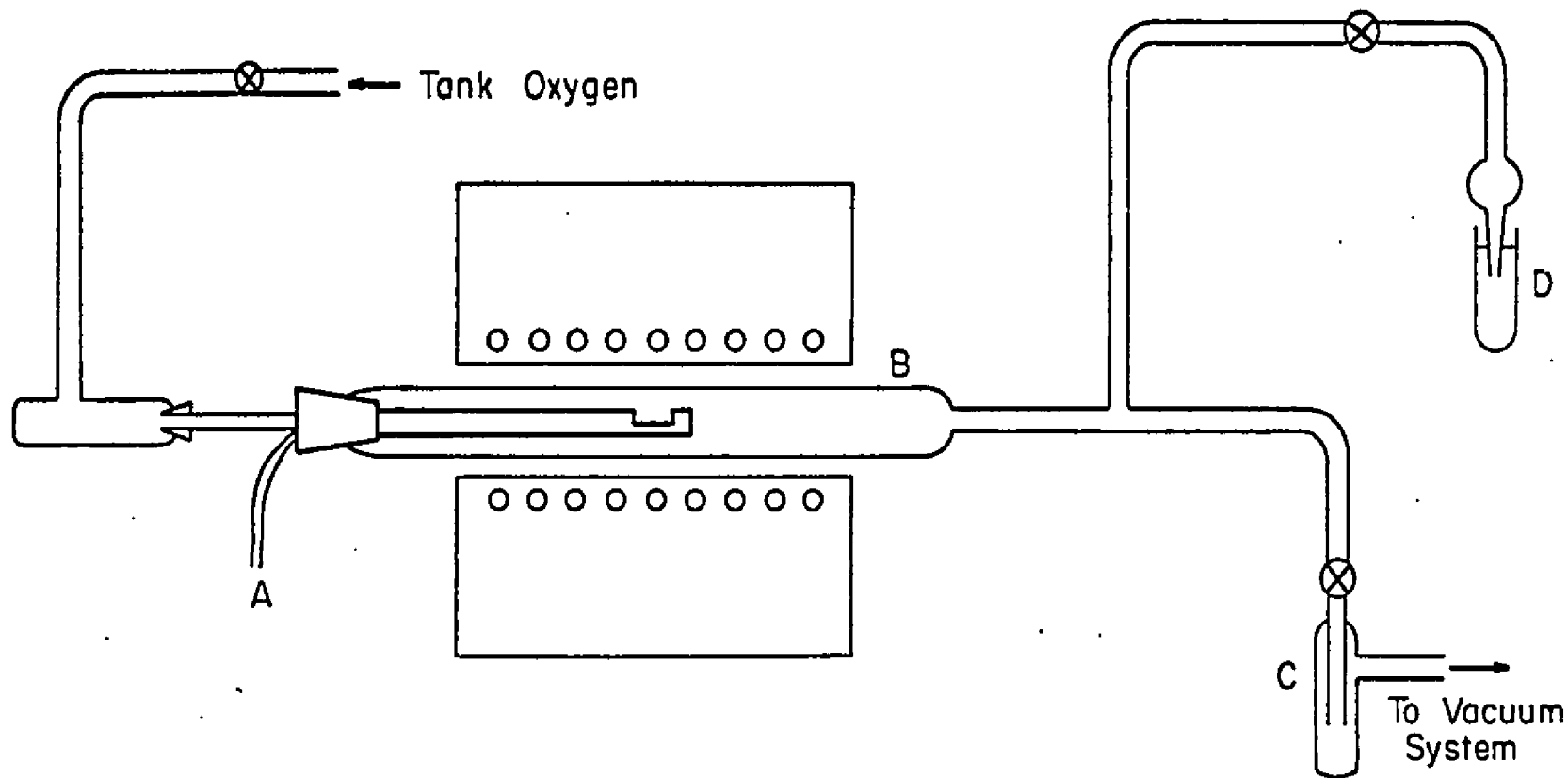


Fig. 12.--Schematic Illustration of the Apparatus Used to Perform the Diffusion Anneals at  $P_{O_2} = 1.0$ .

to the furnace opened and closed with approximately the same frequency as the oscillator and maintained the temperature within  $\pm 1.0^{\circ}\text{C}$  of the desired temperature. An impervious mullite tube was placed through the furnace. One end of the tube was closed with a pyrex cap connected to the tube by a pyrex-to-mullite seal, and the other end was connected to a brass adaptor with epoxy cement. The samples were held in the furnace in an alumina tube as shown in Fig. 13. The tube was connected to a brass holding jig by springs, and an alumina pushrod held the pills together and caused the pressure of the springs to be exerted on the pills to create good surface contact. The brass jig formed a vacuum tight seal by fitting into the brass adaptor on the end of the furnace tube.

To obtain the desired oxygen pressure of 1.0 atmosphere, the system was evacuated using a Welsh duo-seal mechanical pump and filled with oxygen three times. The vacuum pump was then shut out of the system, and oxygen was bubbled off at the ambient pressure.

The apparatus shown in Fig. 14 was used for anneals run at oxygen pressures of  $10^{-2}$  and lower. The temperature was controlled as previously described. An impervious, closed-end, calcia-stabilized zirconia tube was placed half way into the furnace, and a pyrex standard taper joint was connected to the open end of the tube with epoxy cement. The samples were held as previously described with the exception that the pushrod was a closed-end, calcia-stabilized zirconia tube.

The oxygen pressure in the system was controlled and measured with the two calcia-stabilized zirconia tubes. At high temperatures and oxygen pressures, the electrical conductivity in calcia-stabilized zirconia results primarily from the migration of oxygen ions through

### Figure 13 Legend

- A Adjustable brass plunger
- B Stupakoff Vacuum seal
- C Brass adaptor machined to standard taper 3/4/45 joint
- D Epoxy glass-to-mullite seal
- E Intervious mullite furnace tube
- F Alumina holder tube
- G Alumina pushrod
- H Alumina plates
- I NiO single crystal
- J  $\text{NiCr}_2\text{O}_4$  pellets
- K Platinum-Platinum 10% Rhodium thermocouple
- L Tension-loaded springs
- M Brass cell head

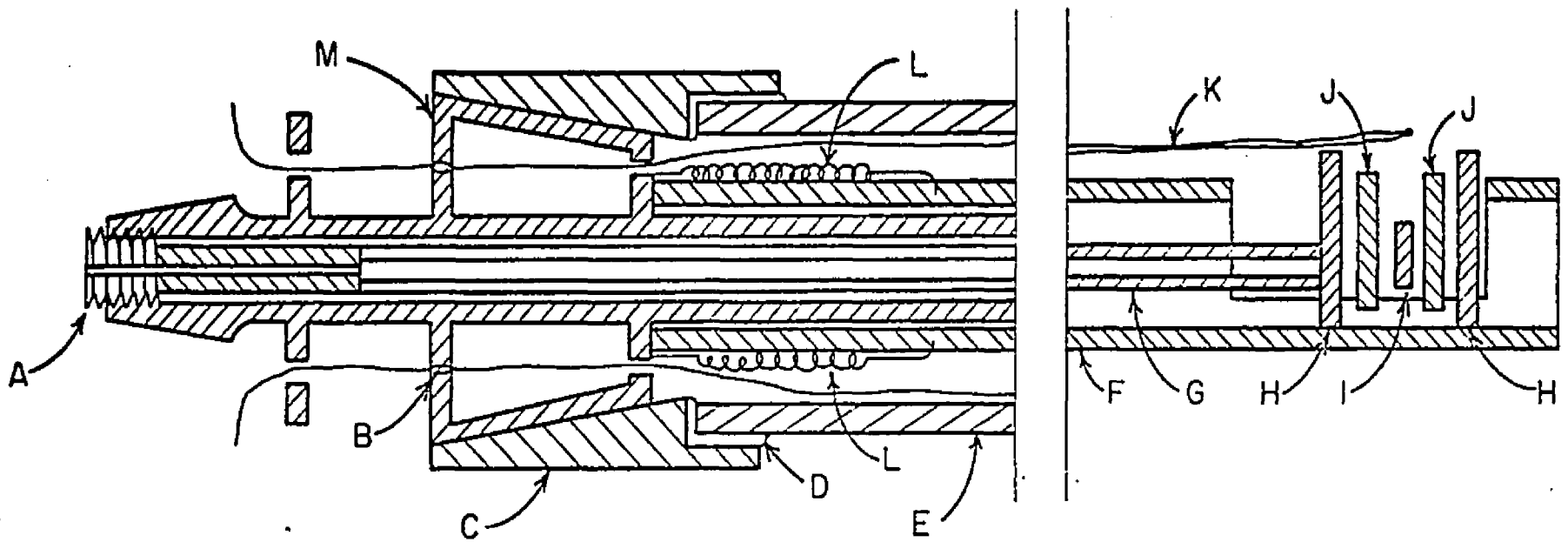


Fig. 13.--Cell Unit Assembly for the Diffusion Anneals at  $P_{O_2} = 1.0$ .

Figure 11, Legend

- A Platinum electrode leads
- B Thermocouple leads
- C Magnesium perchlorate and drierite
- D Bubblers
- E Liquid nitrogen cold trap
- F Calcia stabilized zirconia furnace tube



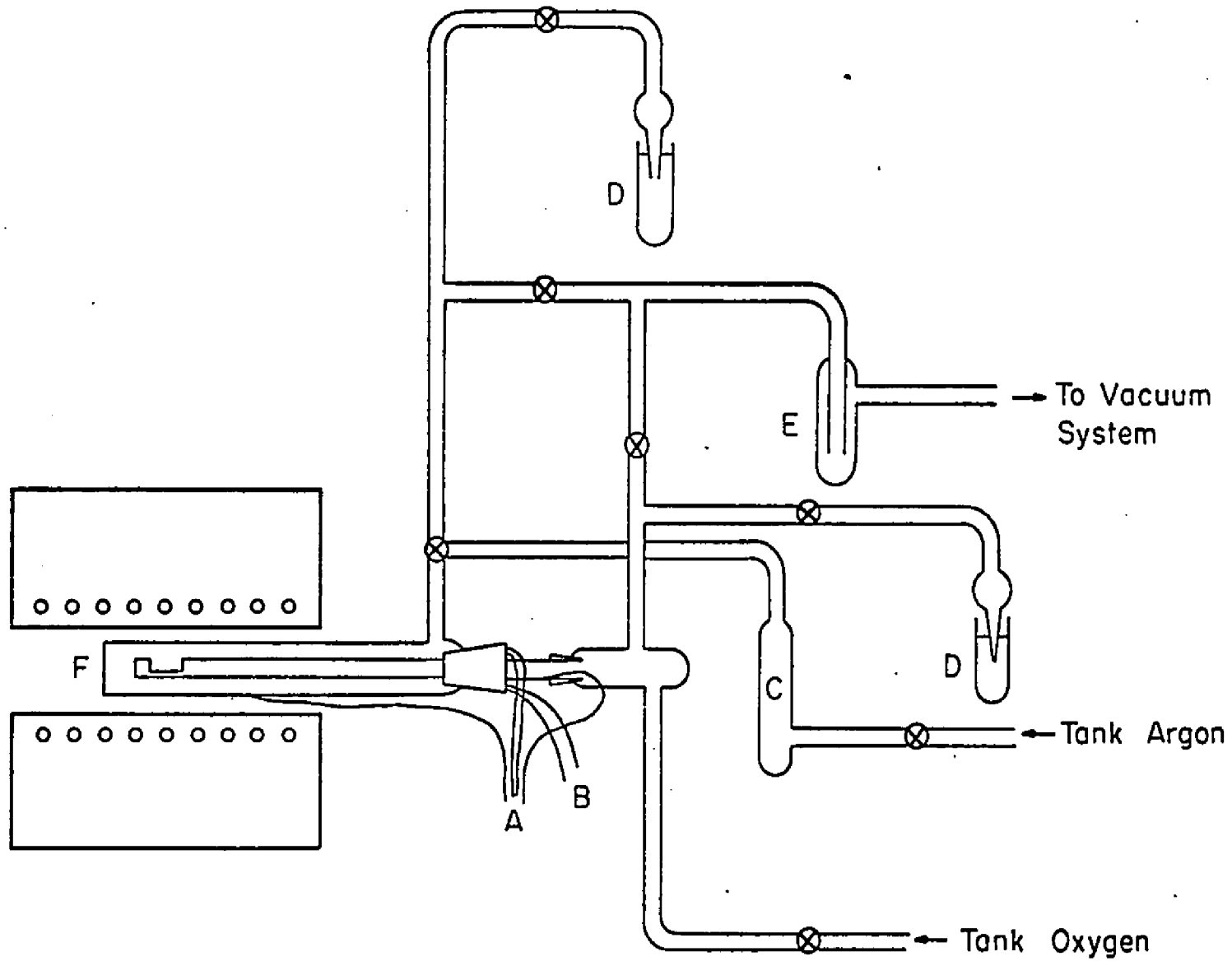


Fig. 14.--Schematic Illustration of the Apparatus Used to Perform the Diffusion Anneals at  $P_{O_2} = 10^{-2}$  and  $10^{-3}$ .

the structure. Stabilized zirconia with platinum contacts can be used as a solid electrolyte in a galvanic cell with different oxygen pressures on the two sides of the electrolyte. In the oxygen pressure range where complete ionic conduction occurs, the cell voltage is given by:

$$E = \frac{RT}{4F} \log \frac{P'_{O_2}}{P''_{O_2}} \quad (68)$$

where  $F$ ,  $R$ , and  $T$  are Faraday's constant, the gas constant, and temperature, respectively, and  $P'_{O_2} > P''_{O_2}$ . From Eq. (68) the calculation of an unknown oxygen pressure at one electrode is possible if the open-circuit cell voltage and a reference oxygen pressure at the other electrode are known. Similarly, a desired oxygen pressure in a closed chamber can be obtained by applying a constant voltage across the cell with a reversible electrode at some known reference pressure. Stabilized zirconia of the composition  $Zr_{0.85}Ca_{0.15}O_{1.85}$  has also been used to pump oxygen into and out of flowing nitrogen<sup>45</sup> and argon<sup>46</sup>.

The outer zirconia tube which pumped oxygen into and out of the system contained 3-4% calcia, and the inner zirconia tube which measured the oxygen pressure in the system contained 7 1/2% calcia. The tubes were impervious, slip cast tubes purchased from Zirconium Corporation of America. Platinum electrodes were painted onto the tubes and the electrode leads were arranged as shown in Fig. 15. The electrodes were applied with Hanovia platinum paste purchased from Engelhard Industries. Both unfluxed platinum paste (No. 6926) and platinum paste fluxed with  $SiO_2$  (No. 6082) were used to make the electrodes with equal

### Figure 15 Legend

- A Adjustable outer plunger
- B Adjustable inner plunger
- C Pyrex standard taper 19/38 joint
- D O-ring seal
- E Stupakoff vacuum seal
- F Pyrex standard taper 34/45 joint
- G Tension-loaded springs
- H 3-4% calcia stabilized zirconiz, closed-end furnace tube
- I Alumina cell holder tube
- J 7 1/2 % calcia stabilized zirconia, closed-end pushrod
- K Brass cell head
- L Epoxy pyrex-to-zirconia seal
- M Epoxy zirconia-to-metal seal
- N Epoxy platinum-to-pyrex seal
- P Platinum electrodes
- R Alumina plates
- S  $\text{NiCr}_2\text{O}_4$  pellets
- T NiO single crystal
- U Platinum-platinum 10% Rhodium thermocouple
- V Platinum electrode leads

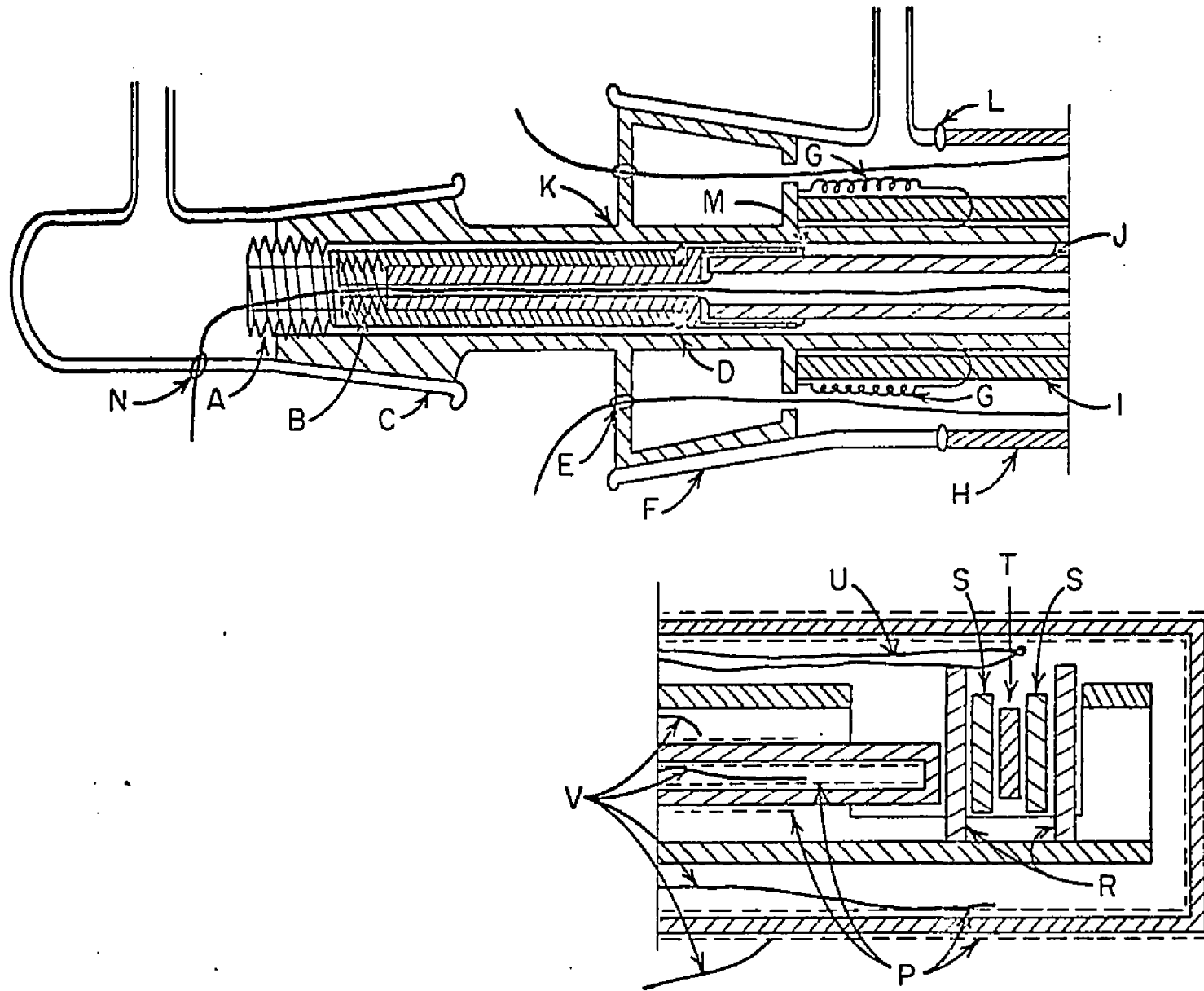


Fig. 15.--Cell Unit Assembly for the Diffusion Anneals at  $P_{O_2} = 10^{-2}$  and  $10^{-5}$ .

success. To coat the inner portions of a tube, a small amount of paste was thinned with xylene and poured into the tube. The xylene was evaporated leaving a thin layer of platinum on the wall of the tube. The tube was then heated slowly to  $870^{\circ}\text{C}$  in air and furnace cooled to remove the organic solvents and cause the platinum to adhere to the zirconia. To coat the outer portions of the tubes, the thinned paste was applied with a brush and heat-treated as before. Successive layers were applied until the resistance of each electrode was approximately two ohms between extreme points on the electrodes. At temperatures of  $1100^{\circ}\text{C}$  and above, the outer electrode of the pumping cell was slowly volatilized; however, this was not observed for the electrodes inside the system. The platinum most likely volatilized as a higher oxide molecule of platinum so the volatilization was suppressed at low oxygen pressures. Therefore, the resistances of the electrodes were measured before each diffusion anneal and additional platinum was applied when necessary. The platinum leads to the outer electrodes on the tubes were wrapped around the electrodes several times, and the leads to the inner electrodes lay in the tubes making a gravity contact.

To obtain the desired oxygen pressure, the system was evacuated with the mechanical pump and filled with argon three times. The argon was then bubbled off to the ambient pressure, and the system was closed to create a stagnant atmosphere. The interior of the measuring cell tube was also evacuated with the mechanical pump and filled with oxygen three times. The vacuum pump was then shut out of the system, and oxygen was bubbled off at the ambient pressure. Because the system was not entirely leak tight, oxygen leaked slowly into the system due to the

difference in oxygen pressures of the system and external atmosphere. However, oxygen could be removed from the system by applying a voltage across the pumping cell. By balancing the rate of oxygen leaking into the system with the rate of oxygen pumped out of the system, a desired oxygen pressure was maintained. The oxygen pressure was determined by measuring the voltage across the small zirconia tube with a Leeds and Northrup volt-potentiometer.

### C. Sectioning Apparatus

To obtain the diffusion profiles, the NiO crystals were sectioned, and the radioactivity of  $^{51}\text{Cr}$  in each section counted after a diffusion anneal. To obtain an accurate profile, the sections must all be parallel to each other and to the original surface of the crystal, and the thickness of each section removed must be very accurately measured. To perform the sectioning, the apparatus shown in Fig. 16 was built. The bell was made of AISI A-2 tool steel hardened to  $R_c$  52. The base of the bell and the inner diameter of the shaft were ground so that the core of the shaft was perpendicular to the base. A piston was cut from a stainless steel drill rod and ground so that the piston face was perpendicular to the outer diameter of the piston and the piston slip-fit the shaft of the bell. Therefore, when the piston was inserted into the shaft of the bell, the face of the piston was parallel to the base of the bell. The platform for the bell was a granite block, purchased from Herman Stone Company, with a surface tolerance of  $\pm 0.00005$  inch from the mean plane of the surface. A plexiglass frame on the granite block aided the rotation of the bell during polishing. An air cushion



Fig. 16.--Apparatus Used to Section the NiO Crystals.

between the bell and the granite block was created by a flow of compressed air into the annular ring in the base of the bell. This air cushion reduced the friction between the bell and block and allowed smooth movement of the bell during polishing.

To measure the thickness of the section removed during a polishing step, the apparatus shown in Fig. 17 was used. A Feathertouch Height Indicator was mounted on a Universal Height Gage Stand and used in conjunction with a Model 12 Accutron Amplifier to measure the height of the piston plus the crystal. These three instruments were purchased from The Bendix Corporation. The Height Gage Stand was placed on a granite block with a surface tolerance of  $\pm 0.000025$  inch, and a plexiglass frame was fastened on the block. The frame had a slot for the Height Gage Stand and a V-shaped slot which matched V-notches machined in the top of the pistons. The stand was stationery, and the piston was slid into and out of its slot with the matching notches insuring that the same point on the crystal was positioned under the Height Indicator for each section. Measurements could be repeated with a precision of  $\pm 0.05$  microns when measuring on the B scale of the amplifier. To calibrate the Accutron Amplifier the difference in thickness of two high tolerance calibration blocks were used. One block was 1.001 millimeters thick, and the other was 1.003 millimeters thick. Because the precision of the calibration measurements was  $\pm 0.05$  microns, the accuracy of the calibration was  $\pm 5\%$ . Therefore the accuracy of the section thickness measurements was approximately 5%.



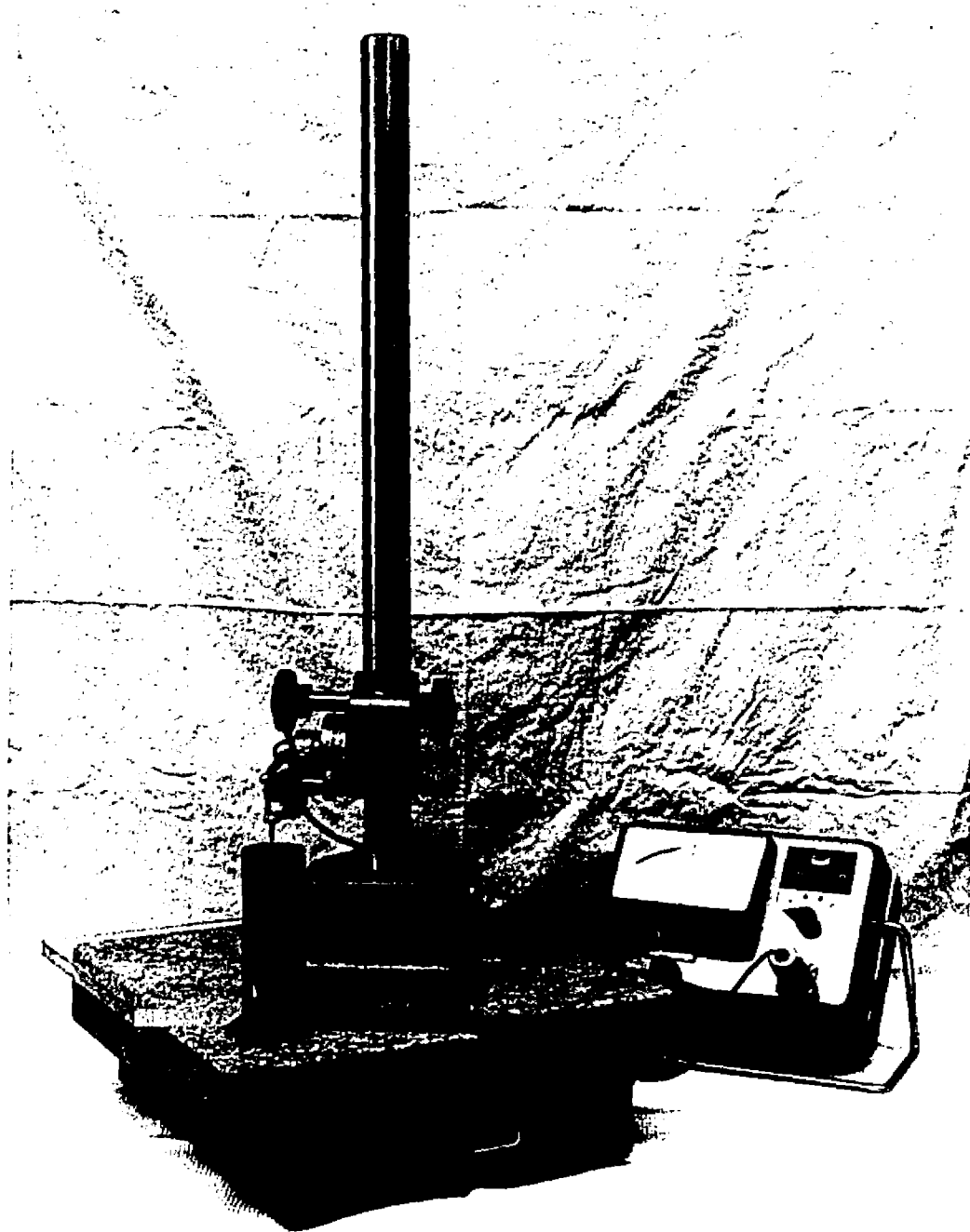


Fig. 17.--Apparatus Used to Measure the Thickness of the Sections Removed from the NiO Crystals.

#### D. Counting Apparatus

To measure the radioactivity of chromium in the material removed for each section, the material was placed in a well-type, thallium-activated sodium iodide crystal used in conjunction with a cesium antimony phototube. The emission of gamma rays was counted with a multichannel analyzer manufactured by Nuclear Data, Incorporated used in conjunction with a ratemeter. The windows of the multichannel analyzer were set so that only channels in the energy range of the photopeak of  $^{51}\text{Cr}$  were counted because the ratio of the counts per second of the sample to the counts per second of the background was much greater for the photopeak range than for the entire energy spectrum. The counting is a statistical process whose accuracy is determined by a Poisson distribution and given by  $\pm\sqrt{N}$  where  $N$  is the total number of counts detected. The samples were counted for a sufficient length of time to obtain an accuracy of  $\pm 1.0\%$  except for when the counting rate was less than twice the background. These latter measurements were taken to determine any residual radioactivity in the crystal.

#### E. Procedure

For the diffusion anneal, a NiO crystal was sandwiched between two  $\text{NiCr}_2\text{O}_4$  pills, and the assembly was placed in the furnace at a constant temperature and oxygen pressure. The duration of the diffusion anneals varied from 11 days at  $1000^\circ\text{C}$  to 3 days at  $1400^\circ\text{C}$ . The furnace was heated to the desired temperature for the anneal and cooled back to room temperature after the anneal with the assembly in place. For anneals shorter than 10 days, the time of the anneal was corrected for

the heating and cooling processes by :<sup>47</sup>

$$t_e = \frac{\int_0^{t_t} \exp (Q/RT(t)) dt}{\exp (Q/RT)} \quad (69)$$

where  $t_e$  is the equivalent time at the diffusion temperature  $T$ ,  $Q$  is the activation energy, and  $t_t$  represents the total time of the anneal. For this correction, the activation energy of the self-diffusion of chromium in NiO obtained by Greskovich<sup>38</sup> was used.

After the anneal, the pills were separated, and the cylindrical edges of the crystal which contacted the gas phase were cleaved off to remove any chromium which diffused rapidly down the edges or entered the crystal at the edges from the vapor phase. The crystal was then glued to the face of the piston with Duco cement in order to section it. To assure that the crystal surface and the granite surface were parallel so that the sections were parallel to the NiO interface in the diffusion couple, the crystal was placed on the granite block with the side to be sectioned down, and the bell was placed over the crystal. The piston, with Duco cement on its face, was inserted into the shaft of the bell. The piston was positioned over the crystal by sighting through the small hole through the center of the piston and lowered until the face of the piston contacted the crystal. The Duco cement was allowed to dry with crystal surface to be sectioned in contact with the granite block. After the crystal was secured to the piston, a piece of 3/0 emery paper was fastened to the granite surface using double-stick scotch tape. The bell with the piston inserted was rotated inside the plexiglass frame,

and the crystal was polished on the emery paper. At the completion of the polishing for a section, the thickness of the residual material was measured with the height gage. Because the change in the height of the crystal plus the piston was measured, the piston was handled with insulated pads so the temperature of the piston was constant; therefore, the length of the piston was constant. During the polishing the material removed became embedded in the emery paper. Therefore the piece of emery polishing paper used to polish the crystal for each section was folded and placed in a 5 ml polyethylene container. The 5 ml container was then placed in a 30 ml container which was sealed to prevent contamination of the counting crystal. The paper was folded similarly for each section to maintain the counting geometry nearly constant for all the measurements. The radioactivity of each sample was measured with the scintillation counter, and a diffusion profile was obtained. Sections approximately ten microns thick were removed from the crystal so the accuracy of the section thickness measurements was approximately  $\pm 6\%$ . The radioactivity of each section was divided by the thickness of the section to get the specific activity. Because of the accuracy of the thickness the accuracy of the specific activity was approximately  $\pm 6\%$ .

## V. RESULTS AND DISCUSSION

The data obtained from the diffusion anneals are tabulated as the specific radioactivity of  $^{51}\text{Cr}$  as a function of distance into the NiO crystal in Appendix D. Diffusion anneals were performed at  $P_{\text{O}_2} = 1.0$  atm at  $1000^\circ\text{C}$  and at  $P_{\text{O}_2} = 1.0, 10^{-2}$  and  $10^{-5}$  atm at  $1100^\circ\text{C}$ ,  $1200^\circ\text{C}$  and  $1300^\circ\text{C}$ . The duration of the diffusion anneals varied from 10 days at  $1000^\circ\text{C}$  to 3 days at  $1300^\circ\text{C}$ . More than two sets of data were obtained from a given diffusion anneal by cleaving the crystal parallel to the direction of chromium diffusion into smaller pieces after the anneal. The radioactivity of a section was divided by the thickness of the section to obtain counts per second per micron (specific activity), and this activity was plotted versus the penetration depth of the center of the section to obtain the concentration profile for chromium diffusing into NiO.

The experimental conditions for the diffusion of the chromium were such that the solution of the diffusion equation was subject to the initial distribution,

$$c = 0, \quad x > 0, \quad t = 0,$$

and the boundary condition,

$$c = c_0, \quad x = 0, \quad t > 0;$$

$c_0$  is the solubility limit of chromium in NiO at a given temperature and

is assumed independent of the oxygen pressure on the basis of the results of Meier and Rapp.<sup>23</sup> The system was semi-infinite, with  $x = 0$  defined as the  $\text{NiCr}_2\text{O}_4$ -NiO interface. The assumption that the NiO boundary was stationary--although some  $\text{NiCr}_2\text{O}_4$  was decomposed to form NiO--and saturated with chromium was made because the chromium concentration in the spinel (approximately 67%) was much greater than  $c_0$  (approximately 1-3%) and because chromium diffuses very slowly away from the boundary.

If the diffusion coefficient for chromium in NiO were independent of the chromium concentration, the solution to the diffusion equation for the given conditions would be of the form of the complementary error function:<sup>48</sup>

$$c = c_0 \operatorname{erfc} \left( x/2(Dt)^{1/2} \right) \quad (70)$$

However, the diffusion coefficient for chromium in NiO was expected and found to be a function of the chromium concentration so that Fick's second law had to be solved for a concentration-dependent diffusion coefficient.

The pertinent diffusion equation was then:

$$\frac{\partial c}{\partial t} = \frac{\partial}{\partial x} \left( D(c) \left( \frac{\partial c}{\partial x} \right) \right) \quad (71)$$

where  $D(c)$  is the concentration-dependent diffusion coefficient and  $c$  is the chromium concentration. Boltzmann,<sup>49</sup> using the substitution:

$$y = x/2t^{1/2} \quad (72)$$

transformed Eq. (71) into the ordinary differential equation:

$$\frac{d}{dy} \left( D(c) \left( \frac{dc}{dy} \right) \right) = -2y \left( \frac{dc}{dy} \right) \quad (73)$$

Integration of Eq. (73) gives:

$$\int_{c_0}^c d \left( D(c) \left( \frac{dc}{dy} \right) \right) = -2 \int_{c_0}^c y \, dc \quad (74)$$

which, because  $t$  is a constant, becomes:<sup>50</sup>

$$\int_{c_0}^c d \left( D(c) \left( \frac{dc}{dx} \right) \right) = \frac{1}{2t} \int_c^{c_0} x \, dc \quad (75)$$

Integration of the left-hand-side of Eq. (75) yields:

$$D(c) \left( \frac{dc}{dx} \right)_c - D_{Cr}^S \left( \frac{dc}{dx} \right)_{c_0} = \frac{1}{2t} \int_c^{c_0} x \, dc \quad (76)$$

where  $D_{Cr}^S$  is the diffusion coefficient of chromium in the saturated NiO lattice.

When the experimental concentration profile is plotted using Cartesian coordinates, the slopes of the curve at the points  $(c, x)$  and  $(c_0, x=0)$  are equal to  $(dc/dx)_c$  and  $(dc/dx)_{c_0}$ , respectively. The right-hand-side of Eq. (76) can be obtained by integrating the area under the diffusion profile graphically from  $c$  to  $c_0$ . Therefore, only  $D(c)$  and  $D_{Cr}^S$  remain to be evaluated. As  $c$  approaches zero, the first term on the left-hand side of Eq. (76) becomes very small, such that

$$\left[ D(c) \left( \frac{dc}{dx} \right)_c \right]_{c \rightarrow 0} \ll D_{Cr}^S \left( \frac{dc}{dx} \right)_{c_0} \quad (77)$$

Then Eq. (76) reduces to:

$$- D_{Cr}^S \left( \frac{dc}{dx} \right)_{c_0} = \frac{1}{2t} \int_{c \rightarrow 0}^{c_0} x \, dc \quad (78)$$

and by graphically integrating the curve from some very small value of  $c$  to  $c_0$ ,  $D_{Cr}^S$  can be calculated. In the actual determination of  $D_{Cr}^S$ , the curve was integrated from  $c = 0$  to  $c_0$ . Because  $D_{Cr}^S$  is a constant for each diffusion profile,  $D(c)$  can be evaluated at various values of  $c$  along the curve by using Eq. (76).

The diffusion profile was obtained by a least-squares fit of a first- or second-order polynomial to the specific radioactivity of  $^{51}Cr$  as a function of distance into the crystal. The polynomial arbitrarily extended the diffusion profile to  $c = 0$  although the profile should have approached the abscissa asymptotically because of the presence of the native vacancies in the crystal. From the assumption that the boundary of the NiO was saturated with chromium, the specific radioactivity was converted to chromium concentration. At  $1000^\circ C$  and  $1100^\circ C$ , the solubility limit is 0.012 and 0.015 cation fraction of chromium, respectively, as reported by Meier and Rapp.<sup>23</sup> These authors also found and explained that the solubility limit was independent of the oxygen pressure. The solubility limit at  $1200^\circ C$  and  $1300^\circ C$  was obtained from the curve in Fig. 18 which also incorporates the solubility values of Greskovich.<sup>38</sup> In his work Greskovich reported his concentration profiles as mole % versus penetration distance from electron microprobe analysis. The points in Fig. 18 attributed to Greskovich were obtained from his concentration profiles at NiO-NiCr<sub>2</sub>O<sub>4</sub> coexistence. The solubility limit



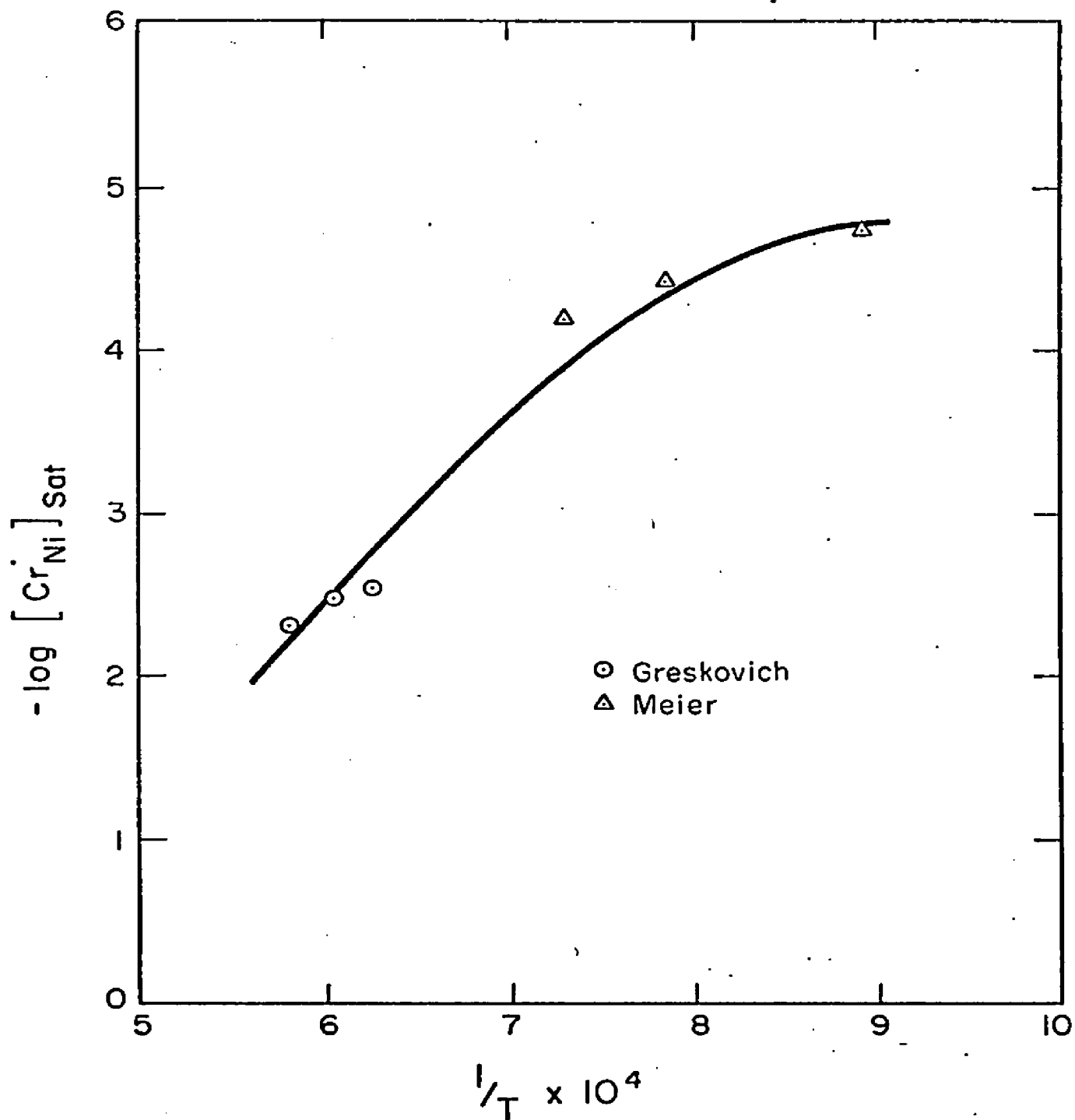


Fig. 18.--Solubility Limit of Chromium in NiO as a Function of Temperature.

is approximately 0.034 and 0.056 cation fraction at 1200°C and 1300°C, respectively. The fitting of the polynomial for the diffusion profile and the calculation of the diffusion coefficient as a function of concentration were performed on an IBM 360 computer using the program shown in Appendix B.

In Fig. 19, the diffusion profile obtained at  $P_{O_2} = 1.0$  atm and 1100°C is shown. The data were plotted as the specific radioactivity versus distance and a least-squares fit of the data to a polynomial was obtained. The least-squares polynomial was either first order as:

$$y = A_0 + ax \quad (79)$$

yielding a linear diffusion profile or second order as:

$$y = A_0 + ax + bx^2 \quad (80)$$

yielding a curved diffusion profile with an increasing slope with penetration depth. In Fig. 19, a first order polynomial fit the data and was extended to the abscissa ( $[Cr_{Ni}] = 0$ ). The radioactivity of the first section taken from the crystal surface was generally very high because some  $NiCr_2O_4$  adhered to the surface, and, therefore, the first section from each set of data was disregarded when plotting the diffusion profile. The uncertainty in the position of the NiO- $NiCr_2O_4$  boundary in the diffusion profile is approximately the same as the accuracy of the first section which is about one micron.

At high temperatures, where only two-member complexes should exist, the diffusion coefficient would be predicted to depend upon the chromium concentration as described by:

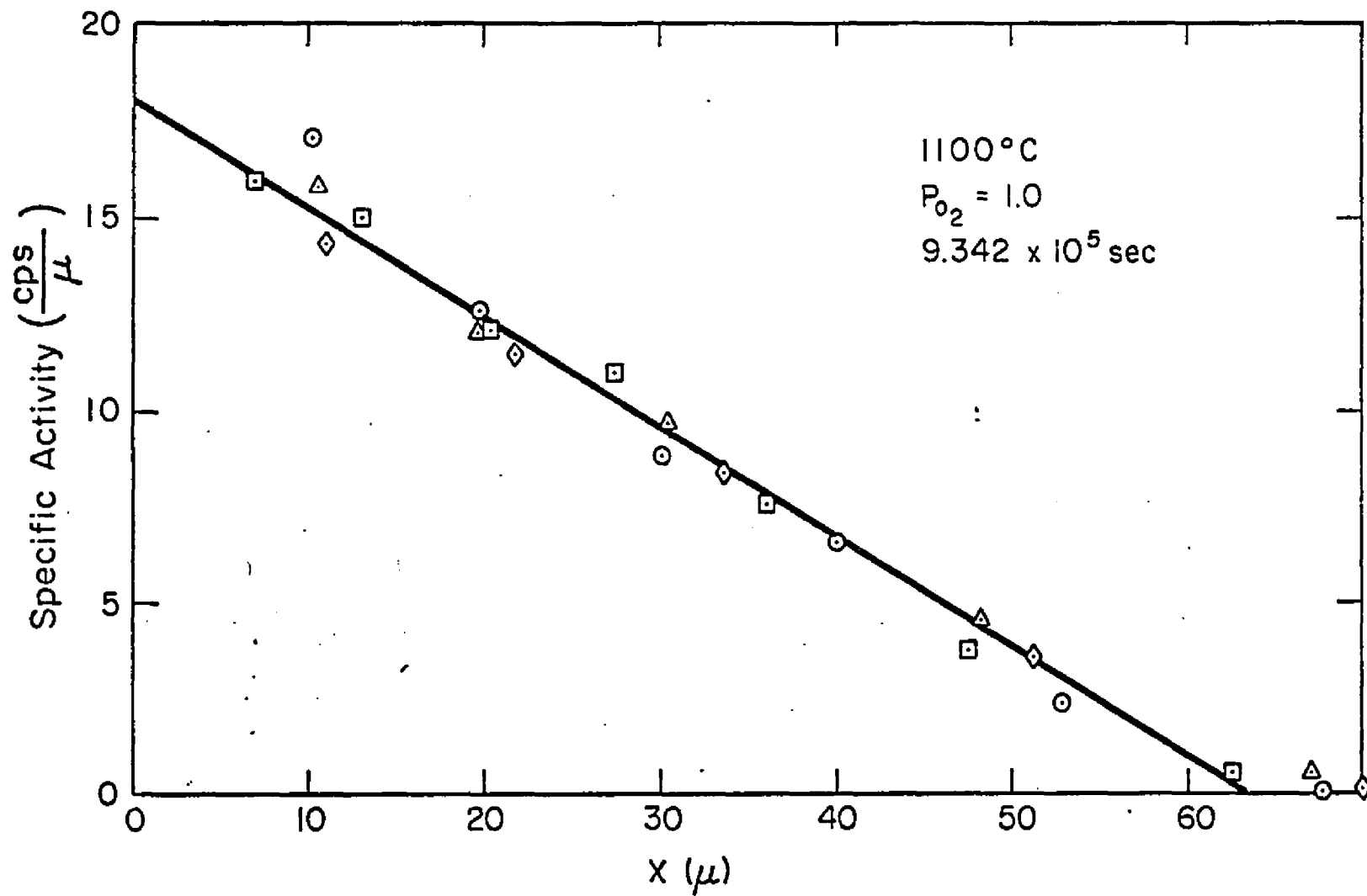


Fig. 19.--Diffusion Profile for Chromium in NiO at 1100°C and  $P_{O_2} = 1.0$ .

$$D(\text{Cr}) = D_0(2) \left( \frac{3}{4} - \left( \frac{c}{8} + \frac{3}{4w} \right) \sqrt{\left( \frac{c^2}{4} + \frac{3c}{w} + \frac{1}{w^2} \right)^{1/2}} \right) \quad (81)$$

where

$$w = Z_2 \exp(\Delta G_3^0/2RT) \quad (82)$$

$D_0(2)$  is the diffusion coefficient of a two-member complex as defined by Eq. (61). This dependence is obtained directly from the derivative of Eq. (56). After the chromium diffusion coefficient was obtained as a function of the chromium concentration from the diffusion profile using Eq. (76), the values of the diffusion coefficient at various concentrations were inserted into Eq. (81), and  $D_0(2)$  and  $\Delta G_3^0$  were evaluated using a method involving successive approximations. Sets of values for  $D_0(2)$  and  $\Delta G_3^0$  were substituted into Eq. (81) at various concentrations and the results for  $D(\text{Cr})$  were compared to the values of the diffusion coefficient obtained from the concentration profile. The set of values for  $D_0(2)$  and  $\Delta G_3^0$  which described the experimental results best for the entire concentration profile was used to construct a curve for  $D(\text{Cr})/D_{\text{Cr}}^S$  versus concentration, again using Eq. (81). The method used to solve for  $D_0(2)$  and  $\Delta G_3^0$  is fully described in Appendix B, and the computer program used for this solution is also shown. The theoretical curve for  $D(\text{Cr})/D_{\text{Cr}}^S$  versus  $c$  was then compared with the experimental results, also plotted as  $D(\text{Cr})/D_{\text{Cr}}^S$  versus  $c$ , to determine the extent to which the model indeed described the diffusion mechanism. The number of two-member complexes present was then calculated by placing the theoretical  $\Delta G_3^0$  into Eq. (56) to obtain the

degree of complexing and multiplying this factor times the chromium concentration.

The diffusion coefficient for chromium along the concentration profile in Fig. 19 was obtained by using Eq. (76), divided by the experimental saturation diffusion coefficient and was plotted versus the chromium concentration in Fig. 20. The solid line represents the experimental results, and the dashed line represents the fit of the theoretical dependence, obtained from Eq. (81) and divided by the experimental saturation diffusion coefficient, to the experimental results. At low concentrations the fit and curvature of the two solutions is good, but at higher concentrations the fit is not as good and the two solutions have different curvature. At high concentrations the experimentally obtained diffusion coefficient does not decrease as rapidly with decreasing concentration as predicted by the theoretical model. This difference between the model and experimental results was observed for every concentration profile.

This difference in curvature at high concentrations might be caused by the difference in the mobility of the vacancies and the chromium ions. The diffusion coefficient of nickel vacancies in NiO is approximately  $1 \times 10^{-7}$  cm<sup>2</sup>/sec at 1000°C so the vacancies are much more mobile than the chromium. Therefore, in the absence of other gradients, the vacancies would tend to diffuse down a vacancy concentration gradient faster than chromium down a chromium concentration gradient. However, if the vacancies were to diffuse ahead of the chromium, the concentration of vacancies in the crystal would be altered as shown schematically by the dashed line in Fig. 21. In Fig. 21,  $[\text{Cr}_{\text{Ni}}^{\bullet}]$  is

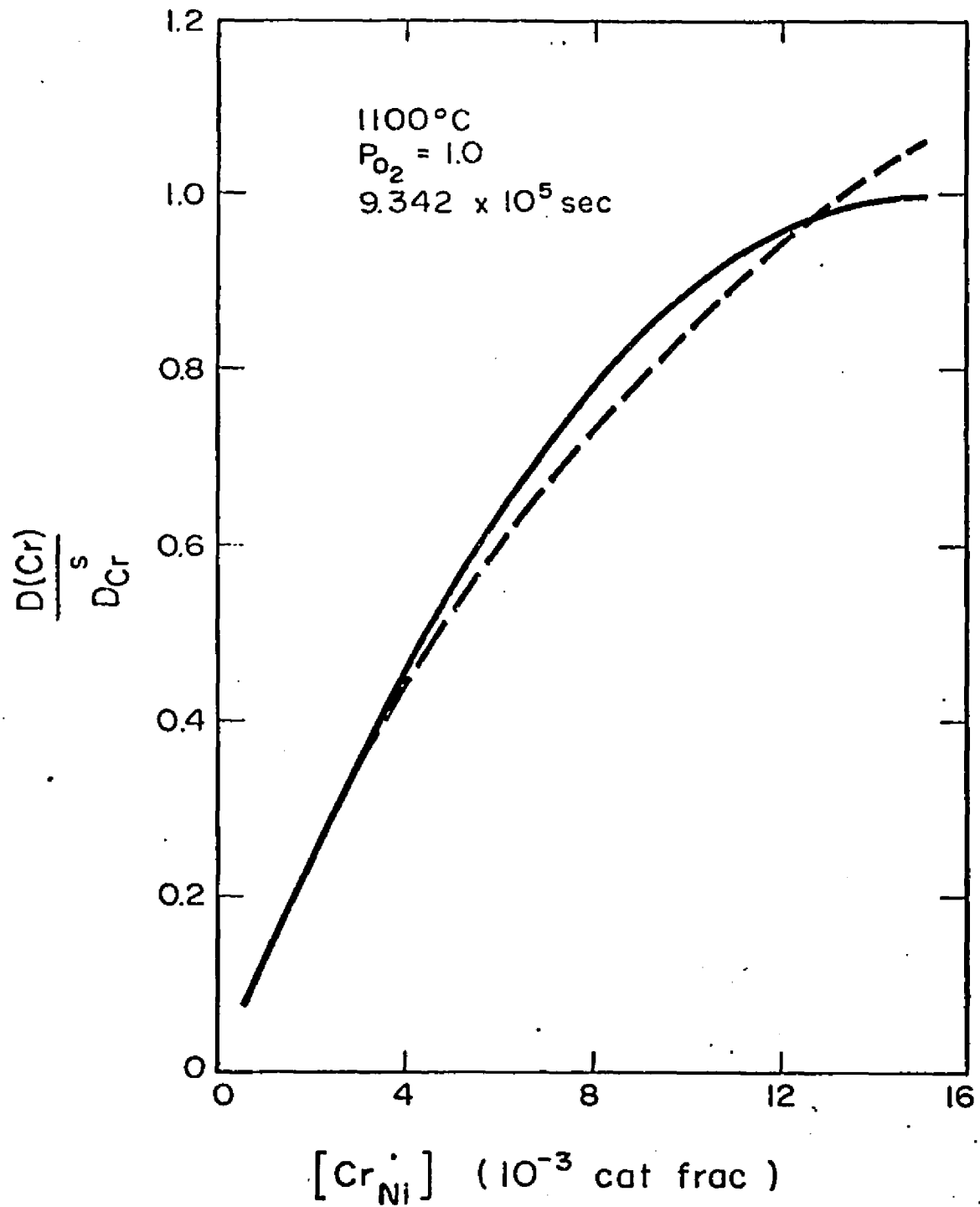


Fig. 20.--Normalized Diffusion Coefficient of Chromium as a Function of the Chromium Concentration at 1100°C and  $P_{O_2} = 1.0$ .

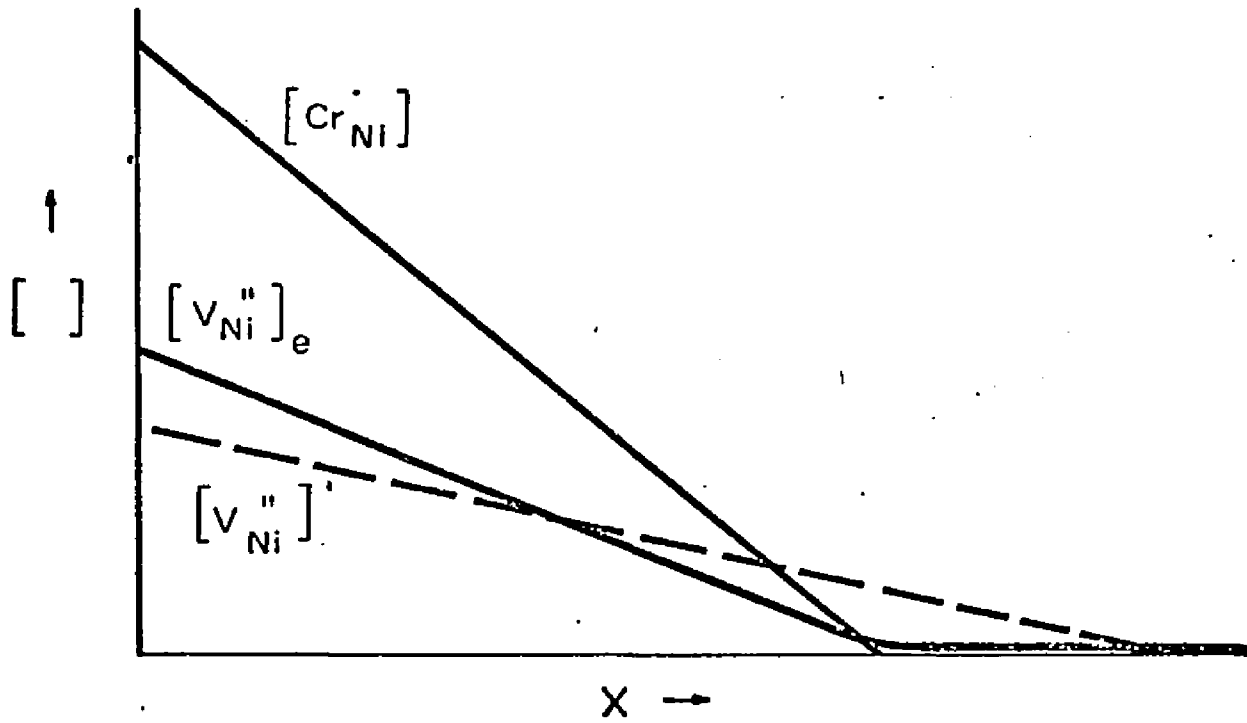


Fig. 21.--Concentration Profile of Chromium and Nickel Vacancies Diffusion into NiO.

the chromium concentration,  $[v_{Ni}^{''}]_e$  is the vacancy concentration if local charge equilibrium defined by Eq. (67) is maintained, and  $[v_{Ni}^{''}]'$  is a schematic vacancy concentration profile if the vacancies would diffuse ahead of the chromium. If the vacancies would diffuse ahead of the chromium, the portion of the concentration profile where  $[v_{Ni}^{''}]' \ll [v_{Ni}^{''}]_e$  would have fewer than the equilibrium number of complexes according to Eq. (32) so the diffusion rate would be decreased. In the portion where  $[v_{Ni}^{''}]' \gg [v_{Ni}^{''}]_e$ , more than the equilibrium number of complexes would be present so the diffusion rate would be relatively increased. If the diffusion coefficient is directly proportional to the concentration, the relative effects of the vacancies diffusing ahead of the chromium would tend to reduce the concentration dependence of the diffusion coefficient.

The electrical energy in the NiO crystal arising from the charges on the vacancies, chromium ions and positive holes can be calculated by using the Debye-Huckel theory according to Eq. (13). The entropy of mixing these species in the crystal can be calculated from statistical mechanics by:

$$S = -k \ln \Omega \quad (83)$$

where

$$\Omega = \frac{N_c!}{\prod_i n_i!} \quad (84)$$

$N_i$  is the number of cation sites in the crystal,  $n_i$  is the number of each type of species occupying cation sites and  $\Omega$  is the number of con-



figuration possible in arranging the various species on the cation sites. From a comparison of the change in the electrical energy and entropy upon moving a vacancy from a position in local charge equilibrium to a position where there would be an excess of vacancies, the likelihood of such an occurrence can be estimated. At 1000°C and  $P_{O_2} = 1.0$  atm, approximately 5000 calories of energy are needed to move a vacancy from a point in local equilibrium with  $10^{-3}$  cation fraction of chromium to a point where only native vacancies exist in equilibrium with the atmosphere. The details of this calculation are more fully described in Appendix C. On this basis, the redistribution seems unfavorable. However, if positive holes were available to move with the vacancies so that no space charge were created in the crystal, much less energy would be needed to move the vacancies. Therefore, the number of vacancies which can move ahead of the chromium is limited by the number of positive holes which are available to move with the vacancies to avoid creating a space charge. The concentration of positive holes present in Cr-doped NiO is given by:<sup>12</sup>

$$p = (2K_1)^{1/2} P_{O_2}^{1/4} / [Cr_{Ni}^{\bullet}]^{1/2} \quad (85)$$

where

$$K_1 = \frac{[V_{Ni}^{\bullet}] p^2}{P_{O_2}^{1/2}} \quad (86)$$

obtained from pure NiO. At 1100°C and  $P_{O_2} = 1.0$  atm, using Tret'yakov and Rapp's<sup>25</sup> value for  $[V_{Ni}^{\bullet}]$  from Table 1,  $K_1 = 5 \times 10^{-10}$ . The hole

concentration is approximately  $8 \times 10^{-5}$  cation fraction at  $1.5 \times 10^{-2}$  cation fraction of chromium and increases as the chromium concentration decreases. In Fig. 22, the effect of the positive holes upon limiting the vacancy distribution is demonstrated for  $1100^{\circ}\text{C}$  and  $P_{\text{O}_2} = 1.0$  atm. In Fig. 22(A) the concentrations of  $\text{Cr}_{\text{Ni}}^{\cdot}$ ,  $V_{\text{Ni}}^{\prime\prime}$ , and  $p^{\cdot}$  are shown for local equilibrium and local electrical neutrality defined by Eq. (67). Area A is related to the number of holes which are present in the chromium-doped portion of the crystal to compensate for the movement of vacancies. Fig. 22(B) shows the maximum redistribution of vacancies which could be accommodated by the positive holes. The redistributed vacancy and hole concentrations are  $[V_{\text{Ni}}^{\prime\prime}]^{\prime}$  and  $p^{\prime}$ , respectively. To avoid creating a space charge,  $\text{Area A} = \text{Area B} = 2 \cdot \text{Area C} = 2 \cdot \text{Area D}$ . The number of vacancies which could possibly move ahead of the chromium is related to Area C. Therefore most of the vacancies would remain in the vicinity of the chromium ions although some would move ahead. If the vacancies were to diffuse ahead, the number of complexes where  $[V_{\text{Ni}}^{\prime\prime}]^{\prime} \ll [V_{\text{Ni}}^{\prime\prime}]_e$  would be lower than expected and result in a reduced diffusion rate. The rate at the saturation limit would be reduced about 10%. The number of complexes where  $[V_{\text{Ni}}^{\prime\prime}]^{\prime} \gg [V_{\text{Ni}}^{\prime\prime}]_e$  would be greater than expected and cause an increase in the rate of diffusion. The magnitude of the increase would be difficult to determine by the current experimental method because of the reduced accuracy of the experimental results at the lowest chromium concentrations. These relative effects would increase the curvature of  $D(\text{Cr})/D_{\text{Cr}}^{\text{S}}$  versus chromium concentration, and could account for the observed difference between the experimental results and theoretical predictions.

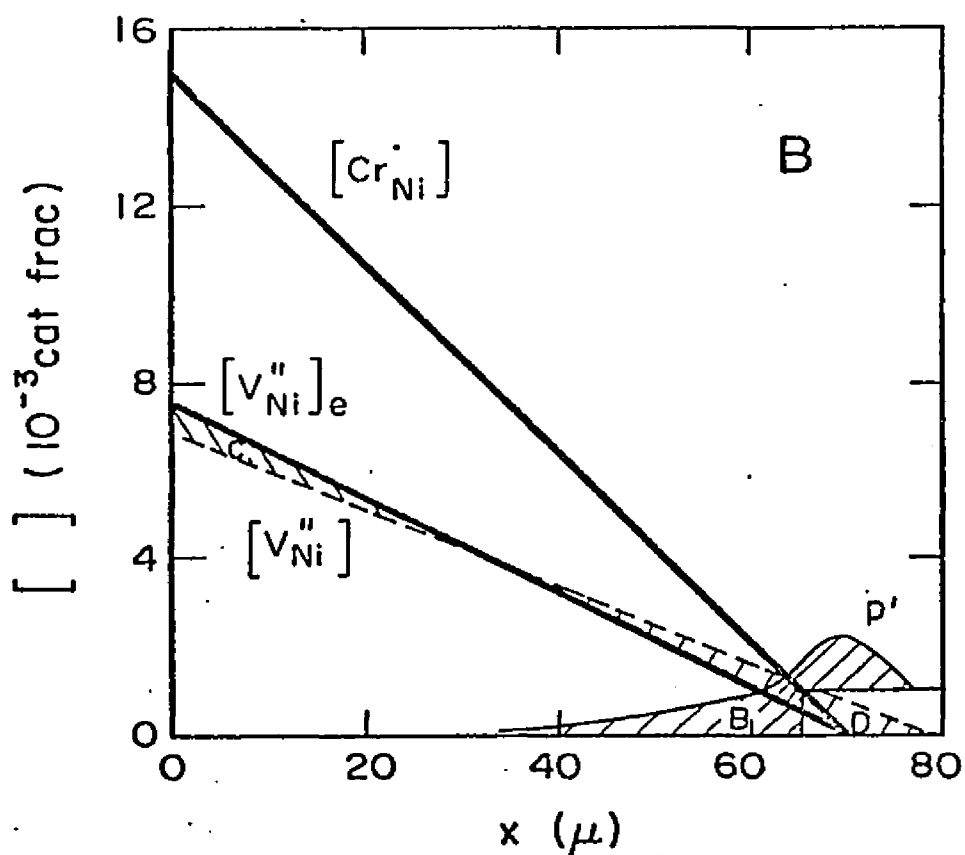
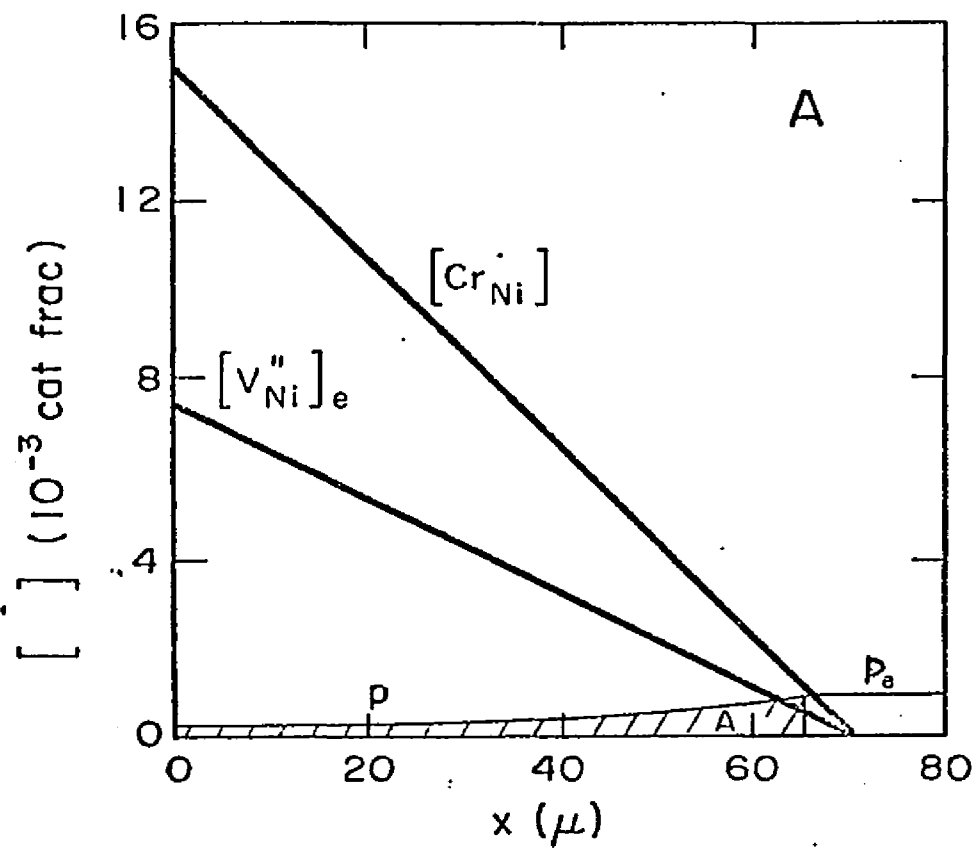


Fig. 22.--Effect of Positive Holes upon the Diffusion of Vacancies Ahead of the Chromium.

The theoretical model and, therefore, Eq. (81) do not consider the native defects of the host lattice which might affect the diffusion of the impurity. As shown in Table 1, an equilibrium number of thermal vacancies will be present in the lattice. Trivalent impurities will also cause native vacancies to maintain electrical neutrality in the lattice. Because the theoretical model only applies for the case in which the native vacancies are of negligible importance, and the experimental diffusion profile was arbitrarily extended to  $c = 0$ , no interpretation for the diffusion coefficient at very low chromium concentrations can be made here. Arbitrarily, the chromium concentration at which the number of vacancies created by the chromium equals the number of native vacancies was chosen as the lower limit for the validity of the present results. The curves showing the dependence of the diffusion coefficient upon the chromium concentration were not extended beyond this limit. The diffusion coefficient would most likely become independent of the chromium concentration as the concentration approaches zero as observed by Seltzer.<sup>40</sup>

The data points obtained from the diffusion anneal at  $1100^{\circ}\text{C}$  and  $P_{\text{O}_2} = 1.0$  atm are plotted using dimensionless coordinates in Fig. 23. The solid line represents the reduced diffusion profile for a constant diffusion coefficient, and the dashed line represents the reduced diffusion profile for the case in which the diffusion coefficient is linearly dependent upon the concentration as treated by Wagner.<sup>51</sup> Wagner assumed that the diffusion coefficient was directly proportional to the concentration so that Fick's second law became:

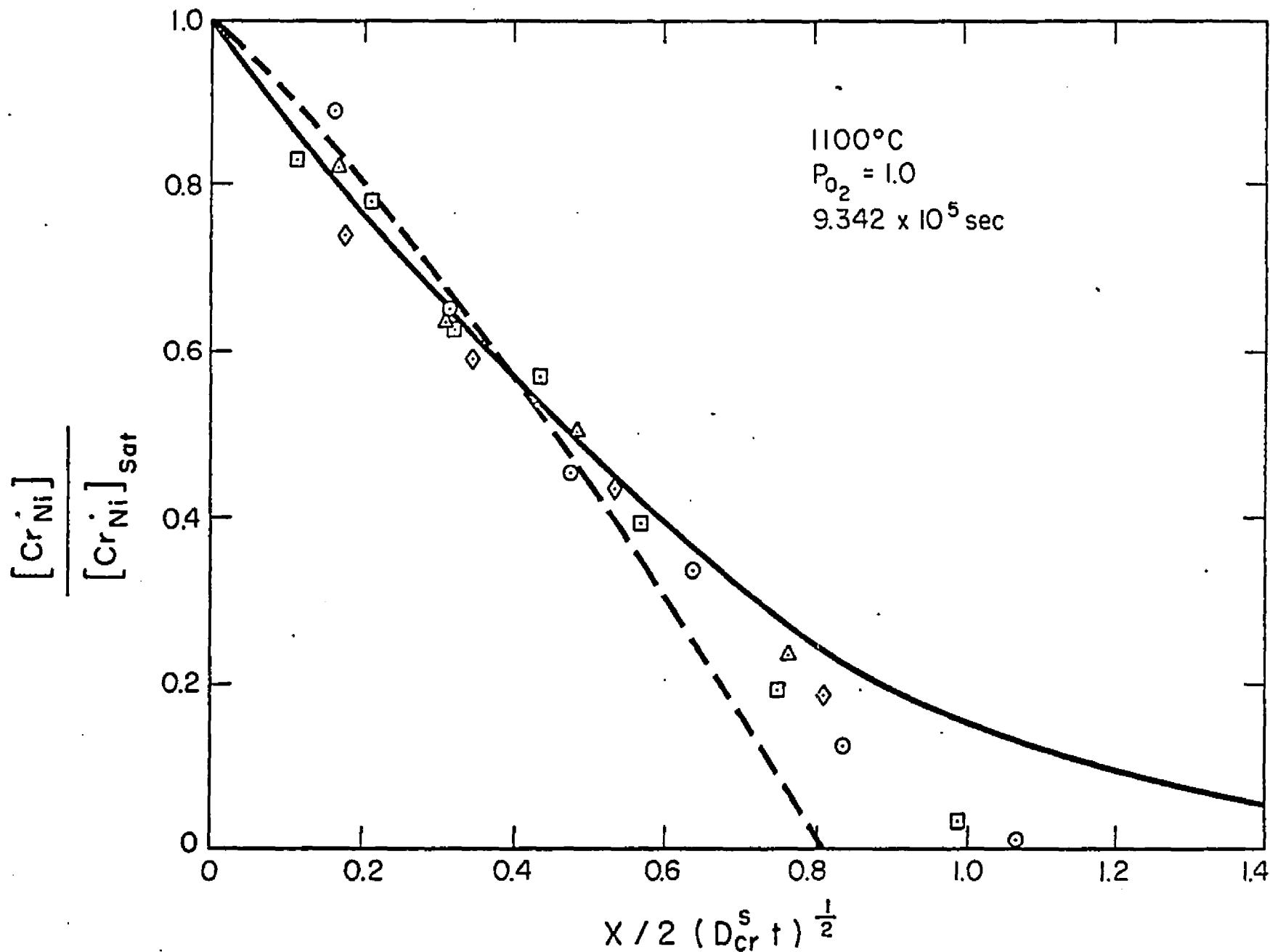


Fig. 23.--Reduced Diffusion Profile for Chromium in NiO at 1100°C and  $P_{O_2} = 1.0$ .

$$\frac{\partial c}{\partial t} = \frac{\partial}{\partial x} \left( D_0 \frac{c}{c_0} \left( \frac{\partial c}{\partial x} \right) \right) \quad (E7)$$

where  $D_0$  represents the diffusion coefficient for a reference concentration which was equated to the saturation concentration  $c_0$ . He then solved Eq. (87) for the case where the boundary concentration is constant and equal to  $c_0$ . A more comprehensive treatment of concentration-dependent diffusion coefficients has been performed by Kass and O'Keefe,<sup>5</sup> and their results for linear dependence of dopant diffusion on concentration agreed very well with Wagner's. As shown in Eq. (66), the diffusion of chromium should be nearly linearly dependent upon its own concentration at high temperatures. As would be expected, the data points lie close to the linear dependent diffusion profile at high concentrations but deviate at low concentrations where the native vacancies become of comparable magnitude to the chromium-induced vacancies. The native vacancies would increase the penetration beyond that which would be attained if vacancies were only created by the presence of chromium. Because the data points lie approximately as expected in Fig. 23, the experimentally obtained  $D_{Cr}^S$ , which was used to refer the data points to dimensionless coordinates, is considered to be fairly accurate.

The results obtained from the analyses of the diffusion experiments are tabulated in Table 4. Included are the experimental  $D_{Cr}^S$  obtained from Eq. (78) and the theoretical  $D_{Cr}^S$  obtained from Eq. (81). The theoretical values  $\Delta G_3^0$  and  $D_0(2)$  from Eq. (81) are also given along with the saturation chromium concentration and the maximum penetration depth. The maximum penetration depth was the point at which the

TABLE 4.--Results of the Analyses of the Diffusion Profiles of Chromium in NiO

T	P <sub>O<sub>2</sub></sub>	t	maximum penetration	expt D <sub>Cr</sub> <sup>S</sup>	theor D <sub>Cr</sub> <sup>S</sup>	Δ G <sub>3</sub> <sup>o</sup>	D <sub>O</sub> (2)
(°C)	(atm)	(10 <sup>5</sup> sec)	(μ) (x for c 0)	(cm <sup>2</sup> /sec)	(cm <sup>2</sup> /sec)	(cal)	(cm <sup>2</sup> /sec)
1000	1.0	8.712	28	2.17 x 10 <sup>-12</sup>	2.2 x 10 <sup>-12</sup>	5980	9.5 x 10 <sup>-12</sup>
1100	1.0	8.712	64	1.24 x 10 <sup>-11</sup>	1.25 x 10 <sup>-11</sup>	4460	5.75 x 10 <sup>-11</sup>
	1.0	9.342	64	9.5 x 10 <sup>-12</sup>	1.12 x 10 <sup>-11</sup>	4800	5.0 x 10 <sup>-11</sup>
	10 <sup>-2</sup>	8.586	53	8.1 x 10 <sup>-12</sup>	8.1 x 10 <sup>-12</sup>	4900	3.75 x 10 <sup>-11</sup>
	10 <sup>-5</sup>	9.684	45	5.2 x 10 <sup>-12</sup>	5.53 x 10 <sup>-12</sup>	4620	2.5 x 10 <sup>-11</sup>
1200	1.0	5.20	107	5.5 x 10 <sup>-11</sup>	5.5 x 10 <sup>-11</sup>	2300	2.1 x 10 <sup>-10</sup>
	1.0	5.194	109	6.0 x 10 <sup>-11</sup>	5.8 x 10 <sup>-11</sup>	2420	2.2 x 10 <sup>-10</sup>
	10 <sup>-2</sup>	5.21	115	6.2 x 10 <sup>-11</sup>	6.3 x 10 <sup>-11</sup>	2300	2.4 x 10 <sup>-10</sup>
	10 <sup>-5</sup>	5.233	81	3.1 x 10 <sup>-11</sup>	3.1 x 10 <sup>-11</sup>	2500	1.15 x 10 <sup>-10</sup>
1300	1.0	3.781	196	2.8 x 10 <sup>-10</sup>	2.8 x 10 <sup>-10</sup>	1240	9.4 x 10 <sup>-10</sup>
	10 <sup>-2</sup>	2.64	160	2.3 x 10 <sup>-10</sup>	2.4 x 10 <sup>-10</sup>	1060	8.15 x 10 <sup>-10</sup>
	10 <sup>-5</sup>	2.64	147	2.1 x 10 <sup>-10</sup>	2.2 x 10 <sup>-10</sup>	1200	7.15 x 10 <sup>-10</sup>

diffusion profile as drawn by the least-squares polynomial intersected the abscissa at zero specific activity.

At a given temperature, but at lower  $P_{O_2}$ , the maximum penetration depth was less as can be seen in Table 4. This decrease can be attributed to the reduced native vacancy concentration at lower  $P_{O_2}$  in the NiO which in pure NiO has a  $P_{O_2}^{1/6}$  dependence. As the chromium diffuses inward, the native vacancies allow a chromium-independent rate of diffusion at the front of the diffusion profile where the native vacancy and chromium concentrations are comparable. The native vacancies, therefore, cause a deeper penetration than would occur if there were no native vacancies. Because  $D_{Cr}^S$  is obtained by integrating the diffusion profile from  $c = 0$  to  $c_0$  as shown by Eq. (78), the native vacancies would also increase the value of  $D_{Cr}^S$  over that which would be obtained if the crystal contained no native vacancies. The concentration of native vacancies decreased with decreased  $P_{O_2}$ ; therefore, the penetration depth would also be expected to decrease and result in an apparent decrease in  $D_{Cr}^S$ . The theoretical model, Eq. (81), fits the experimental results well at low concentrations so the native vacancies would seem to contribute to the diffusion only at the very low chromium concentrations. This increase in the diffusion rate at low concentrations would have a gradual effect upon the diffusion profile and would not greatly affect the concentration dependence above the lower limit of the theoretical and experimental results. In Table 4, the diffusion coefficient of the two-member complex,  $D_0(2)$ , seemed to depend upon  $P_{O_2}$ . The only variables in Eq. (61) for  $D_0(2)$  are the jump frequencies which will not vary



with  $P_{O_2}$ . Therefore this variance must result from the effect of the native vacancies upon the experimental results to which the theoretical solution was fit.

In Fig. 24, the experimental  $D_{Cr}^S$  is plotted versus  $\log P_{O_2}$ ;  $D_{Cr}^S$  is not a function of  $P_{O_2}$  and should be represented by a horizontal line, but the native vacancies seem to cause an apparent increase in  $D_{Cr}^S$  with  $P_{O_2}$ . As  $P_{O_2}$  decreases,  $D_{Cr}^S$  should approach a value which is independent of the native defects. Therefore the values of  $D_{Cr}^S$  at the lowest oxygen pressure are most nearly the values representing the system if no native vacancies are present in the crystal.

From fitting the theoretical model to the experimental results using Eq. (81) as described in Appendix B, a value for the energy of association of a two-member complex was also obtained. This association energy should be independent of the oxygen pressure so the average value of  $\Delta G_2^0$  at each temperature was used to calculate the number of two-member complexes as a function of the chromium concentration. At  $1000^\circ\text{C}$ ,  $RT/\Delta G_3^0$  was 0.425 so that at this and higher temperatures only two-member complexes were assumed to be present in the crystal. This assumption was made from referring to Figs. 3-6. For this reason the use of Eq. (81) to fit the experimental results was justified. In Fig. 25 the concentration of two-member complexes is plotted versus the chromium concentration for  $1000^\circ\text{C}$ ,  $1100^\circ\text{C}$ ,  $1200^\circ\text{C}$  and  $1300^\circ\text{C}$ . The concentration of complexes is given as the cation fraction of chromium atoms existing in two-member complexes.

As the concentration increases the slope in Fig. 25 increases,

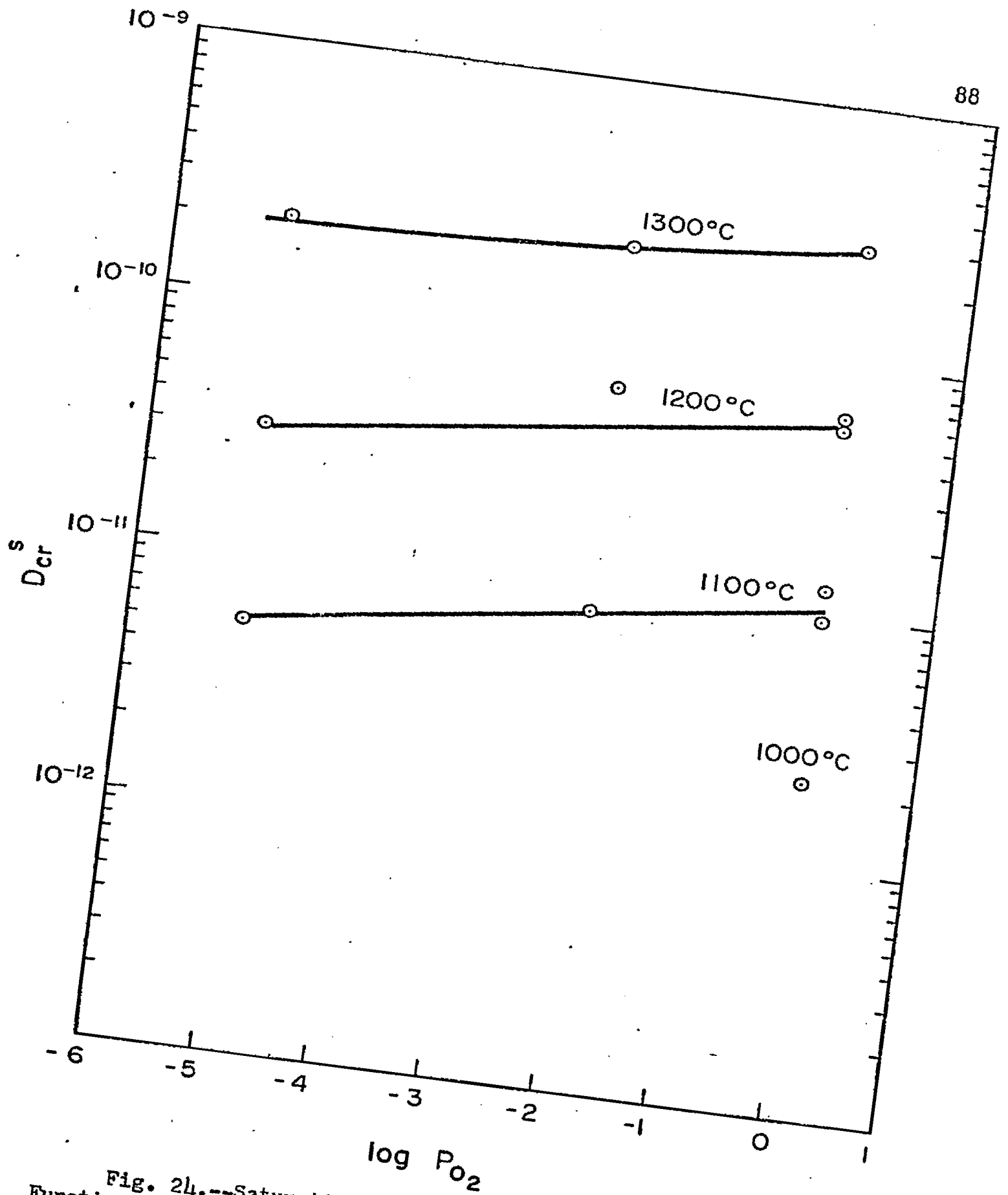


Fig. 24.--Saturation Diffusion Coefficient of Chromium as a Function of Temperature.

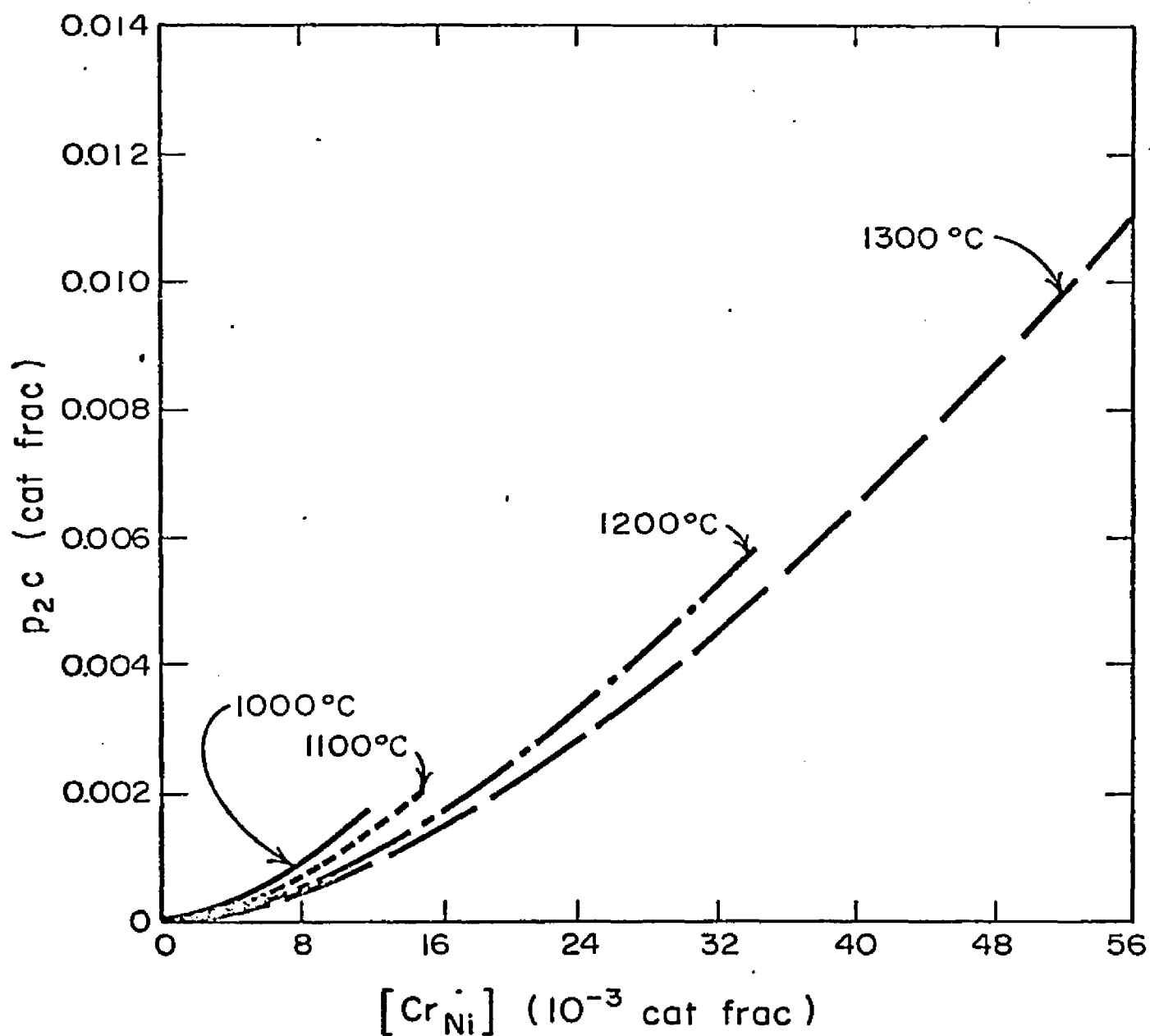


Fig. 25.--Concentration of Chromium-Vacancy Complexes as a Function of Temperature and Chromium Concentration.

and because:

$$D(\text{Cr}) = D_0 \frac{d(p_2 c)}{dc} \quad (88)$$

$D(\text{Cr})$  should increase with the chromium concentration as has been observed. At a specific chromium concentration, the degree of complexing and therefore the number of complexes decreased as the temperature increased. However, the diffusion coefficient increased because the jump frequencies increased faster than  $d(p_2 c) / dc$  decreased.

The temperature dependence of the diffusion coefficient is given by:

$$D(t) = \frac{a^2}{3} \omega_2(T) N_c(T) \quad (89)$$

where  $\omega_2$  is the frequency of a chromium vacancy interchange and  $N_c$  is the number of complexes, i.e., the number of chromium atoms which have a vacancy for a nearest neighbor. The temperature dependence is clarified if the activation energies are inserted into Eq. (89) so that:

$$D(t) = \frac{a^2}{2} \nu \exp\left(\frac{-E_j}{RT}\right) p_2(T) [\text{Cr}_{\text{Ni}}^\bullet] \quad (90)$$

where  $\nu$  is the lattice vibration frequency,  $E_j$  is the activation energy for a chromium-vacancy interchange,  $p_2$  is the degree of association as defined by Eq. (56), and  $[\text{Cr}_{\text{Ni}}^\bullet]$  is the chromium concentration.

In order to calculate the energy of activation of a chromium ion exchanging with a vacancy, the assumption that  $\omega_2 \ll \omega_1$ , is made so

that the diffusion coefficient is described by Eq. (89) and is dependent only upon  $\omega_2$ . Also in plotting the diffusion coefficient as a function of temperature there must be an equal number of chromium ions which are available to jump and, therefore, an equal number of two-member complexes present at each temperature. From Fig. 25 the chromium concentration for each temperature at which a specific concentration of complexes were present in the crystal could be obtained. In the analysis a complex concentration of  $10^{-3}$  cation fraction was chosen. The diffusion coefficients for each temperature and chromium concentration at one atmosphere of oxygen were then calculated from the appropriate diffusion profiles. The logarithm of the diffusion coefficient is plotted versus the reciprocal of the temperature for  $10^{-3}$  cation fraction of complexes and  $P_{O_2} = 1.0$  atmosphere in Fig. 26. From the slope in Fig. 26 the activation energy for the jump of a chromium ion was calculated to be approximately 52 kcal / mole. At  $1000^\circ\text{C}$   $\omega_1 \approx 10\omega_2$  so the assumption that  $\omega_1 \gg \omega_2$  was justified; however, as the temperature increased the ratio of jump frequencies decreased, and at  $1200^\circ\text{C}$   $\omega_1 \approx 8\omega_2$ . At  $1100^\circ\text{C}$  and  $P_{O_2} = 1$  atm the self-diffusion coefficient of nickel is  $1.255 \times 10^{-10}$   $\text{cm}^2/\text{sec}$ , and the diffusion coefficient for chromium in saturated NiO is  $7 \times 10^{-12}$   $\text{cm}^2/\text{sec}$ . The diffusion coefficient for nickel tracers in NiO is given by

$$D_{Ni}^T = 1/6 (12 [v_{Ni}^{''}] \omega_1) r^2 f \quad (91)$$

where  $r$  is the jump distance,  $f$  is the correlation factor, and  $[v_{Ni}^{''}]$  and  $\omega_1$  are as previously defined. From Eq. (91)  $\omega_1$  can be calculated,

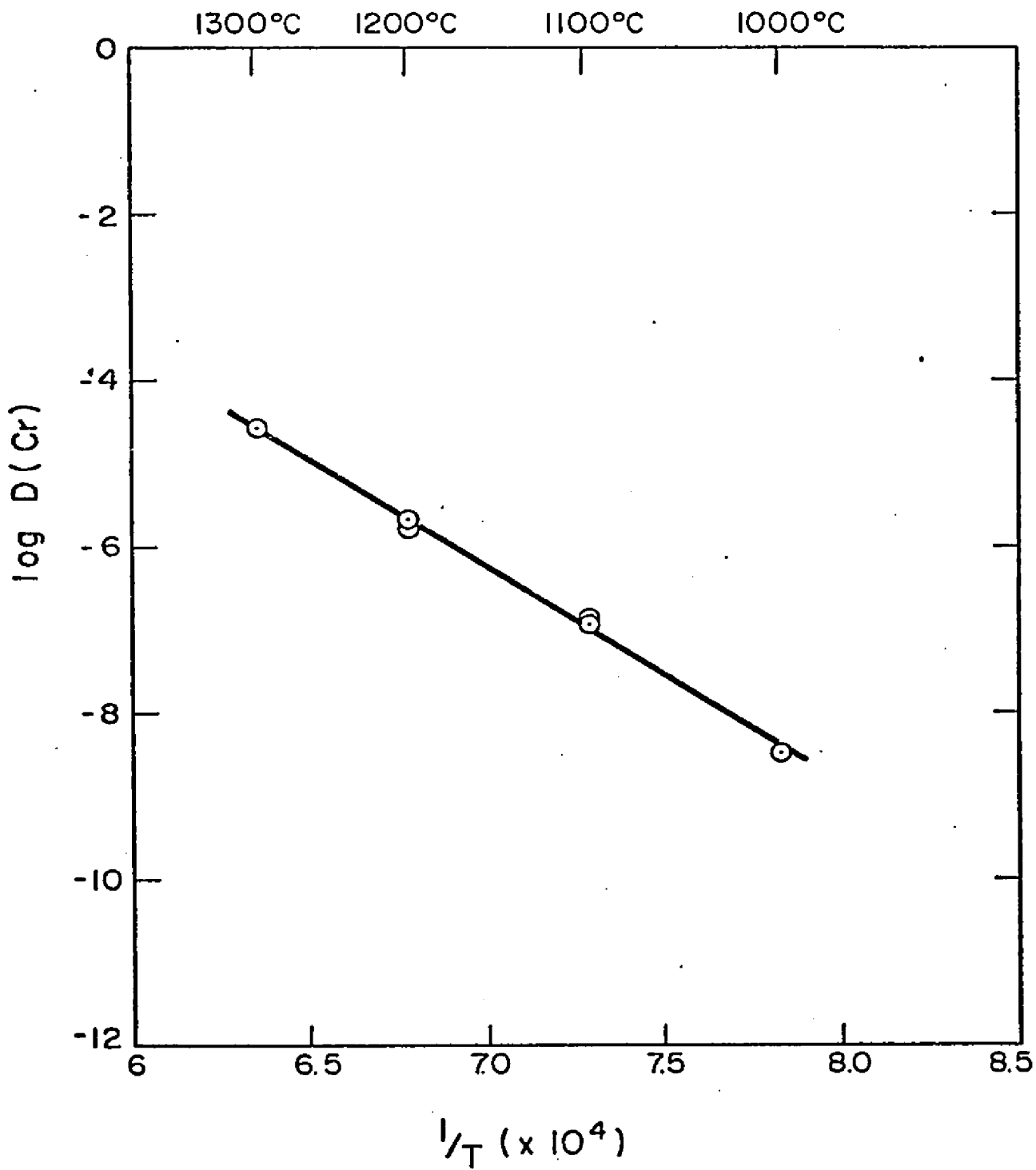


Fig. 26.--Log  $D(\text{Cr})$  as a Function of  $1/T$  for  $10^{-3}$  Cation Fraction of Chromium-Vacancy Complexes.

and because  $\omega_1 \approx 9\omega_2$ ,  $\omega_2$  can be calculated. The correlation factor for the diffusion of chromium can be obtained by substitution of the concentration of two-member complexes for  $[V_{Ni}^{''}]$  and  $\omega_2$  for  $\omega_1$ . The correlation factor was evaluated to be approximately 0.1. Although the chromium increases the concentration of nickel vacancies, the diffusion of chromium is slower than the nickel self-diffusion because only a fraction of the chromium ions exist in complexes simultaneously,  $\omega_2$  is smaller than  $\omega_1$ , and the chromium jumps are highly correlated. The calculation of the correlation factor is rather inaccurate because of the large uncertainty in the native vacancy concentration and the uncertainty in the activation energies for the nickel-vacancy and chromium-vacancy exchange jumps. The correlation factor calculated from the jump frequencies is about 0.9 which is reasonably close to the above value.

According to Nowick<sup>53</sup> the effective activation energy for the diffusion coefficient at low impurity concentrations and high temperatures is:

$$E_j \approx \Delta H_j - \Delta H_2^0 \quad (92)$$

where  $\Delta H_j$  is the enthalpy of activation for an impurity-vacancy interchange and  $\Delta H_2^0$  is the enthalpy of formation of a complex. A vacancy formation energy was not included because the vacancies are present to maintain electrical neutrality in the crystal rather than being thermally produced defects. This relation would apply for a divalent impurity in an alkali halide where the impurity and vacancy have equal but opposite charges. According to Lidiard<sup>26</sup> at the limiting case  $c \exp$

$(\Delta G^{\circ}/RT) \ll 1$ , the diffusion coefficient is given by:

$$D(c) = 8 a^2 \omega_2 c \exp (\Delta G^{\circ}/RT), \quad (93)$$

where  $\Delta G^{\circ}$  is the energy of association of the complex. However, in the present system at the limit of  $c \exp (\Delta G_3^{\circ}/RT) \ll 1$ , the diffusion coefficient is given by Eq. (66) which reduces to:

$$D(\text{Cr}) = \frac{a^2}{3} \omega_2 \left( \frac{2 Z_2 c \exp (\Delta G_3^{\circ}/2RT)}{3 Z_2 c \exp (\Delta G_3^{\circ}/2RT) + 1} \right) \quad (94)$$

Obviously Eq. (92) would not apply to the present system, but the energy of association would be expected to affect the effective activation energy of the diffusion coefficient. In Fig. 27 the logarithm of the diffusion coefficient is plotted versus the reciprocal of the temperature at one atmosphere of oxygen and chromium concentration of  $1.2 \times 10^{-2}$  cation fraction. From the slope in Fig. 27 the effective activation energy was evaluated to be 49.0 kcal / mole. Therefore the activation energy for the diffusion coefficient is affected by the energy of association for the complexes but the effect is not described by Eq. (92).

In Fig. 28 the diffusion coefficient is plotted versus the chromium concentration at  $P_{O_2} = 1.0$  atm and 1000°C, 1100°C, 1200°C, and 1300°C. As the temperature increases the theoretical model would predict that the dependence of the diffusion coefficient upon the chromium concentration becomes more linear. In Fig. 29 the experimental results for  $D(\text{Cr})/D_{\text{Cr}}^S$  versus the chromium concentration are shown for  $P_{O_2} = 1.0$  at 1100°C and 1300°C. In Fig. 29, the solid line is the experimental



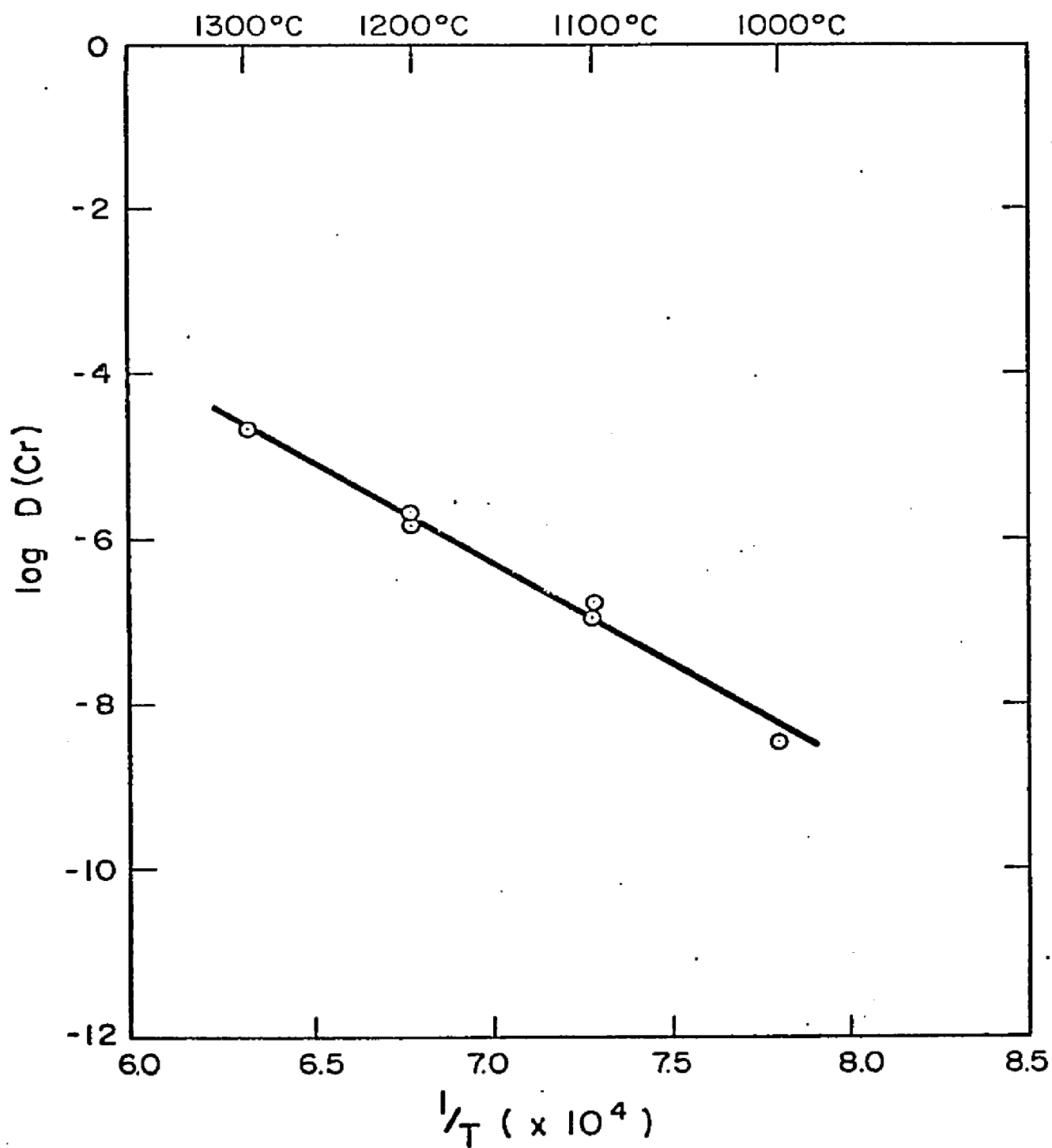


Fig. 27.--Log  $D(\text{Cr})$  as a Function of  $1/T$  for  $1.2 \times 10^{-2}$  Cation Fraction of Chromium.

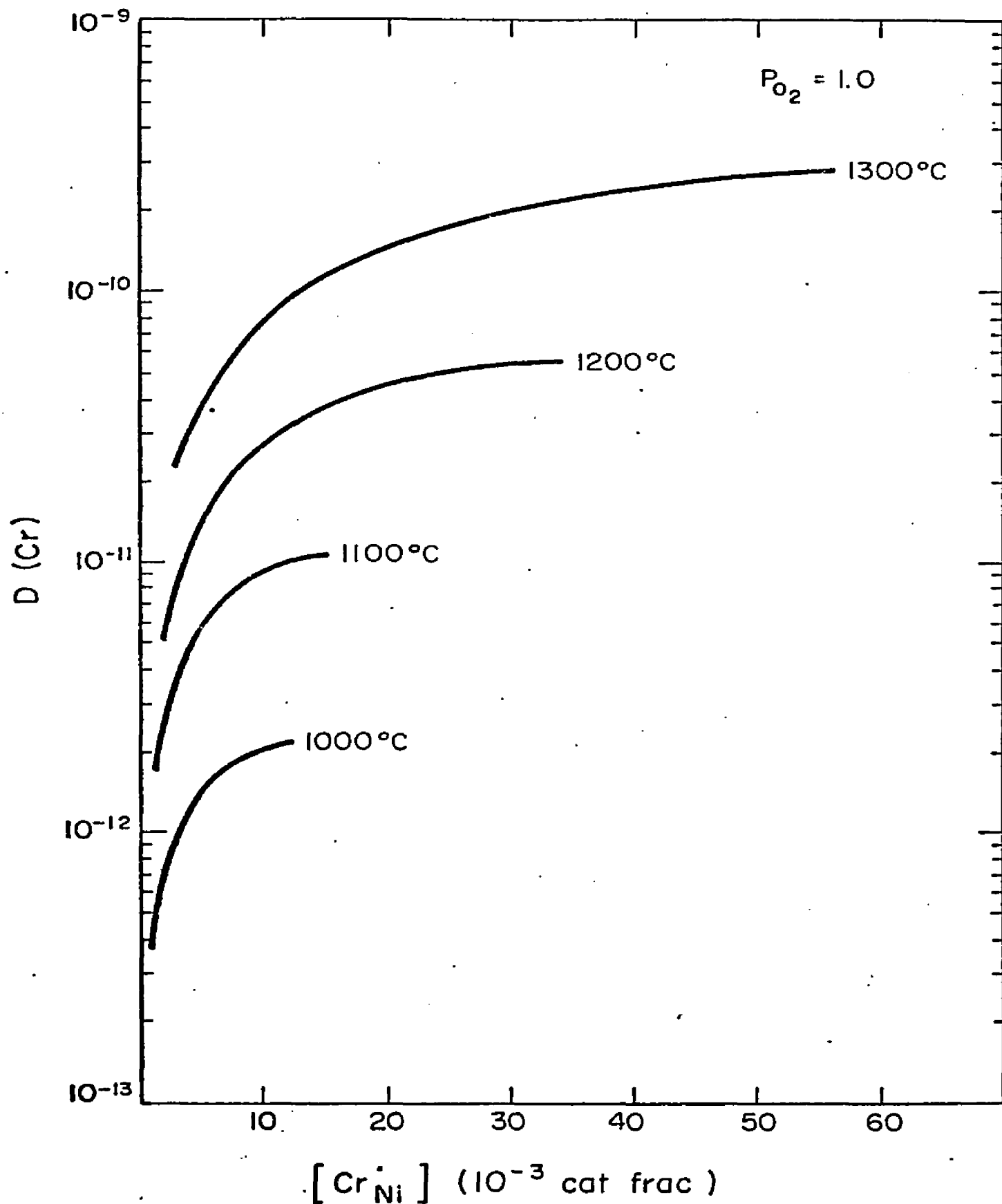


Fig. 28.--Diffusion Coefficient of Chromium as a Function of Chromium Concentration and Temperature.

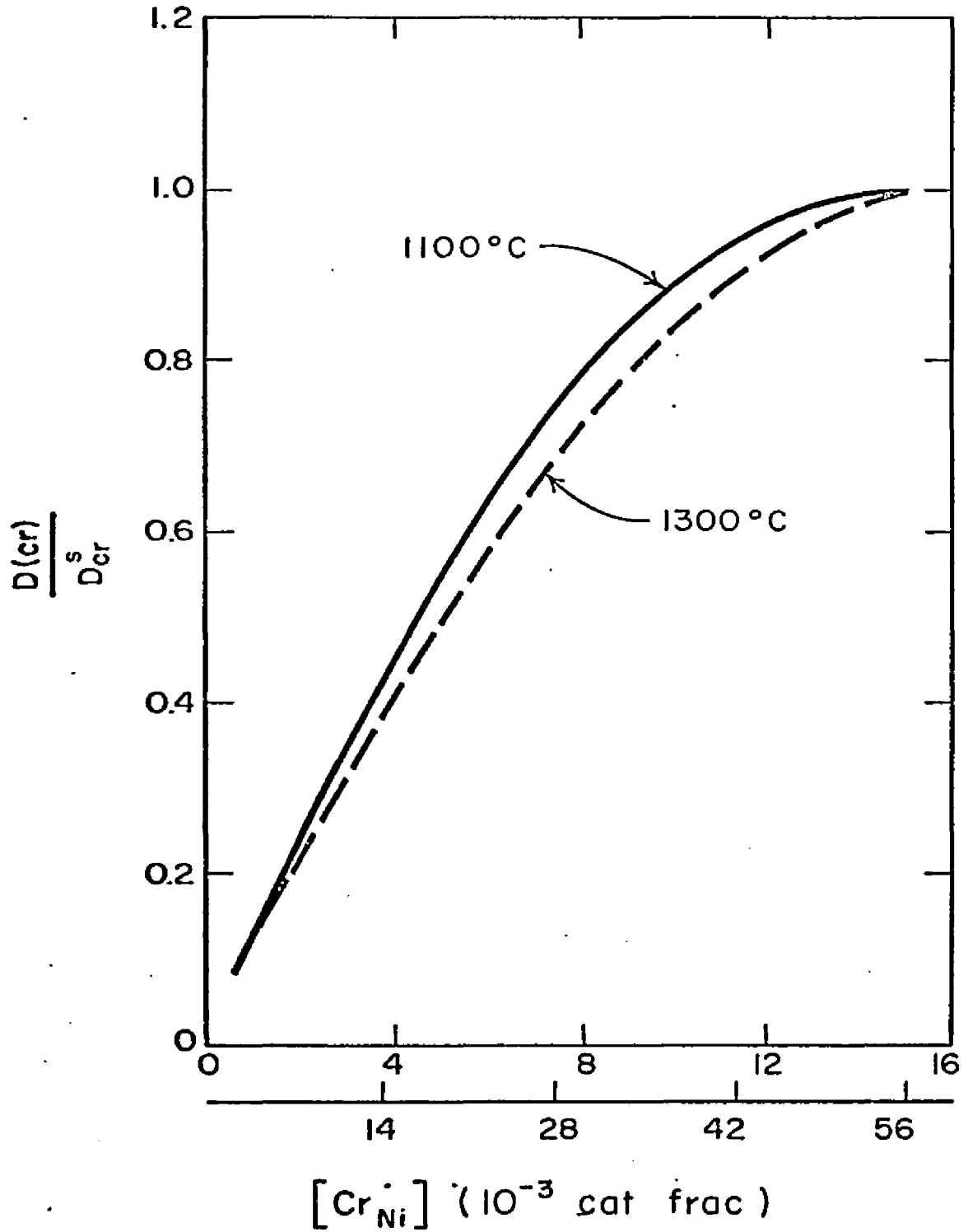


Fig. 29.--Normalized Diffusion Coefficient of Chromium as a Function of the Chromium Concentration at 1100°C and 1300°C.

results for 1100°C and the dashed line is the results for 1300°C. The curvature for the high temperature curve is less than for the low temperature curve. With the assumption that the effect of the vacancies diffusing ahead of the chromium is fairly constant, the experimental results indicate that the dependence of the diffusion coefficient upon the chromium concentration becomes more linear as the temperature is increased. Greskovich<sup>38</sup> found that the interdiffusion coefficient of chromium and nickel in NiO was linearly dependent upon the chromium concentration at 1330°C and above. Because the diffusion of chromium was the rate determining step, the diffusion coefficient of chromium was then linearly dependent upon the chromium concentration. At 1330°C at approximately  $10^{-2}$  cation fraction of chromium and above he observed a linear dependence which would correspond fairly well to the results obtained in this work at 1300°C. No meaningful direct comparison to Seltzer's<sup>40</sup> work can be made except to note that he also observed a concentration dependence for the diffusion of chromium in NiO at 1100°C to 1250°C.

The activation energy for a chromium ion-vacancy interchange was evaluated as 51.9 kcal / mole. This value can be compared with the activation energy for tracer diffusion of chromium in NiO which has been evaluated as 55.0 kcal / mole by Greskovich and 47.0 kcal / mole by Seltzer. These latter two activation energies are the activation energy of the vacancy-chromium exchange and compare well with the value obtained in this work.

## VI. SUMMARY AND CONCLUSIONS

A theory has been developed to describe the diffusion of trivalent impurities in a divalent metal oxide. The theory has been evaluated for the diffusion of trivalent chromium in NiO.

At 1000°C and above, from the reasonable fit of the experimental results to the theory, chromium seems to diffuse in NiO by a mechanism involving the diffusion of two-member complexes composed of a chromium ion and cation vacancy. The presence of chromium ions in the NiO lattice causes the formation of cation vacancies to maintain electrical neutrality. Because chromium diffuses by a vacancy mechanism and causes the creation of vacancies, the diffusion coefficient is a function of the chromium concentration.

The presence of native vacancies affects the diffusion of chromium at low concentrations which causes deeper penetration than results from the theory which neglects native defects. Because the concentration of native vacancies varies with the oxygen pressure, a slight apparent dependence of the diffusion coefficient upon the oxygen pressure is caused.

The diffusion coefficient of chromium in NiO saturated with chromium increases from approximately  $2 \times 10^{-12}$  cm<sup>2</sup>/sec at 0.012 cation fraction of chromium at 1000°C to  $2 \times 10^{-10}$  cm<sup>2</sup>/sec at 0.056 cation fraction of chromium at 1300°C.

The diffusion of chromium is slower than nickel self-diffusion

because the equilibrium number of complexes is small, the jump frequency of a chromium ion-vacancy exchange is about a tenth of that for a nickel ion-vacancy exchange, and the chromium ion-vacancy exchanges are highly correlated, i.e.  $f = 0.1$ .

The activation energy for the chromium-vacancy exchange is approximately 52 kcal, and the effective activation energy for the chromium diffusion coefficient is approximately 49.0 kcal. The bonding energy of the chromium-vacancy complex accounts for the difference between the effective activation energy and the jump activation energy.

From the model which has been developed and the reasonable fit of the theory to the experimental results, the diffusion coefficient for chromium in NiO above 1000°C is described by:

$$D(\text{Cr}) = D_0(2) \left( \frac{3}{4} - \frac{\left( \frac{[\text{Cr}_{\text{Ni}}^\bullet]}{8} + \frac{3}{4W} \right)}{\left( \frac{[\text{Cr}_{\text{Ni}}^\bullet]^2}{4} + \frac{3[\text{Cr}_{\text{Ni}}^\bullet]}{W} + \frac{1}{W^2} \right)^{1/2}} \right) \quad (81)$$

where

$$W = Z_2 \exp(\Delta G_2^\circ/RT) \quad (82)$$

$D_0(2)$  is the diffusion coefficient of the two-member complex,  $Z_2$  is the number of distinct configurations of a two-member complex, and  $\Delta G_2^\circ$  is the energy of association of a two-member complex which was found to decrease from approximately 3000 calories at 1000°C to approximately 600 calories at 1300°C.

## APPENDIX A

This computer program was used to draw the diffusion profile through the data points by a least squares fit to a polynomial and evaluate the diffusion coefficient as a function of the chromium concentration from the diffusion profile according to Eq. (76)

```

DIMENSION X(500),CPSM(500),CPS(500),BLOCK1(100),BLOCK2(100),
2C(10,10),YCAL(500),XIN(500),YOUT(500),RMS(10),VAR(10),DZERO(10),
3DCONC(500),DCDX(500),CONC(500),DCDCO(500),W(500),DIST(500),
4RATIO(500),CIN(500),DXDC(500),XOUT(500),BLOCK3(500),BLOCK4(500),
5CC(10,10),XCAL(500),SMR(10),RAV(10),DELTA(10)
100 FORMAT (8F10.0)
200 FORMAT (10X,'IER',I10)
300 FORMAT (5X,'OUTPUT',5X,'K',I5)
400 FORMAT (10X,'DZERO',E15.5,5X,'DCONC',E15.5,5X,'CONC',E15.5,
15X,'DCDCO',E15.5)
500 FORMAT (10X,'X',E15.5,5X,'CPSM',E15.5,5X,'W',E15.5)
600 FORMAT (10X,'K',I5,5X,'KK',I5,5X)
650 FORMAT (2X,'C1-CK',10E12.5)
700 FORMAT (10X,'RMS',E15.5,5X,'VAR',E15.5)
750 FORMAT (10X,'TEMP',E15.5,5X,'PRESS',E15.5)
800 FORMAT (10X,'CIN',E15.5,5X,'XOUT',E15.5,5X,'CPS',E15.5,5X,'DCDX',
1,E15.5)
850 FORMAT (5X,'XIN',E15.5,5X,'YOUT',E15.5)
920 FORMAT (10X,'RATIO',E15.5,5X,'DIST',E15.5)
TEMP = 1300.0
PRESS = 0.00001
TIME = 264000.0
NN = 39
NOPT = 11
DIV = 15.0
CSAT = 0.056
INCRE = 20
TINCRE = INCRE
NUM = INCRE + 1
NNN = NN + 1
READ (5,100) (X(I),I=1,NN)
READ (5,100) (CPSM(I),I=1,NN)
READ (5,100) (W(I),I = 1,NNN)
DO 1100 K = 1,3
WRITE (6,300) K

```



```

-----
KK = K - 1
C OBTAIN LEAST SQUARE FIT TO THE DATA
-----
CALL PCFI (X,CPSM,V,1,NN,KK,2,BLOCK1,BLOCK2,C,YCAL,RMS,VAR)
DO 900 J = 1,NOPT
TJ = J
XIN(J) = (-DIV + (DIV*TJ))
-----
900 CONTINUE
C CHANGE CURVE TO INCREMENTS OF X
-----
CALL PCFE (XIN,NOPT,KK,YOUT)
WRITE (6,850) (XIN(J),YOUT(J),J = 1,NOPT)
DELTA(K) = YOUT(1)/TINCRE
IF (K.EQ.1) X(500) = XIN(1)
IF (K.EQ.2) X(499) = XIN(1)
IF (K.EQ.3) X(498) = XIN(1)
IF (K.EQ.1) CPSM(500) = YOUT(1)
IF (K.EQ.2) CPSM(499) = YOUT(1)
IF (K.EQ.3) CPSM(498) = YOUT(1)
WRITE (6,650) (C(K,J),J = 1,K)
WRITE (6,700) (RMS(K),VAR(K))
-----
1100 CONTINUE
DO 1300 K = 1,3
WRITE (6,300) K
IF (K.EQ.1) X(NNN) = X(500)
IF (K.EQ.2) X(NNN) = X(499)
IF (K.EQ.3) X(NNN) = X(498)
IF (K.EQ.1) CPSM(NNN) = CPSM(500)
IF (K.EQ.2) CPSM(NNN) = CPSM(499)
IF (K.EQ.3) CPSM(NNN) = CPSM(498)
-----
KK = K - 1
C OBTAIN LEAST SQUARE FIT FOR NEW COORDINATES
-----
CALL PCFI (CPSM,X,W,0,NNN,KK,2,BLOCK3,BLOCK4,CC,XCAL,SMR,RAV)
DO 875 I = 1,NUM
TI = I
CIN(I) = (-DELTA(K) + DELTA(K)*TI)
-----

```

875 CONTINUE

C CHANGE TO INCREMENTS OF CONCENTRATION

CALL PCFE (CIN, NUM, KK, XOUT)

DO 950 I = 1, NUM

CONC(I) = CIN(I)\*CSAT/CIN(NUM)

950 CONTINUE

C INTEGRATE AREA UNDER THE CURVE

CALL QTFG (CONC, XOUT, CPS, NUM)

C OBTAIN SLOPES FROM THE CURVE

CALL DGT3 (CONC, XOUT, DXDC, NUM, IER)

WRITE (6, 200) IER

IF (K.EQ.1) GO TO 1025

DO 885 I = 1, NUM

DCDX(I) = 1.0/DXDC(I)

885 CONTINUE

WRITE (6, 800) (CIN(I), XOUT(I), CPS(I), DCDX(I), I=1, NUM)

DZERO(K) = CPS(NUM)/(2.0\*TIME\*DCDX(NUM))

DO 1000 I = 1, NUM

DCONC(I) = CPS(I)/(2.0\*TIME\*DCDX(I))

DCDCO(I) = DCONC(I)/DZERO(K)

1000 WRITE (6, 400) DZERO(K), DCONC(I), CONC(I), DCDCO(I)

DO 910 I = 1, NN

RATIO(I) = CPSM(I)/YOUT(1)

DIST(I) = X(I)/(2.0\*(DZERO(K)\*TIME)\*\*0.5)

WRITE (6, 920) RATIO(I), DIST(I)

910 CONTINUE

WRITE (6, 750) TEMP, PRESS

WRITE (6, 600) K, KK

1025 CONTINUE

1300 CONTINUE

CALL EXIT

END

## APPENDIX B

This computer program was used to fit the theoretical model described by Eq. (81) to the experimentally evaluated diffusion coefficient, evaluate the association energy and diffusion coefficient of the two-member complex, and evaluate the theoretical dependence of the diffusion coefficient as a function of the chromium concentration again using Eq. (81).

The theory was fit to Eq. (81) for a particular diffusion profile by assuming a value for  $D_o(2)$  and for a specific concentration varying  $\Delta G_3^o$  until  $D(\text{Cr})$  calculated from the equation is within 5% of the value of the diffusion coefficient obtained from the appropriate diffusion profile at that concentration. The value of  $\Delta G_3^o$  which yielded the best fit was then inserted into Eq. (81) and  $D_o(2)$  was varied until  $D(\text{Cr})$  was again within 5% of the experimental value. The value of  $D_o(2)$  which yielded the best fit was then inserted into Eq. (81) and  $\Delta G_3^o$  was again varied. This process was reiterated until  $D_o(2)$  and  $\Delta G_3^o$  became constant through two successive iterations. The values of  $D_o(2)$  and  $\Delta G_3^o$  obtained from several concentrations were averaged, and these averaged values were the theoretical parameters which related the theoretical model to the experimental results for the diffusion profile under consideration. By placing these parameters into Eq. (81) and varying the concentration, the theoretical dependence of the diffusion coefficient upon the concentration was obtained.

```
DIMENSION DG3(25),DCO(25),DCONC(50),CONC(50),DELTA(25,2),  
2DZERO(25,25),DC(50),DCDU(50),DCD0-2(50),CON(50)
```

```
10 FORMAT (5E15.5)
```

```
11 FORMAT (5X, 'I', I4, 5X, 'L', I4, 5X, 'J', I4, 5X, 'DCONC', E15.5, 5X,  
2'DCALC', E15.5, 5X, 'DELTA', E15.5)
```

```
12 FORMAT (5X, 'I', I4, 5X, 'L', I4, 5X, 'J', I4, 5X, 'DCONC', E15.5, 5X,  
2'DCALC', E15.5, 5X, 'DELTA', E15.5)
```

```
13 FORMAT (5X, 'I', I4, 5X, 'L', I4, 5X, 'J', I4, 5X, 'DCONC', E15.5, 5X,  
2'DCALC', E15.5, 5X, 'ZERO', E15.5)
```

```
14 FORMAT (5X, 'I', I4, 5X, 'L', I4, 5X, 'K', I4, 5X, 'LOOP K = Z', E15.5)
```

```
15 FORMAT (5X, 'I', I4, 5X, 'L', I4, 5X, 'DELTA', E15.5, 5X, 'ZERO', E15.5)
```

```
16 FORMAT (5X, 'I', I4, 5X, 'L', I4, 5X, 'DG3', E15.5, 5X, 'DCO', E15.5)
```

```
17 FORMAT (5X, 'CONC', E15.5, 5X, 'DCONC', E15.5, 5X, 'DG3', E15.5, 5X,  
2'DCO', E15.5)
```

```
18 FORMAT (10X, 'DCO', E15.5, 5X, 'Z', E15.5)
```

```
19 FORMAT (5X, 'DC', E15.5, 5X, 'DC', E15.5, 5X, 'DCD0', E15.5,  
25X, 'DCD02', E15.5)
```

```
20 FORMAT (10X, 'OUTPUT')
```

```
44 FORMAT (10X, 'TEMP', E15.5, 5X, 'PRESS', E15.5)
```

```
NR = 10
```

```
TEMP = 1200.0
```

```
PRESS = 1.0
```

```
TIME = 520000.0
```

```
CSAT = 0.034
```

```
DELTA = 0.002
```

```
LL = 17
```

```
T = 1573.0
```

```
DOEXP = 0.0054775
```

```
Z = 12.0
```

```
R = 1.9872
```

```
WRITE (6,20)
```

```
WRITE (6,44) TEMP, PRESS
```

```
READ (5,10) (CONC(I), I = 1, NR)
```

```
READ (5,10) (DCONC(I), I = 1, NR)
```

```
DO 1202 JJ = 1, R
```

```
TJJ = JJ
```

```

DSTART = 0.015 + 0.001*TJJ
DO 1000 I = 1, NM
DO 600 L = 1, 20
DO 200 J = 1, 31
TJ = J
DELTA(I, L) = 200.0*TJ
IF (L.EQ.1.AND.J.FO.1) DZERU(I, L-1) = DSTART
DCALC = DZERU(I, L-1)*(3.0/4.0 - ((CONC(I))/3.0) + (3.0/(4.0*Z*
2*EXP(DELTA(I, L)/(2.0*R*T)))))/((CONC(I))**2.0/4.0) + ((3.0*
3*CONC(I))/(Z*EXP(DELTA(I, L)/(2.0*R*T)))) + (1.0/(Z*EXP(DELTA(I,
4(I, L)/(2.0*R*T))**2.0))**0.5))
IF (ABS(DCONC(I) - DCALC)/DCONC(I)).GT.0.05) GO TO 150
GO TO 250
150 CONTINUE
200 CONTINUE
250 CONTINUE
DO 400 K = 1, 31
TK = K
DZERU(I, L) = 0.01 + 0.001*TK
DCALC = DZERU(I, L)*(3.0/4.0 - ((CONC(I))/3.0) + (3.0/(4.0*Z*
2*EXP(DELTA(I, L)/(2.0*R*T)))))/((CONC(I))**2.0/4.0) + ((3.0*
3*CONC(I))/(Z*EXP(DELTA(I, L)/(2.0*R*T)))) + (1.0/(Z*EXP(DELTA(I,
4(I, L)/(2.0*R*T))**2.0))**0.5))
IF (ABS(DCONC(I) - DCALC)/DCONC(I)).GT.0.05) GO TO 350
GO TO 450
350 CONTINUE
400 CONTINUE
450 CONTINUE
IF (L.EQ.1) GO TO 550
IF (ABS(DELTA(I, L) - DELTA(I, L-1))/DELTA(I, L)).NE.0.0.
2 OR ABS(DZERU(I, L) - DZERU(I, L-1))/DZERU(I, L).NE.0.0)
3 GO TO 550
DCR(I) = DELTA(I, L)
DCO(I) = DZERU(I, L)
GO TO 650

```

550 CONTINUE

DG3(I) = DELTA6(I,20)  
DC0(I) = DZER0(I,20)

650 CONTINUE  
1000 CONTINUE

WRITE (6,17) (CONC(I),DCONC(I),DG3(I),DC0(I), I = 1,N)

TIM = TIM  
SUMA = 0.0  
DO 1050 I = 1,N  
SUMA = SUMA + DG3(I)

DG1 = SUMA/TIM  
SUMB = 0.0  
DO 1100 I = 1,NM  
SUMB = SUMB + DC0(I)

DZ0 = SUMB/TIM  
WRITE (6,18) DG0,DZ0  
DO 1200 M = 1,11  
TM = M

C = DELTA6\*TM  
DC(M) = DZ0\*((3.0/4.0 - ((C/8.0) + (3.0/(4.0\*Z\*EXP(DG0/(2.0  
2\*\*8\*1)))))/((C\*\*2.0)/4.0) + ((3.0\*C)/(Z\*EXP(DG0/(2.0\*\*8\*1))))  
3 + (1.0/((Z\*EXP(DG0/(2.0\*\*8\*1))))\*\*2.0))\*\*0.5)))  
DC0(M) = DC(M)/DZ0  
DC02(M) = DC(M)/DZ\*XP  
WRITE (6,19) M,C,DC(M),DC0(M),DC02(M)

1200 CONTINUE  
1202 CONTINUE

CALL EXIT  
END

## APPENDIX C

To calculate the energy necessary to move a vacancy beyond the limit of the possible rearrangement of positive holes both the entropy of mixing and the electrical energy must be considered. For an illustrative calculation,  $10^{-3}$  cation fraction of vacancies were assumed to be moved from a  $1 \text{ cm}^3$  of NiO in local equilibrium with  $10^{-2}$  cation fraction of chromium to  $1 \text{ cm}^3$  of NiO in equilibrium with the atmosphere. The electrical energy for the species in the NiO lattice was calculated from Eq. (13). With Stirling's approximation, Eq. (83) becomes:

$$S = -k (N_c \ln N_c - \sum_i n_i \ln n_i) \quad (95)$$

from which the entropy of mixing the species in the lattice can be calculated.

From Eq. (13) and Eq. (95), the electrical energy and entropy for each piece of NiO was calculated before and after the vacancies were redistributed. At  $1000^\circ\text{C}$  and  $P_{\text{O}_2} = 1.0$ , the change in the electrical energy would be approximately + 10000 calories per vacancy and the change in the entropy would be approximately - 5000 calories. Therefore, approximately 5000 calories are necessary to move a cation vacancy from a position in equilibrium with  $10^{-3}$  cation fraction of chromium to a position with no chromium if positive holes were not available to maintain local electrical neutrality. If holes were available to maintain the local electrical neutrality, the change in the electrical energy would be reduced and the cation vacancies would be moved more easily.

## APPENDIX D

TABLE 5. Diffusion Data for Chromium in Nickel Oxide

Symbols used in Table:

$x$  = distance to the center of the section (microns)

$\sigma$  = specific activity of the section (counts per second per  
micron)

$t$  = length of the diffusion anneal (sec)

$T$  = temperature of the diffusion anneal ( $^{\circ}\text{C}$ )

$P_{\text{O}_2}$  = oxygen pressure during the diffusion anneal (atm)



TABLE 5. Continued

T (°C)	P <sub>O<sub>2</sub></sub> (atm)	t (sec)	x(μ)	σ (cps/μ)			
1000	1.0	8.712 x 10 <sup>5</sup>	4.86	0.664			
			9.88	0.564			
			17.35	0.2537			
			12.18	0.0764			
			9.18	0.477			
			17.56	0.206			
			26.79	0.051			
			6.0	0.66			
			15.88	0.305			
			27.06	0.0582			
			5.51	0.627			
			14.00	0.315			
			25.72	0.353			
			1100	1.0	8.712 x 10 <sup>5</sup>	5.90	31.2
						12.69	30.3
18.98	28.5						
25.98	24.7						
35.00	18.91						
48.25	8.23						
62.45	2.02						
4.87	34.7						
9.79	32.3						
15.19	29.45						
20.53	27.85						
27.18	21.6						
35.30	16.28						
44.69	10.63						
55.03	3.51						
66.27	0.084						
1100	1.0	9.312 x 10 <sup>5</sup>	10.17	17.1			
			19.64	12.5			
			30.06	8.73			
			40.10	6.5			
			52.84	2.33			
			67.61	0.11			
			10.42	15.78			
			19.43	12.12			
			30.38	9.67			

TABLE 5. Continued

<u>T (°C)</u>	<u>P<sub>O<sub>2</sub></sub> (atm)</u>	<u>t (sec)</u>	<u>x(μ)</u>	<u>σ(cps/μ)</u>			
1100	1.0	9.342 x 10 <sup>5</sup>	48.16	4.46			
			66.98	0.506			
			6.99	15.95			
			13.10	15.01			
			19.97	12.05			
			27.31	10.95			
			35.95	7.58			
			47.47	3.73			
			62.45	0.537			
			11.14	14.24			
			21.71	11.4			
			33.62	8.36			
			51.3	3.52			
			69.95	0.106			
1100	10 <sup>-2</sup>	8.586 x 10 <sup>5</sup>	6.67	11.92			
			13.02	8.34			
			20.01	8.14			
			29.22	4.57			
			37.77	2.63			
			50.97	0.67			
			17.74	7.37			
			32.03	4.84			
			51.72	1.11			
			1100	10 <sup>-5</sup>	9.684 x 10 <sup>5</sup>	10.90	.519
19.45	.468						
27.95	.259						
38.78	.0804						
10.28	.496						
19.80	.337						
31.90	.169						
44.27	.0345						
1200	1.0	5.2 x 10 <sup>5</sup>				7.11	57.0
						12.37	53.8
			17.76	50.1			
			23.41	48.0			
			30.32	43.5			
			36.54	41.0			
			43.45	32.93			
			50.87	30.41			

TABLE 5. Continued

T (°C)	P <sub>O<sub>2</sub></sub> (atm)	t (sec)	x(μ)	σ(cps/μ)			
1200	1.0	5.2 x 10 <sup>5</sup>	58.35	26.88			
			66.72	22.93			
			77.83	14.22			
			95.47	4.75			
			112.67	0.58			
			9.68	56.8			
			20.0	49.1			
			29.83	46.3			
			39.19	41.1			
			47.22	36.7			
			1200	1.0	5.194 x 10 <sup>5</sup>	8.90	21.25
						13.52	22.2
						20.47	20.65
						29.74	19.65
						38.38	15.3
51.00	13.0						
65.08	10.27						
75.36	8.25						
87.61	4.76						
101.1	1.75						
114.4	.082						
9.58	21.2						
15.69	21.63						
22.18	19.6						
28.85	18.15						
35.77	16.39						
43.48	15.68						
8.38	20.19						
14.26	22.19						
19.94	19.84						
28.58	18.39						
39.43	18.0						
52.33	12.69						
63.95	10.78						
73.20	8.47						
84.24	5.15						
96.94	1.93						
111.1	.181						
1200	10 <sup>-2</sup>	5.21 x 10 <sup>5</sup>	8.34	7.08			
			15.31	7.77			

TABLE 5. Continued

<u>T (°C)</u>	<u>P<sub>O<sub>2</sub></sub> (atm)</u>	<u>t (sec)</u>	<u>x(μ)</u>	<u>σ(cps/μ)</u>
1200	10 <sup>-2</sup>	5.21 x 10 <sup>5</sup>	24.87	7.29
			35.34	6.49
			46.76	5.52
			60.75	4.41
			76.34	3.19
			88.84	2.27
			100.2	1.07
			114.7	.183
			5.69	8.64
			10.98	8.47
			18.47	7.88
			26.15	7.27
			33.82	6.90
			42.68	5.92
			52.49	5.26
			63.03	4.44
			75.60	3.325
			91.41	1.738
			111.8	.334
			11.11	8.74
			18.80	7.61
			26.60	7.24
			34.87	6.14
			44.42	5.10
			55.14	4.28
			67.77	3.63
			83.82	2.24
			99.04	1.012
			113.1	.121
			1200	10 <sup>-5</sup>
16.83	2.94			
24.51	2.63			
33.05	2.18			
42.61	1.75			
54.71	1.218			
70.63	.352			
86.47	.047			
99.9	.075			
5.54	3.51			
11.53	3.24			
18.38	3.00			

TABLE 5. Continued

T (°C)	P <sub>O<sub>2</sub></sub> (atm)	t (sec)	x(μ)	σ (cps/μ)			
1200	10 <sup>-5</sup>	5.233 x 10 <sup>5</sup>	26.44	2.59			
			36.15	2.075			
			46.24	1.61			
			56.39	1.04			
			68.20	.375			
			81.95	.0754			
			10.79	2.69			
			19.10	2.78			
			27.29	2.54			
			36.93	2.02			
			47.84	1.485			
			61.97	.758			
			77.37	.227			
			7.93	3.65			
			15.96	3.20			
			24.93	2.575			
			35.53	2.025			
			46.77	1.58			
			60.54	.716			
			76.70	.1045			
			1300	1.0	3.781 x 10 <sup>5</sup>	30.45	32.1
						43.30	28.3
						55.39	28.0
						67.48	24.2
						79.40	22.8
						91.49	22.0
						103.4	19.85
114.4	18.3						
127.3	15.45						
141.5	13.18						
157.3	9.58						
171.2	6.38						
185.9	3.80						
32.28	32.25						
44.07	29.4						
56.52	27.4						
68.32	26.7						
81.37	26.7						
93.84	22.15						
107.6	17.75						
122.0	16.0						

TABLE 5. Continued

$T$ ( $^{\circ}\text{C}$ )	$P_{\text{O}_2}$ (atm)	$t$ (sec)	$x$ ( $\mu$ )	$\sigma$ (cps/ $\mu$ )
1300	1.0	$3.781 \times 10^5$	137.9	13.6
			154.0	9.57
			168.8	6.63
			13.04	38.44
			20.58	35.3
			30.28	31.6
			39.68	32.7
			49.93	28.6
			59.67	27.0
			68.81	26.0
			79.28	22.3
			89.56	23.1
			99.97	20.0
			112.2	17.4
			124.5	14.17
			136.2	11.51
			149.3	8.1
			163.3	6.72
			178.4	2.2
			14.13	35.5
			23.33	32.4
			33.68	31.3
			44.34	29.7
			54.68	27.8
			65.62	25.6
			76.88	25.2
			87.73	21.9
98.11	20.2			
108.3	18.25			
118.4	16.0			
130.6	14.05			
145.7	10.65			
164.7	5.90			
182.1	2.50			
1300	$10^{-2}$	$2.64 \times 10^5$	4.92	3.58
			8.13	3.41
			12.03	3.60
			18.42	3.39
			27.25	3.28
			37.22	2.88
			47.77	2.78
			57.97	2.60

TABLE 5. Continued

$T$ ( $^{\circ}\text{C}$ )	$P_{\text{O}_2}$ (atm)	$t$ (sec)	$x$ ( $\mu$ )	$\sigma$ (cps/ $\mu$ )			
1300	$10^{-2}$	$2.64 \times 10^5$	69.28	2.24			
			81.58	1.94			
			94.78	1.66			
			109.4	1.26			
			127.7	.733			
			146.4	.231			
			5.88	3.59			
			9.06	4.25			
			12.90	3.66			
			17.39	3.55			
			21.91	3.39			
			26.38	3.31			
			31.18	2.89			
			37.56	2.94			
			46.02	2.63			
			55.77	2.51			
			66.36	2.22			
			77.51	2.13			
			91.09	1.66			
			102.1	1.32			
			108.5	1.221			
			115.4	1.015			
			124.0	.769			
			136.7	.468			
			154.6	.0899			
			1300	$10^{-5}$	$2.64 \times 10^5$	21.45	1.66
						30.14	1.95
39.97	1.61						
49.93	1.71						
59.07	1.39						
69.32	1.252						
81.48	1.09						
94.14	.917						
106.5	.687						
118.6	.49						
130.6	.290						
143.9	.112						
17.84	1.849						
23.36	1.714						
30.05	1.742						
38.23	1.663						

TABLE 5. Continued

$T$ ( $^{\circ}\text{C}$ )	$P_{\text{O}_2}$ (atm)	$t$ (sec)	$x$ ( $\mu$ )	$\sigma$ (cps/ $\mu$ )
1300	$10^{-5}$	$2.64 \times 10^5$	47.21	1.463
			57.94	1.415
			67.97	1.233
			78.76	1.126
			89.47	.934
			98.92	.817
			109.0	.640
			122.0	.386
			136.6	.204
			151.4	.0514
			10.25	2.105
			18.82	1.44
			29.55	1.99
			37.67	1.985
			46.11	1.801
			55.44	1.519
			65.09	1.427
			75.63	1.171
			86.43	1.003
			97.61	.805
			110.3	.552
			123.6	.290
			136.1	.098



#### REFERENCES

1. G. E. Zima: Trans. ASM, 1957, Vol. 49, pp. 924-947.
2. F. R. Billman: Ph. D. Thesis, Ohio State University, 1967.
3. E. A. Gulbransen and K. F. Andrew: J. Electrochem. Soc., 1954, Vol. 101, pp. 128-40.
4. O. Kubaschewski and B. E. Hopkins: Oxidation of Metals and Alloys, Ch. 1, Butterworth Publications, London, 1953.
5. M. T. Shim and W. J. Moore: J. Chem. Phys., 1957, Vol. 26, pp. 802-804.
6. M. O'Keefe and W. J. Moore: J. Phys. Chem., 1961, Vol. 65, pp. 1438-1439.
7. C. Wagner and K. Zimens: Acta Chemica Scand., 1947, Vol. 1, pp. 547-565.
8. H. Pfeiffer and K. Hauffe: Z. Metallk., 1952, Vol. 43, pp. 364-69.
9. L. Horn: Z. Metallk., 1949, Vol. 40, pp. 73-76.
10. H. R. Copson and F. S. Lang: Corrosion, 1959, Vol. 15, pp. 194t-198t.
11. C. S. Giggins and F. S. Pettit: Trans. TMS-AIME, 1969, Vol. 245, pp. 2495-2507.
12. G. H. Meier: Ph. D. Thesis, Ohio State University, 1968.
13. R. A. Rapp: Corrosion, 1965, Vol. 21, pp. 382-401.
14. R. W. Cairns and E. J. Ott: J. Am. Chem. Soc., 1933, Vol. 55, pp. 527-544.
15. C. A. Hogarth: Proc. Phys. Soc., 1951, Vol. B64, pp. 691-700.
16. G. Parravano: J. Chem. Phys., 1955, Vol. 23, pp. 5-10.
17. F. J. Morin: Phys. Rev., 1954, Vol. 93, pp. 1199-1204.

18. F. J. Morin: Semiconductors, (N. B. Hanay, ed.), Ch. 14, Reinhold Publishing Corp., New York, 1959.
19. H. H. von Arnim and C. Wagner: Z. Physik. Chem. (Leipzig), 1934, Vol. B24, pp. 59-67.
20. M. G. Erer and J. B. Wagner: Phys. Stat. Sol., 1969, Vol. 35, pp. 641-651.
21. I. Bransky and N. M. Tallan: J. Chem. Phys., 1968, Vol. 49, pp. 1243-49.
22. S. P. Mitoff: J. Chem. Phys., 1961, Vol. 35, pp. 882-89.
23. G. H. Meier and R. A. Rapp: Z. Physik. Chem., 1971, Vol. 73, p.
24. W. C. Tripp and N. M. Tallan: J. Am. Cer. Soc., 1970, Vol. 53, pp. 531-33.
25. Y. D. Tret'yakov and R. A. Rapp: Trans. TMS - AIME, 1969, Vol. 245, pp. 1235-41.
26. O. Muller, R. Roy and W. B. White: J. Am. Cer. Soc., 1968, Vol. 51, pp. 693-99.
27. H. Falkenhagen: Electrolytes, Ch. 11, pp. 250-257, Oxford University Press, Oxford, 1934.
28. A. B. Lidiard: Handbuch der Physik, Vol. XX, (S. Flugge, ed.), pp. 298-339, Springer-Verlag OHG., Berlin, Göttingen, Heidelberg, 1957.
29. P. G. Shewmon: Diffusion in Solids, pp. 100-111, Mc Graw-Hill, New York, 1963.
30. V. O. Stasiw and J. Teltow: Ann. Physik, 1947, Vol. 1, pp. 261-72.
31. J. E. Hanlon: J. Chem. Phys., 1960, vol. 32, pp. 1492-1500.
32. F. J. Keneshea and W. J. Fredericks: J. Chem. Phys., 1963, Vol. 38, pp. 1952-58.
33. F. J. Keneshea and W. J. Fredericks: J. Phys. Chem. Solids, 1965, Vol. 26, pp. 501-8.
34. C. A. Allen, D. T. Ireland and W. J. Fredericks: J. Chem. Phys., 1967, Vol. 46, pp. 2000-1.
35. J. S. Choi and W. J. Moore: J. Phys. Chem., 1962, Vol. 66, pp. 1308-11.

36. R. Lindner and A. Akerstrom: *Disc. Far. Soc.*, 1957, Vol. 23, pp. 133-36.
37. W. B. Crow, Ph. D. Thesis, Ohio State University, 1969.
38. C. Greskovich: *J. Am. Cer. Soc.*, 1970, Vol 53, pp. 498-502.
39. K. J. Richards and F. E. Wagstaff: *J. Phys. Chem.*, 1966, Vol. 70, pp. 1553-57.
40. M. S. Seltzer: *J. Electrochem. Soc.*, 1971, Vol. 118, pp. 802-5.
41. J. E. Wentz : NBS Special Publication 296, 1968, pp. 11-23.
42. A. B. Lidiard: *Phys. Rev.*, 1954, Vol. 94, pp. 29-37.
43. J. Jennings: Mathematical Solutions of Engineering Problems, Ch. 1, E. and F. N. Spon, LTD, London, 1951.
44. K. Hauffe: *Ann. Physik (Leipzig)*, 1950, Vol. 8, pp. 201-10.
45. D. Yuan and F. A. Kroger: *J. Electrochem. Soc.*, 1969, Vol. 116, pp. 594-600.
46. Y. Agarwal: M. S. Thesis, Ohio State University, 1970.
47. S. M. Makin, A. H. Rowe and A. D. LeClaire: *Proc. Phys. Soc.*, 1957, Vol. B70, pp. 545-52.
48. J. Crank: The Mathematics of Diffusion, p. 19, Clarendon Press, Oxford, England, 1956.
49. J. Crank: The Mathematics of Diffusion, pp. 148-9, Clarendon Press, Oxford, England, 1956.
50. W. Jost: Diffusion in Solids, Liquids and Gases, p. 32, Academic Press, Inc., New York. 1960.
51. C. Wagner: *J. Chem. Phys.*, 1950, Vol. 18, pp. 1227-30.
52. W. Kass and M. O'Keefe: *J. Appl. Phys.*, 1966, Vol. 37, pp. 2377-79.
53. A. S. Nowick: personal Communication.